NACA RM L57I13

CONFIDENTIAL

Copy 5
RM L57I13

c. 2

CLASSIFICATION CHANGED

To UNCLASSIFIED

NACA

By authority of NASA #14 effective Date 2-8-60

RESEARCH MEMORANDUM

STATIC LATERAL CHARACTERISTICS AT HIGH SUBSONIC SPEEDS OF A COMPLETE AIRPLANE MODEL WITH A HIGHLY TAPERED WING HAVING THE 0.80 CHORD LINE UNSWEPT AND WITH SEVERAL TAIL CONFIGURATIONS

By Kenneth W. Goodson

Langley Aeronautical Laboratory
Langley Field, Va.

NATIONAL ADVISORY COMMITTEE FOR AERONAUTICS

WASHINGTON

October 28, 1957

CONFIDENTIAL

UNCLASSIFIED

NATIONAL ADVISORY COMMITTEE FOR AERONAUTICS

RESEARCH MEMORANDUM

STATIC LATERAL CHARACTERISTICS AT HIGH SUBSONIC SPEEDS OF A COMPLETE AIRPLANE MODEL WITH A HIGHLY TAPERED WING HAVING THE 0.80 CHORD LINE UNSWEPT AND WITH SEVERAL TAIL CONFIGURATIONS

By Kenneth W. Goodson

SUMMARY

An investigation was made at high subsonic speeds of a complete model having a highly tapered wing and several tail configurations. The aspect-ratio-3.50 wing had a taper ratio of 0.067 and an unswept 0.80 chord line. The complete model was tested with a wing-chord-plane tail, a T-tail, and a biplane tail (combined T-tail and wing-chord-plane tail). The model was tested in the Langley high-speed 7- by 10-foot tunnel at Mach numbers from 0.60 to 0.92 over a range of angle of attack of about $\pm 20^{\circ}$ and a range of sideslip of -15° to 13°. Some data were obtained with the horizontal stabilizer deflected. A few tests were also made with the wing tips clipped to an aspect ratio of 3.00.

The data show that shock-interference effects between the tail surfaces (T-tail) can have considerable influence on the directional stability and effective dihedral. For example, the T-tail configuration with horizontal-tail leading-edge overhang showed a considerable loss in directional stability as the angle of attack was reduced to zero or negative values; whereas, the T-tail with zero leading-edge overhang showed the loss to be considerably less. The directional stability of the model with the low tail was essentially constant over a range of angle of attack of $\pm 15^{\circ}$. All configurations tested showed a large reduction in stability at positive and negative angles of attack larger than about 15°, probably because of adverse sidewash associated with wing stall.

The data show that a wing-chord-plane horizontal tail (low tail) tends to give a positive pitching-moment increment with increase in sideslip angle; whereas, a high tail (T-tail) tends to give negative increments in pitching moment.

[redacted]

INTRODUCTION

Experience has shown that many high-performance airplanes are deficient in longitudinal and lateral stability at high subsonic and transonic speeds, especially at moderate and high angles of attack. These deficiencies, nonlinearities in pitching-moment curves and reductions in directional stability, along with aerodynamic and inertia cross-coupling effects, have resulted in violent inadvertent motions for some airplanes. The difficulties caused by the nonlinearities in pitching moment (pitch-up) can be minimized by proper selection of the wing and tail configuration. A program directed toward the development of suitable longitudinal configurations is reported in references 1 and 2. The lateral characteristics, by using the model of reference 2, have been determined over a large range of angle of attack and of sideslip, and the results are presented herein.

The model used in the present investigation has a wing of aspect ratio 3.50, a taper ratio of 0.067, and a zero sweep of the 0.80 chord line. The wing has an NACA 65A004 airfoil section parallel to the plane of symmetry. Static lateral derivatives and sideslip data were obtained on the complete model for several tail configurations. Limited data for lateral derivatives also were obtained for the model with the wing tips clipped to an aspect ratio of 3.00.

COEFFICIENTS AND SYMBOLS

The lateral-stability data are referred to the body axes, except for the lift and drag data which are referred to the stability axes. (See fig. 1.) The moment coefficients are referred to a center-of-gravity position which is located at the quarter-chord point of the aspect-ratio-3.50 wing. The force and moment coefficients of the wing configurations having aspect ratios of 3.50 and 3.00 are based on the area, mean aerodynamic chord, and span of the wing under consideration.

C_L lift coefficient, $\frac{\text{Lift}}{qS}$

C_D' drag coefficient, $\frac{\text{Drag (approx.)}}{qS}$

C_Y side-force coefficient, $\frac{\text{Side force}}{qS}$

C_m pitching-moment coefficient, $\frac{\text{Pitching moment}}{qS\bar{c}}$

C_l rolling-moment coefficient, $\frac{\text{Rolling moment}}{qSb}$

C_n yawing-moment coefficient, $\frac{\text{Yawing moment}}{qSb}$

q dynamic pressure, $\frac{\rho V^2}{2}$, lb/sq ft

ρ mass density of air, slugs/cu ft

V free-stream velocity, ft/sec

M Mach number

S wing area, sq ft

$\bar{c}$ wing mean aerodynamic chord, $\frac{2}{S}\int_0^{b/2} c^2 dy$, ft

c local chord parallel to plane of symmetry, ft

c_r root chord, ft

c_t tip chord, ft

$\bar{c}_h$ horizontal-tail mean aerodynamic chord, ft

$\bar{c}_v$ vertical-tail mean aerodynamic chord, ft

b wing span, ft

y spanwise distance from plane of symmetry, ft

Δx change of mean aerodynamic quarter-chord location due to clipping tip of wing, in.

l_h horizontal-tail length measured between the mean aerodynamic quarter-chord points of the wing and horizontal-tail surfaces, in.

l_v vertical-tail length measured between the mean aerodynamic quarter-chord points of the wing and vertical-tail surfaces, in.

α angle of attack, deg

β angle of sideslip, deg

i_t stabilizer deflection, positive when trailing edge is down, deg

A aspect ratio

λ taper ratio

Λ sweep angle, deg

C_{l_β} rate of change of rolling-moment coefficient with sideslip angle

C_{n_β} rate of change of yawing-moment coefficient with sideslip angle

C_{Y_β} rate of change of side-force coefficient with sideslip angle

MODEL AND APPARATUS

A three-view drawing of the complete model with the aspect ratio 3.50 wing having a taper ratio of 0.067 and an unswept 80-percent chord line is shown in figure 2(a). The wing tips of the aspect ratio 3.50 wing were clipped to form the aspect ratio 3.00 wing (fig. 2(b)).

The model was fitted with a vertical tail having an unswept trailing edge $\left(\Lambda_{\frac{c}{4}} = 28.37^{\circ}\right)$ and with a delta horizontal tail which could be mounted in two positions. (See figs. 2(a) and 2(c).) The horizontal tail could be mounted on the rear end of the fuselage in the wing-chord plane extended and also on the tip of the vertical tail in a T-tail arrangement. The apex of the horizontal tail (basic T-tail arrangement) overhung the leading edge of the vertical-tail tip by 1.93 inches. The various tail configurations of the basic model are shown in figure 2(c).

In addition to the tail configurations of the basic model, the model was modified to provide zero overhang of the horizontal tail (T-tail) and also to keep the original tail length for this configuration (fig. 2(d)). In order to keep the same horizontal-tail length, a reduced-sweep vertical tail was constructed for the zero overhang configuration (tail configuration 7).

The incidence of the horizontal tail of the T-tail configuration could be varied by use of several mounting brackets. The incidence of the chord-plane horizontal tail was fixed at 0°. Dimensions of the fuselage which has a fineness ratio of 10.94 are presented in table I. A photograph of the model mounted on the sting support of the Langley high-speed 7- by 10-foot tunnel is shown in figure 2(e).

TESTS

The sting-supported model was tested in the Langley high-speed 7- by 10-foot tunnel through a Mach number range of 0.60 to 0.92. The Reynolds number based on the mean aerodynamic chord varied with Mach number from about 2.6×10^{6} to 3.4×10^{6}.

Tests for lateral derivatives of the aspect-ratio-3.50 model with several tail configurations were made at $\beta = \pm 4^{\circ}$ over a range of angle of attack of about -20° to 24°, with the range covered being dependent upon the model loads and tunnel operating conditions. The aspect-ratio-3.50 wing was also tested in sideslip over a range from -15° to 13° at angles of attack of 0°, 9.5°, and 15.6°. In addition, several tests were made in order to determine the effect of stabilizer deflection on the lateral aerodynamic characteristics. Some tests for lateral derivatives were made for the model with the wing tips clipped to an aspect ratio of 3.00.

CORRECTIONS

Blockage corrections were applied to the results by the method of reference 3. Jet-boundary corrections to the angle of attack and drag were applied in accordance with reference 4. Corrections for effects of the longitudinal pressure gradient in the wind-tunnel test section have been applied to the data.

Model-support tares have not been applied, except for a fuselage base-pressure correction to the drag. The corrected drag data represent a condition of free-stream static pressure at the fuselage base. Past experience indicates that the influence of the sting support on the model characteristics is negligible with regard to the lift and pitching moment.

The angle of attack has been corrected for deflection of the balance and sting support. No attempt has been made to correct the data for aeroelastic distortion of the steel-wing model.

PRESENTATION OF RESULTS

The results are presented in figures 3 to 24 as follows:

The results are presented about a center of gravity located at the quarter-chord point of the mean aerodynamic chord of the aspect-ratio-3.50 wing.

DISCUSSION

Currently many high-performance airplanes have experienced violent cross-coupling effects in some maneuvers which resulted in large angular displacements of the airplane. For this reason, lateral-derivative data of the present investigation were obtained at rather large positive and negative angles of attack in order to gain insight into the aerodynamic characteristics at these large angles. To further extend these results, sideslip data (both lateral and longitudinal coefficients) were obtained over a moderate range of sideslip for several angles of attack. A detailed discussion of these results is presented in the following paragraphs.

Lateral Derivatives

Directional stability.- The directional instability of the tail-off configuration (tail configuration 1, fig. 3) remains essentially constant through the Mach number range and through an angle-of-attack range of about ±15°, at which point the instability becomes larger probably because of wing stall. (See ref. 2.) When a vertical tail is added to the model (tail configuration 2), the directional stability is increased by an increment of about 0.0064 through the Mach number range investigated, with the gain being somewhat larger at positive angles of attack than at negative angles of attack. This variation with angle of attack is opposite to that which would be expected on the basis of vertical-tail effective sweep angle alone, thus the indication is that interference (sidewash and dynamic pressure) is the more important factor. The addition of a horizontal tail on the wing-chord plane extended (tail configuration 3) gives an added increment to the stability as a result of the end-plate effect. When the horizontal tail is raised to the top of the vertical tail (T-tail arrangement with leading-edge overhang, tail configuration 4), a considerably larger increase in stability is obtained through the range of angle of attack at $M = 0.60$, again as a result of the end-plate effect. Note that the small effect of the wing-fuselage wake (sidewash) still prevails through the range of angle of attack. Similar results were obtained with the biplane tail configuration (tail configuration 5). Note, also, that the increase in stability diminishes rather markedly with an increase in Mach number, especially in the range of angle of attack from moderate positive values to large negative values. In fact, at moderate to large negative angles of attack (below the wing stall) and at high Mach numbers, a negative end-plate effect due to the horizontal surfaces is indicated.

In order to help explain the loss of directional stability as the angle of attack is reduced to negative values, data were obtained with the wing removed from the T-tail model. These results (fig. 4) show the same trends with angle of attack as indicated for the complete wing-on configuration, although the wing-wake effects are eliminated. This similarity in the data of the wing-on and wing-off configurations leads to the conclusion that above a critical Mach number, shock interference between the horizontal tail (with leading-edge overhang) and the vertical tail is the probable cause of the large reduction in stability. In order to further investigate the shock-interference effects, the T-tail was modified to give zero leading-edge overhang of the horizontal-tail root chord. This shift in the maximum-thickness position of the horizontal tail relative to the vertical tail (shift of transonic shock pattern) proved to be effective in that the directional stability was considerably improved over the range of angle of attack from moderate positive values to large negative values. (See fig. 5.) Reduction in sweep of the vertical tail to maintain the original horizontal-tail length for the case of zero overhang did not appreciably affect the directional stability (fig. 5, tail configurations 6 and 7). Some of these results were previously presented in reference 5. Note that all wing-on configurations showed an abrupt reduction in directional stability at positive and negative angles of attack at or near the wing stall ($\alpha = \pm 15^{\circ}$ approximately).

Additional losses in directional stability also are incurred, especially at and above the critical Mach number, when the stabilizer is deflected negatively for the zero leading-edge overhang configuration (tail configuration 4, fig. 6). These losses probably result from increased shock-interference effects as the stabilizer is deflected. This trend is true over the unstalled range of angle of attack up to high negative values, at which point shock-stall effects on the horizontal tail apparently give a temporary gain in stability in the range of angle of attack of -5° to -10°. When the horizontal tail is moved rearward to give a zero leading-edge overhang, a small increase in directional stability (fig. 7) is obtained at high angles of attack for negative stabilizer deflections. At low positive and negative angles of attack, the stability losses still occur when the critical Mach number is reached or exceeded. The results obtained with the reduced-sweep vertical-tail configuration having zero leading-edge overhang are very similar to those obtained for the basic T-tail configuration having zero leading-edge overhang. (See figs. 7 and 8.)

Figure 9 presents lateral-derivative data for the model with the wing tips clipped to give an aspect ratio of 3.00. The effect of reducing the aspect ratio of the wing from 3.50 to 3.00 is to increase the overall directional stability of the tail-on configurations, although most of the increase is due to the effects of reduction in wing area and span on the coefficients. For example, C_{n_β} values based on the area and span of the aspect-ratio-3.50 wing rather than on the aspect-ratio-3.00 wing reduces C_{n_β} by about 0.0007. (See fig. 7(a); $M = 0.60$.) The remaining increment between the curves based on the span of the aspect-ratio-3.50 wing and on the area probably result from improved sidewash at the tail.

Effective dihedral.- The effective dihedral parameter C_{l_β} of the wing-body configuration (tail configuration 1, fig. 3) is negative for positive angles of attack and positive for negative angles of attack, as would be expected for a sweptback wing. These trends are magnified by an increase in Mach number. The curve of effective dihedral at stall also breaks in the expected direction . The addition of a vertical tail to the model (tail configuration 2) increases the effective dihedral throughout the range of angle of attack and of Mach number by a value of ΔC_{l_β} of about -0.002. The addition of a wing-chord-plane horizontal tail to the vertical-tail-on configuration (tail configuration 3) reduced the effective dihedral a small amount, probably because of the lower center of load caused by the end-plate effect of the horizontal tail. The addition of the horizontal tail to the top of the vertical tail (tail configuration 4, with leading-edge overhang) gave a considerable increase in negative C_{l_β} at positive angles of attack as a result of the end-plate effect of the high horizontal tail. This increase diminishes as the angle of attack approaches negative values, especially at Mach numbers above the critical value. Similar results were obtained when the wing-chord-plane horizontal tail was added to the T-tail configuration to form the biplane tail configuration (tail configuration 5), although there was some reduction in C_{l_β} caused by the end-plate effect of the low tail.

The reduction in effective dihedral of the high horizontal-tail configuration (with leading-edge overhang) as the angle of attack becomes negative is believed to be caused, in part, by shock interference between the horizontal and vertical tail surfaces in a manner similar to that previously discussed in the section on directional stability. This conclusion is substantiated by the wing-off data of figure 4 which shows, for the body—vertical-tail configuration (wing-off), a negative increase in C_{l_β} in the negative angle-of-attack direction and the opposite effect when the horizontal tail with leading-edge overhang is on the model. This trend is still evident when the wing is added to the model. (See fig. 5, tail configurations 2 and 4.) When the horizontal tail is moved rearward, the interference effect is reduced. (See tail configuration 6.) The reduced-sweep vertical tail did not appreciably affect the results with zero overhang of the horizontal tail other than for a small negative increase in C_{l_β}.

The use of stabilizer deflection for longitudinal trim considerably reduces the effective dihedral at moderate angles of attack, especially at the higher Mach numbers, for the configuration with the horizontal-tail root-chord leading-edge overhang (fig. 6). Moving the horizontal tail rearward to obtain zero overhang reduced the effect on C_{l_β} of stabilizer deflection at positive angles of attack. Similar results were obtained with the reduced-sweep vertical-tail configuration. (See fig. 8, tail configuration 7.)

The effect of a reduction in wing aspect ratio on the effective dihedral was small for the wing-fuselage configuration. (See fig. 9, tail configuration 1.) Small increases in C_{l_β} were obtained with a a vertical tail on the model, probably because of a favorable increase in sidewash at the tail. When a horizontal tail with zero overhang was added to the tip of the vertical tail (T-tail, tail configuration 6), a somewhat larger increase in C_{l_β} was obtained because of the reduction in aspect ratio. (See fig. 5.)

Side-force characteristics.- The side-force characteristics are generally what would be expected, based on the previous discussion of C_{n_β} and C_{l_β}.

Sideslip Characteristics

In general, lateral derivatives measured from sideslip data at low Mach numbers (M = 0.60) agree with values obtained from pitch tests at $\beta = \pm 4^{\circ}$ (as shown by a comparison of the values of fig. 3 with the values of slopes from figs. 10, 11, and 12). A study of the sideslip results shows, however, that the lateral-derivative data at Mach numbers above the critical Mach number and at high angles of attack were made at sideslip angles where nonlinearities occur. Further examination of the sideslip data shows, however, that the same trends with angle of attack are indicated by either method, although the magnitude of values are somewhat different. These nonlinearities are believed to be associated with shock interference effects on the wing and tail surfaces. The occurrence of shock effects at the tail is further substantiated when the horizontal tail (T-tail) is moved rearward to give zero leading-edge overhang, since the nonlinearities in the sideslip curves then are minimized. (See figs. 13 and 14.) The lateral-derivative plots (figs. 6, 7, and 8) indicate that horizontal-stabilizer deflection for trim had a detrimental effect on the lateral characteristics at some angles of attack; however, the sideslip data (figs. 16 to 24) show that stabilizer deflection in most cases only shifted the coefficient level when the nonlinearities (shock effects) occurred, without appreciably affecting the slopes.

The nonlinearities observed in the lateral results are also evident in the longitudinal coefficients under sideslipped conditions. Inspection of the pitching-moment data of figures 10, 11, and 12 shows that a wing-chord-plane horizontal tail (low tail), in general, tends to give a positive pitching-moment increment at the higher sideslip angles; whereas, the high horizontal-tail configurations tend to give negative increases in pitching moment. It can be seen, therefore, that location of the horizontal tail can have considerable influence on the pitching-moment characteristics when sideslipped, and thus on aerodynamic cross-coupling effects. The effects of stabilizer deflection on the longitudinal characteristics in sideslip are what would normally be expected.

CONCLUDING REMARKS

An investigation of the lateral characteristics of the model, which was previously found to have favorable longitudinal characteristics at high subsonic speeds, has indicated the following results:

A high horizontal tail (T-tail) with leading-edge overhang contributes a large increment to the directional stability at large positive angles of attack; however, this increment diminishes rather markedly at Mach numbers above the critical Mach number as the angle of attack is reduced to zero or negative values. The loss in directional stability is considerably smaller when the horizontal tail is moved rearward to a zero leading-edge overhang position, indicating, therefore, that shock interference effects at the tail alter the stability appreciably. The directional stability with a low horizontal tail was essentially constant over a range of angle of attack of about $\pm 15^{\circ}$. The wing-fuselage configuration also showed a constant increment over this range of angle of attack. All configurations showed an abrupt reduction in directional stability at positive and negative angles of attack larger than about 15°, probably as a result of wing stall. The effects of shock interference at the tail (T-tail configurations) are also evident in the effective dihedral results.

The data show that a wing-chord-plane horizontal tail (low tail) tends to give a positive pitching-moment increment with increase in sideslip angle; whereas a high tail (T-tail) tends to give negative increments in pitching moment. These data, in general, show that the degree of aerodynamic cross coupling (between the longitudinal and lateral results) is dependent upon the tail configuration.

Langley Aeronautical Laboratory,
National Advisory Committee for Aeronautics,
Langley Field, Va., August 27, 1957.

REFERENCES

1. Few, Albert G., Jr., and Fournier, Paul G.: Effects of Sweep and Thickness on the Static Longitudinal Aerodynamic Characteristics of A Series of Thin, Low-Aspect-Ratio, Highly Tapered Wings at Transonic Speeds - Transonic-Bump Method. NACA RM L54B25, 1954.

2. Goodson, Kenneth W.: Static Longitudinal Characteristics at High Subsonic Speeds of a Complete Airplane Model With a Highly Tapered Wing Having the 0.80 Chord Line Unswept and With Several Tail Configurations. NACA RM L56J03, 1956.

3. Herriot, John G.: Blockage Corrections for Three-Dimensional-Flow Closed-Throat Wind Tunnels, With Consideration of the Effect of Compressibility. NACA Rep. 995, 1950. (Supersedes NACA RM A7B28.)

4. Gillis, Clarence L., Polhamus, Edward C., and Gray, Joseph L., Jr.: Charts for Determining Jet-Boundary Corrections for Complete Models in 7- by 10-Foot Closed Rectangular Wind Tunnels. NACA WR L-123, 1945. (Formerly NACA ARR L5G31.)

5. Polhamus, Edward C., and Hallissy, Joseph M., Jr.: Effect of Airplane Configuration on Static Stability at Subsonic and Transonic Speeds. NACA RM L56A09a, 1956.

TABLE I.- FUSELAGE ORDINATES

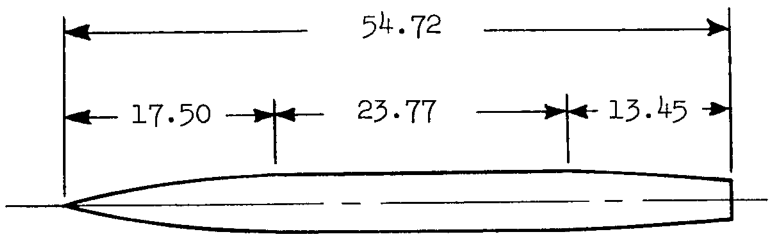

Station, in.	Radius, in.
0	0
2.00	.53
4.00	1.00
6.00	1.44
8.00	1.80
10.00	2.07
12.00	2.30
14.00	2.42
16.00	2.47
17.50	2.50
41.27	2.50
43.27	2.42
45.27	2.35
47.27	2.25
48.30	2.14
54.72	1.65

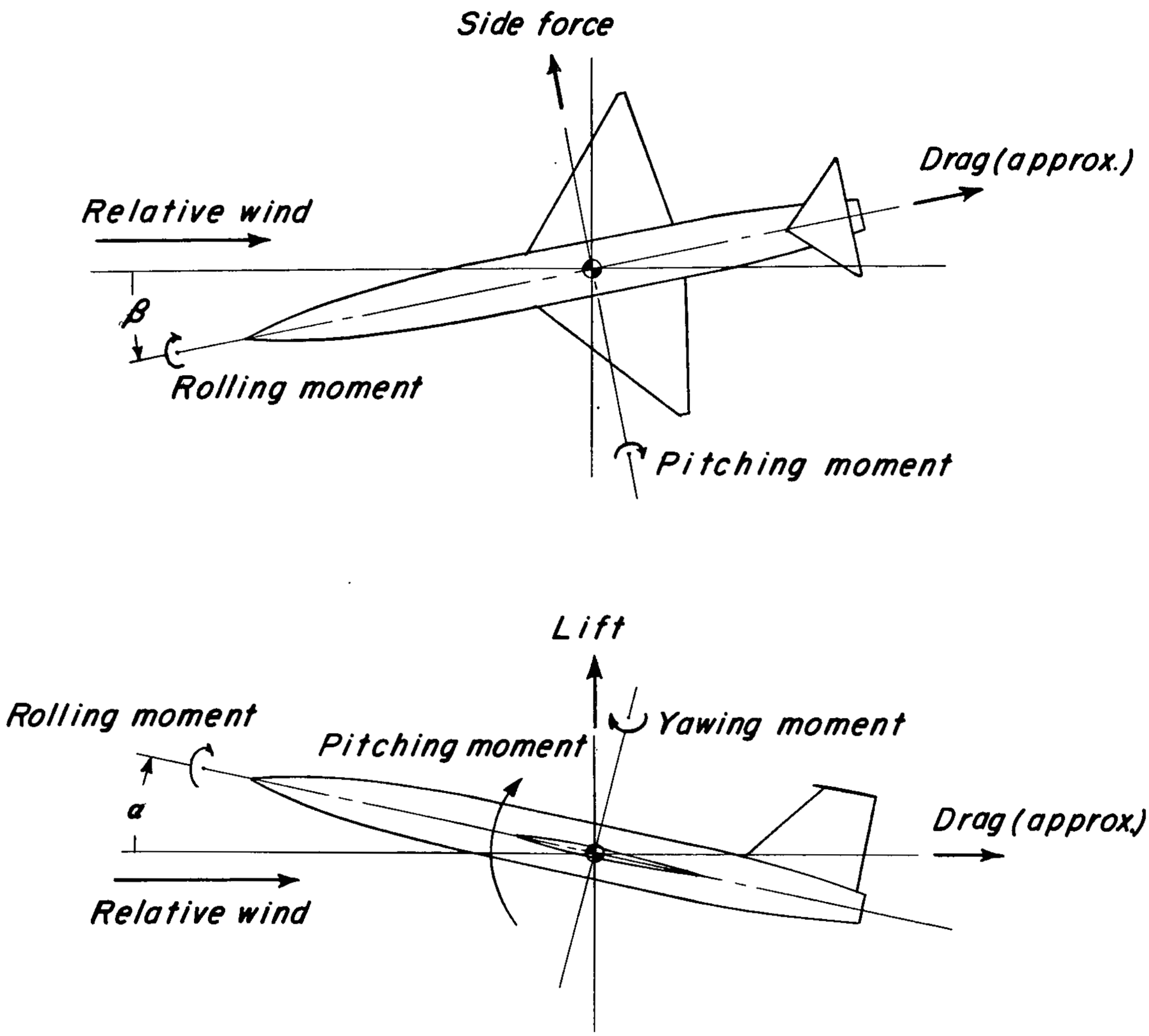

Figure 1.- Systems of axes. Positive values of forces, moments, and angles are indicated by arrows.

[redacted]

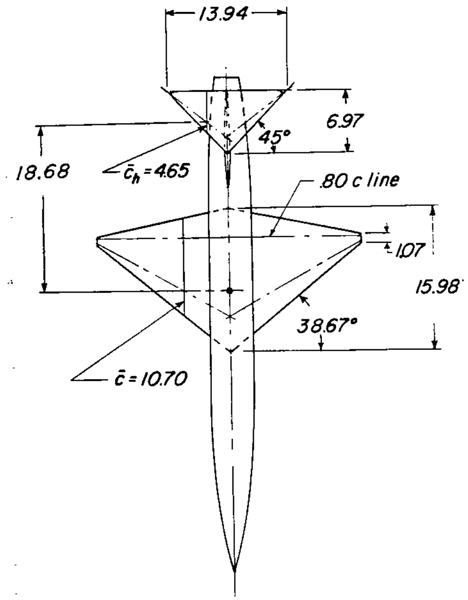

Geometric Characteristics Of Model	Wing	Horiz. tail	Vert. tail
Area, ft^2	1.77	.337	.603
Aspect ratio	3.50	4.00	1.16
Taper ratio	.067	0	.411
$\Lambda_{c/4}$, deg	28.82	36.85	28.37
NACA airfoil section parallel to airstream	65A004	65A006	65A006

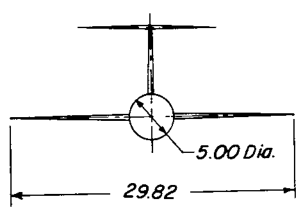

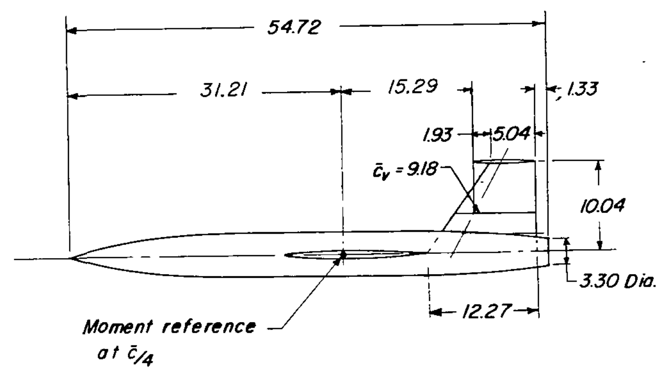

(a) Three-view drawing of basic model. Wing aspect ratio, 3.50. All dimensions are in inches.

Figure 2.- Geometric characteristics of model.

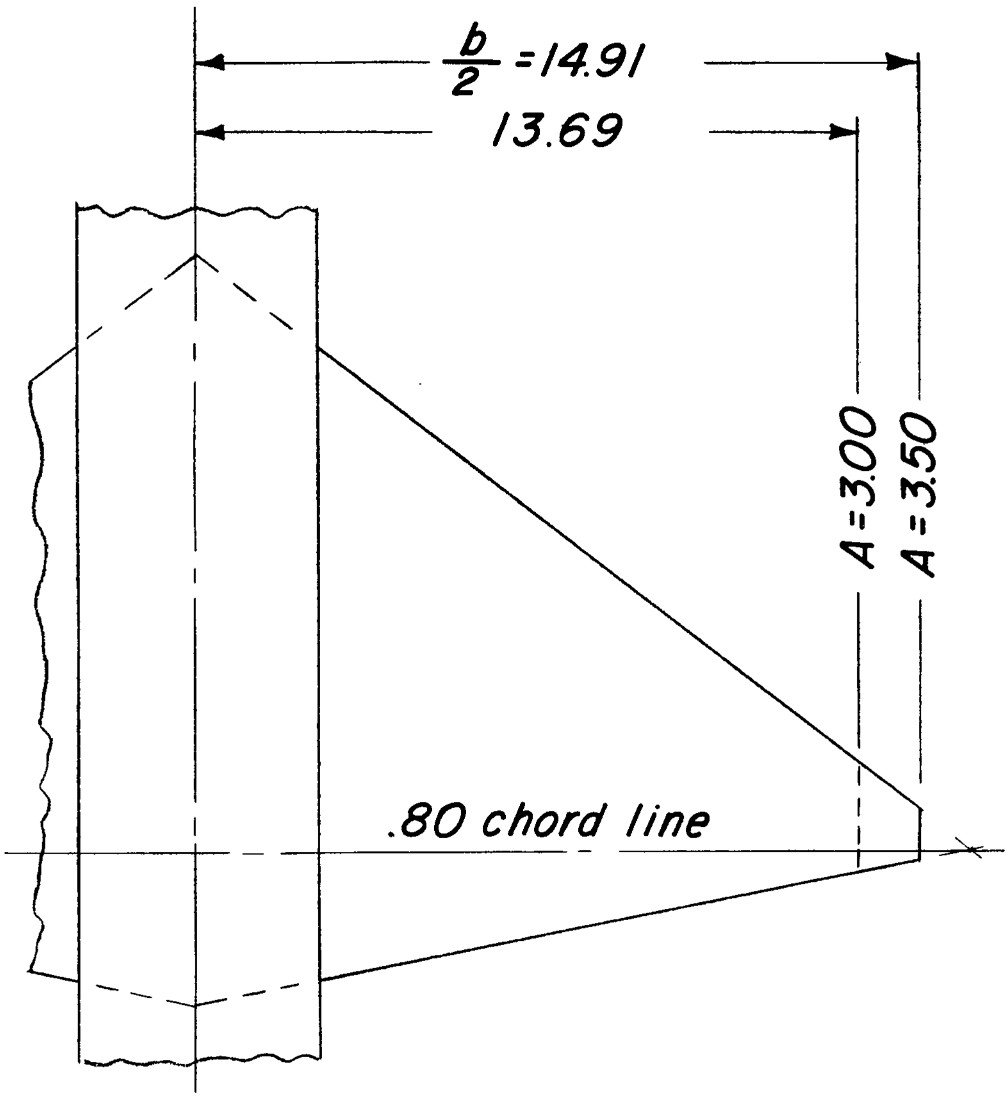

A	λ	$\Lambda_{.80c}$	c_r	c_t	$\bar{c}$	S	Δx
3.50	.067	0°	15.98	1.07	10.70	1.77	0
3.00	.143	↓	↓	2.28	10.83	1.74	-.078

(b) Wing-tip modification of aspect-ratio-3.50 wing. All dimensions are in inches.

Figure 2.- Continued.

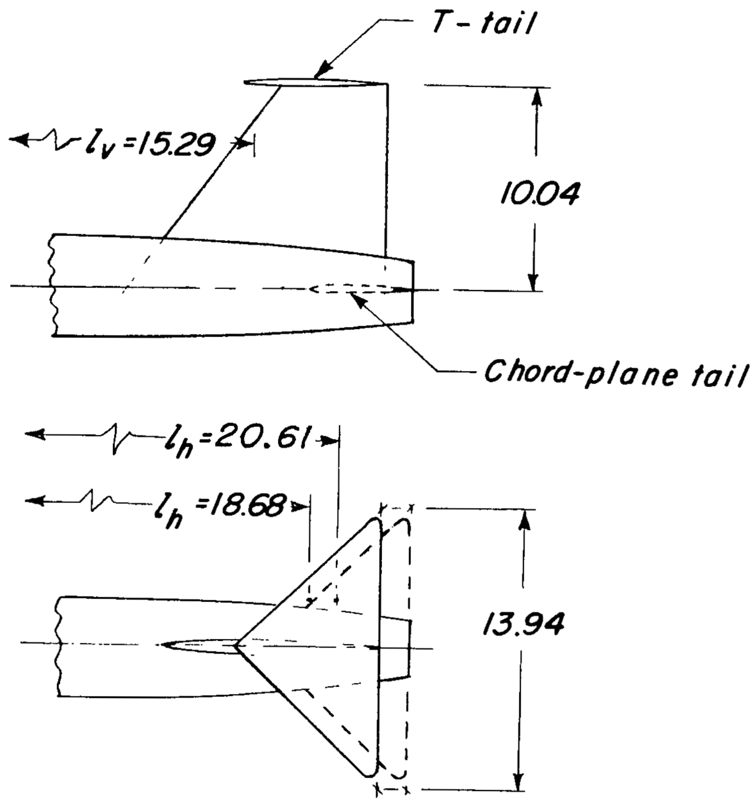

Tail Configuration	Horizontal tail	Vertical tail (Unswept trailing edge)
1	Off	Off
2	Off	On
3	Chord-plane tail	On
4	T-tail	On
5	Biplane tail	On

(c) Model tail configurations with unswept trailing-edge vertical tail.

Figure 2.- Continued.

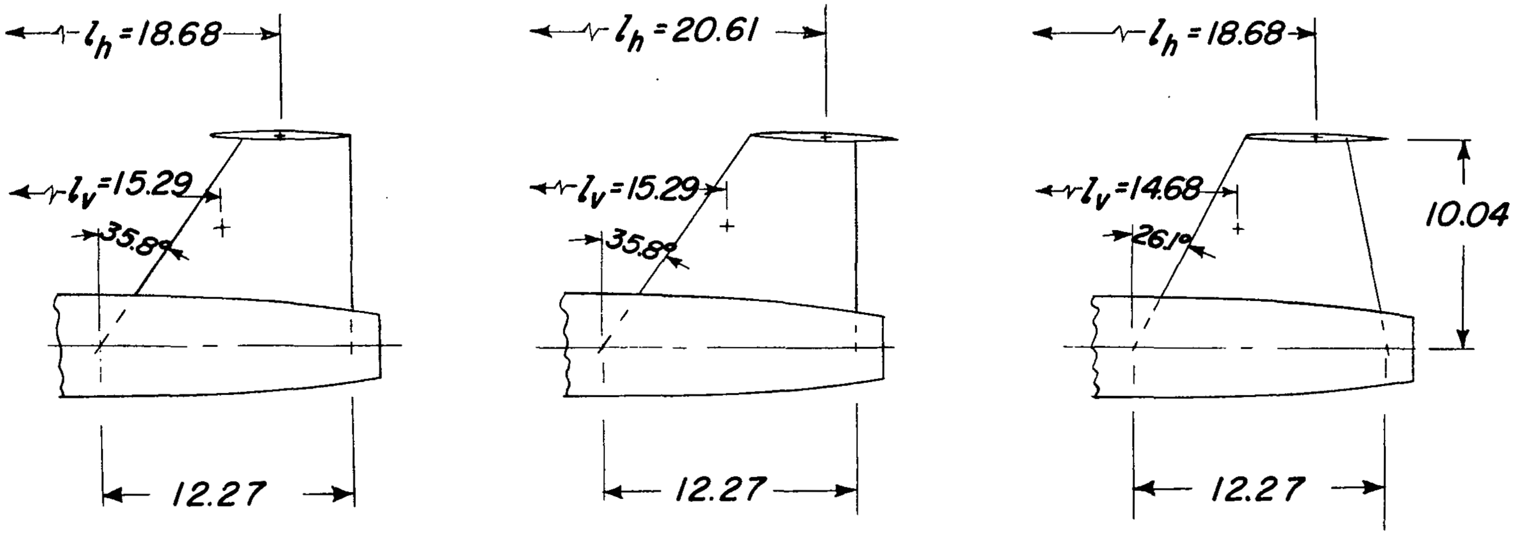

Tail configuration 4 *Tail configuration 6* *Tail configuration 7*

(d) Horizontal-tail overhang and tail length.

Figure 2.- Continued.

[redacted]

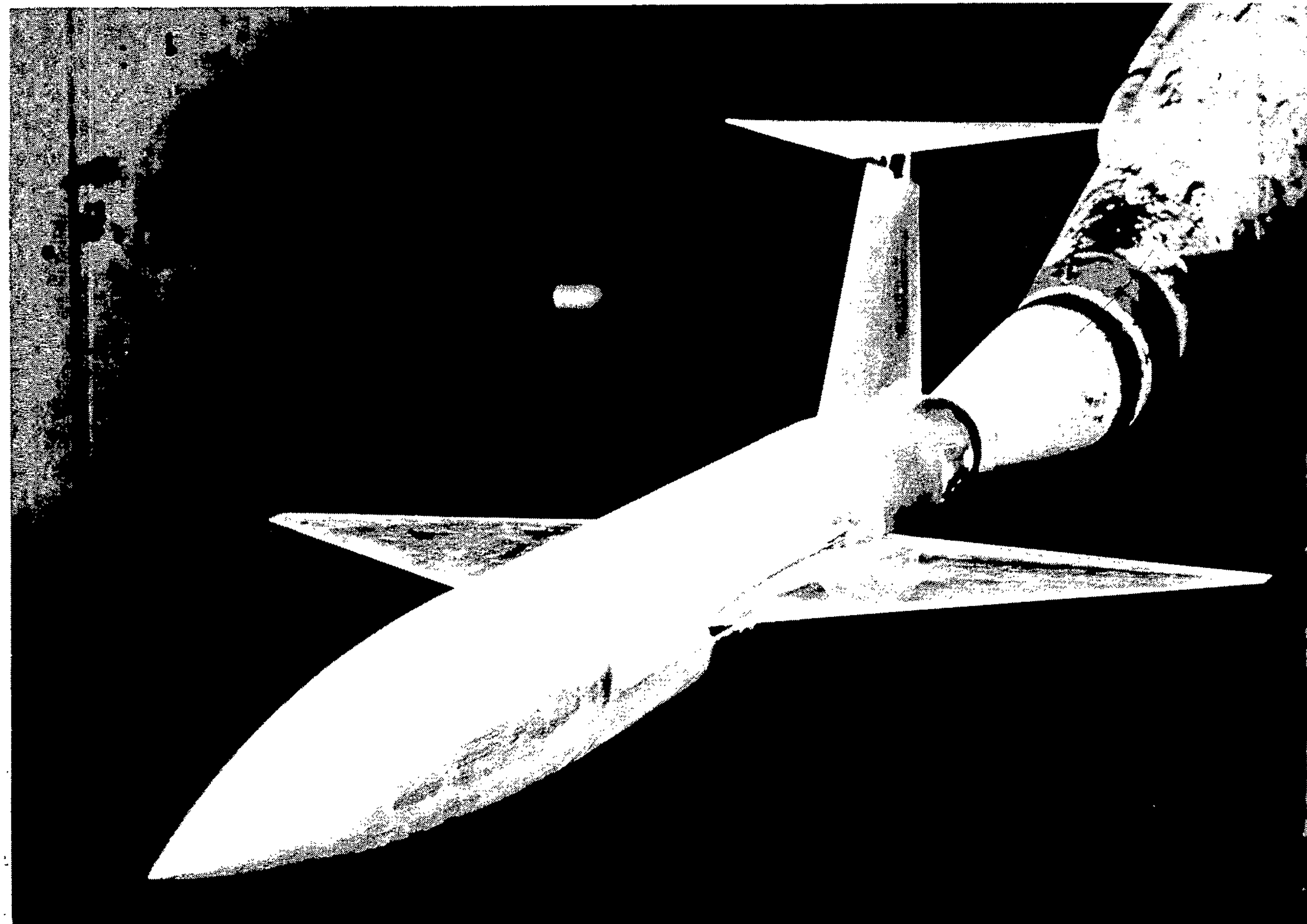

(e) Photograph of model mounted in tunnel. L-89250

Figure 2.- Concluded.

[redacted]

[redacted]

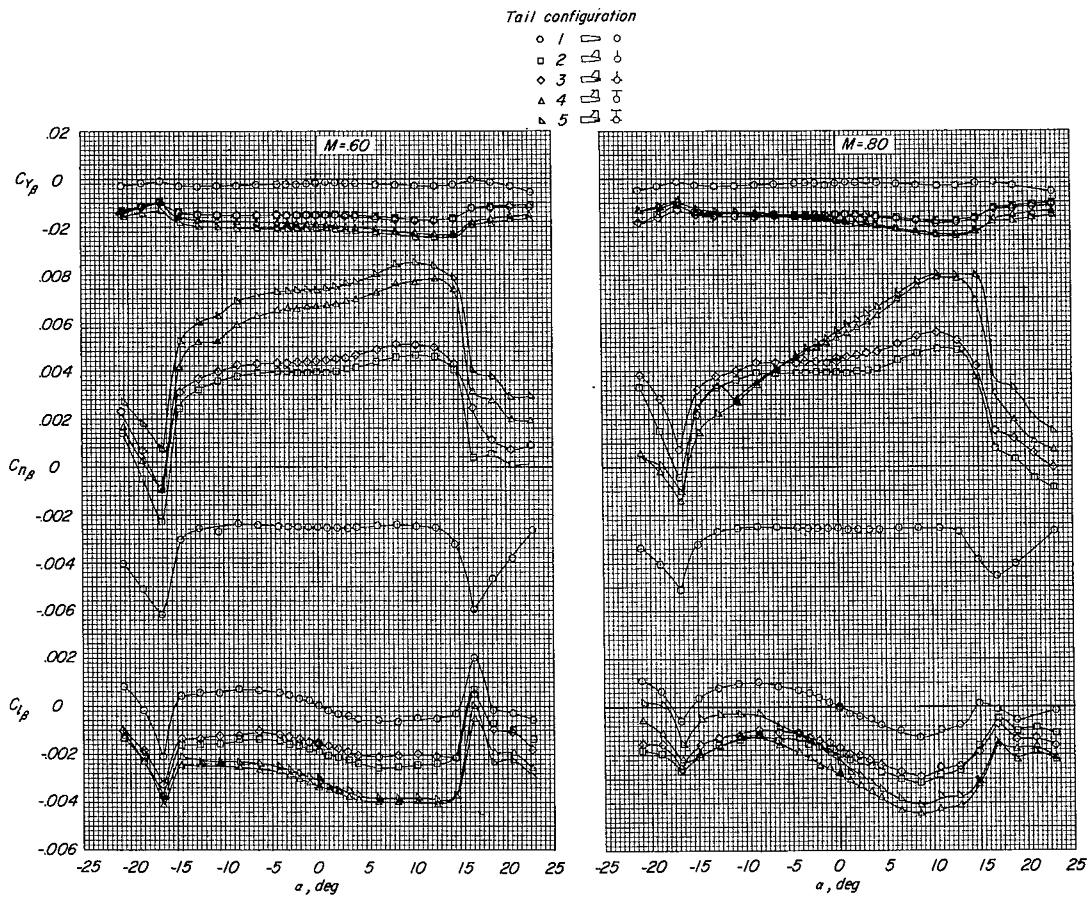

(a) M = 0.60 and 0.80.

Figure 3.- Lateral derivatives of the model for several tail configurations. Wing aspect ratio, 3.50; $i_t = 0^\circ$.

[redacted]

[redacted]

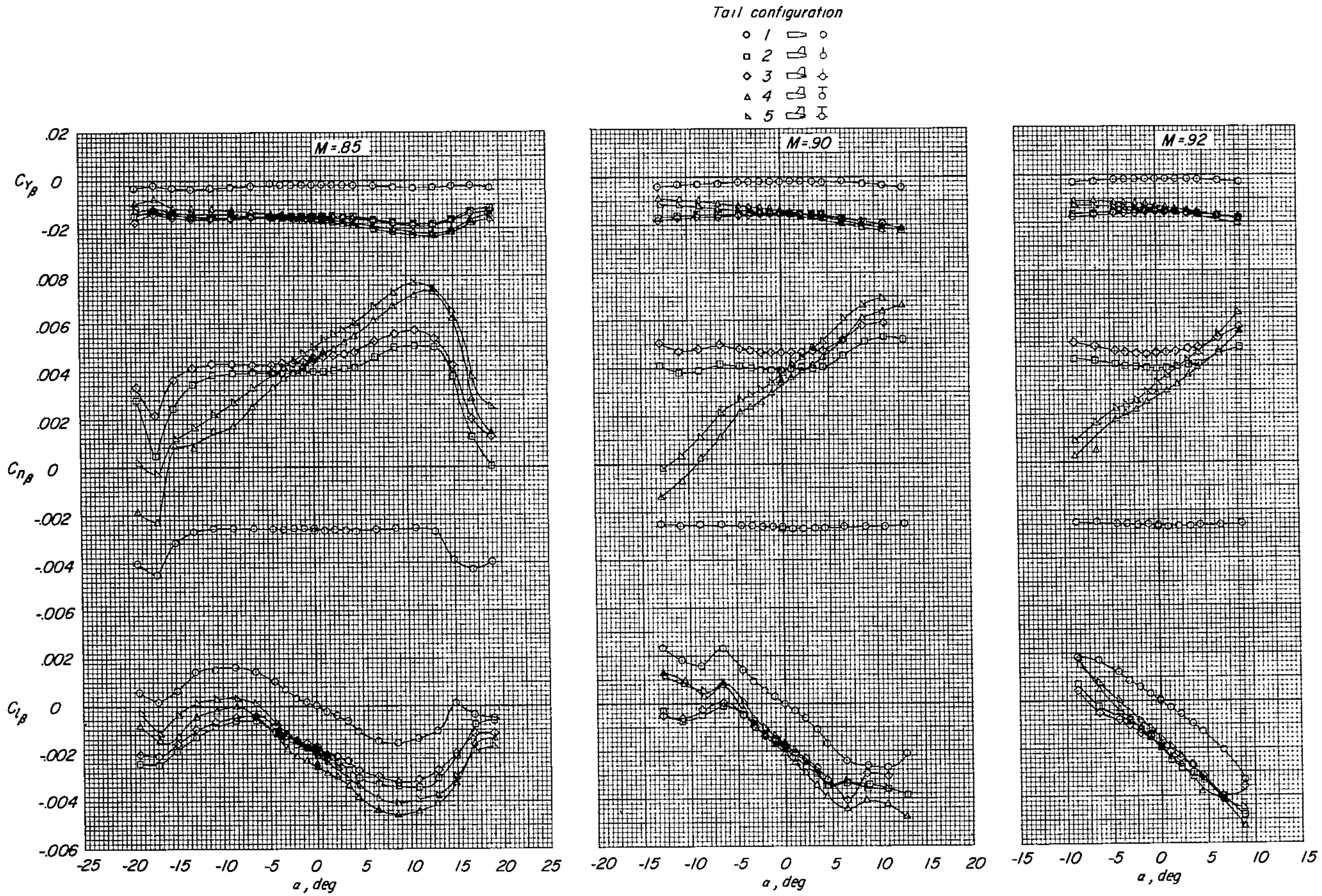

(b) M = 0.85, 0.90, and 0.92.

Figure 3.- Concluded.

[redacted]

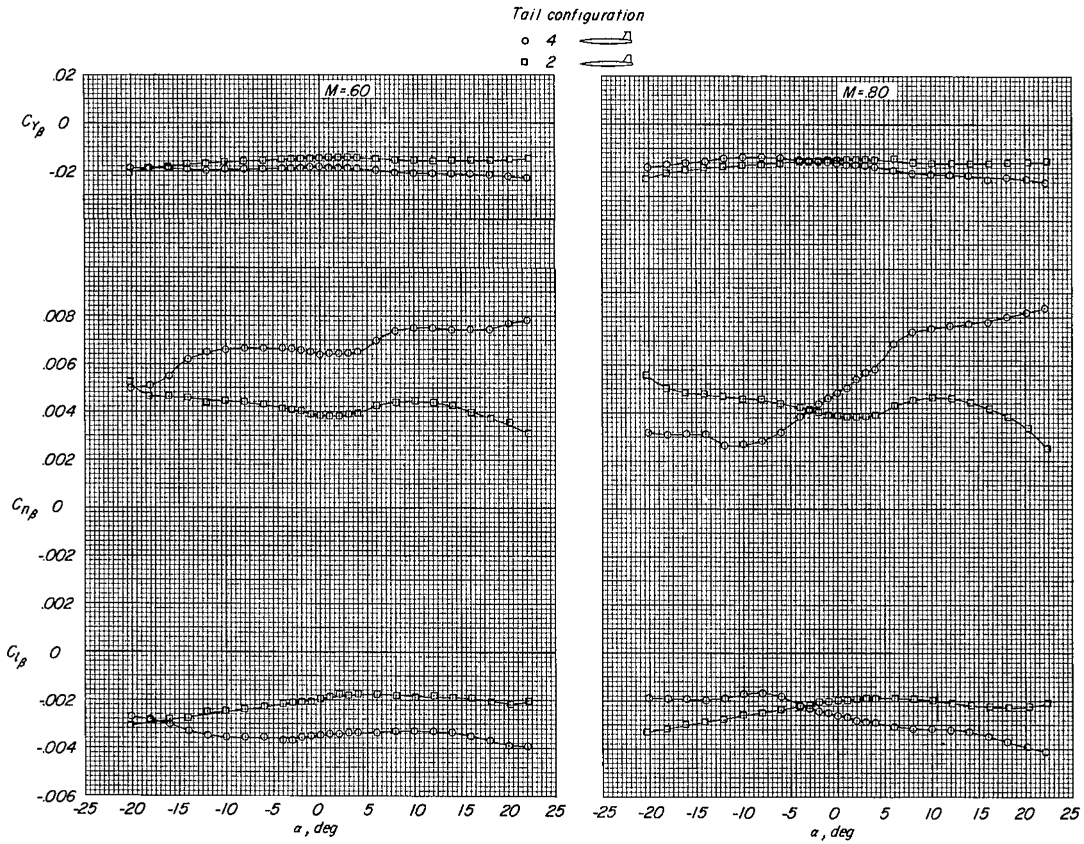

(a) M = 0.60 and 0.80.

Figure 4.- Lateral derivatives of several fuselage-tail configurations with the wing removed. Wing aspect ratio, 3.50.

[redacted]

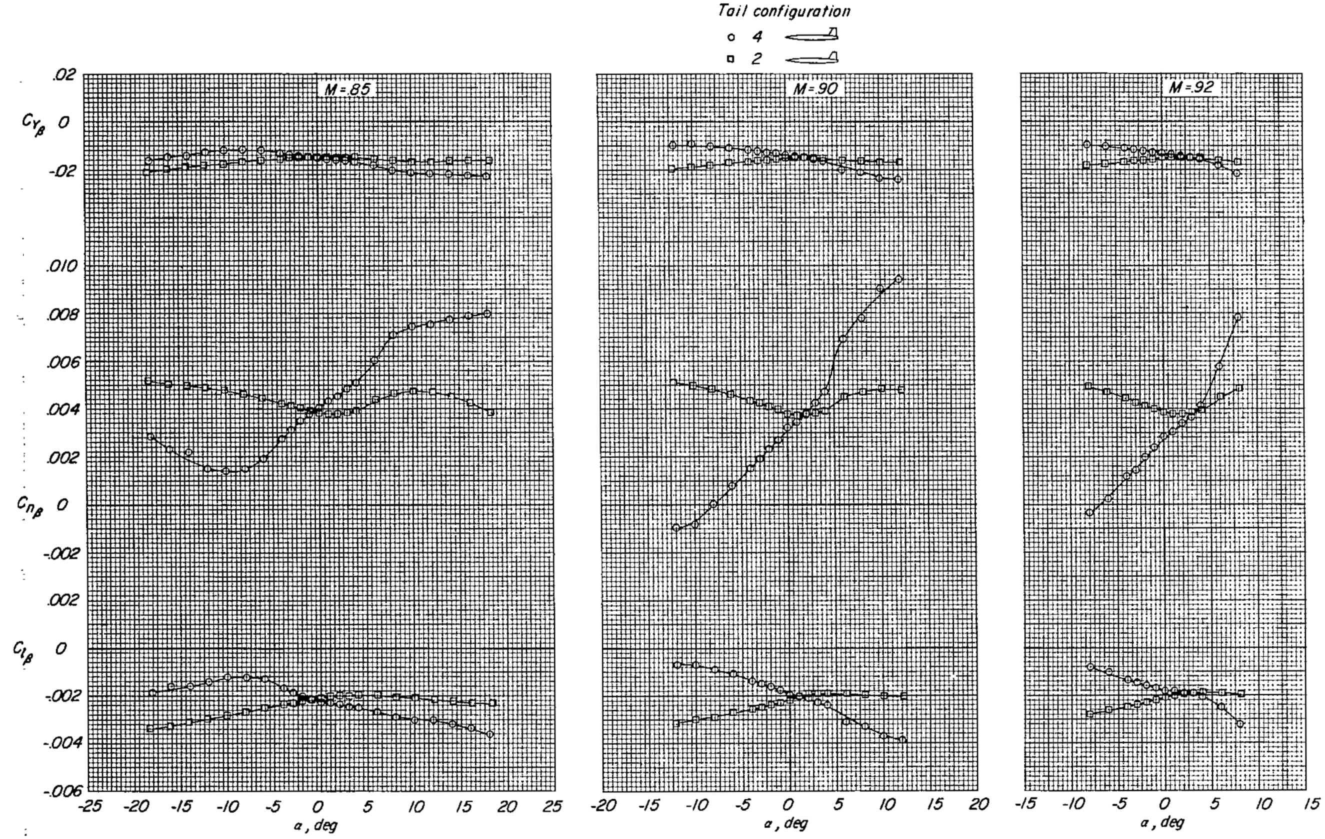

(b) M = 0.85, 0.90, and 0.92.

Figure 4.- Concluded.

[redacted]

~~CONFIDENTIAL~~

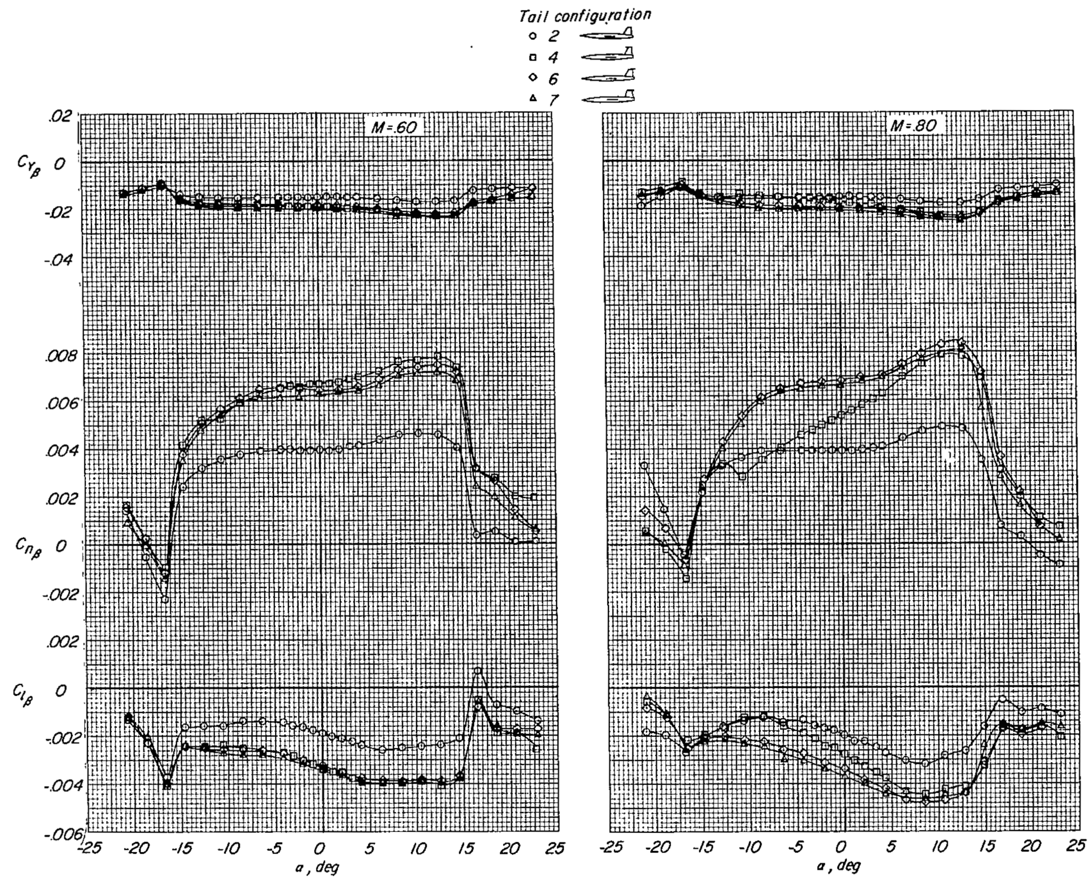

(a) M = 0.60 and 0.80.

Figure 5.- Lateral derivatives of the model for several variations of the T-tail arrangement. Wing aspect ratio, 3.50; $i_t = 0^{\circ}$.

~~CONFIDENTIAL~~

[redacted]

[redacted]

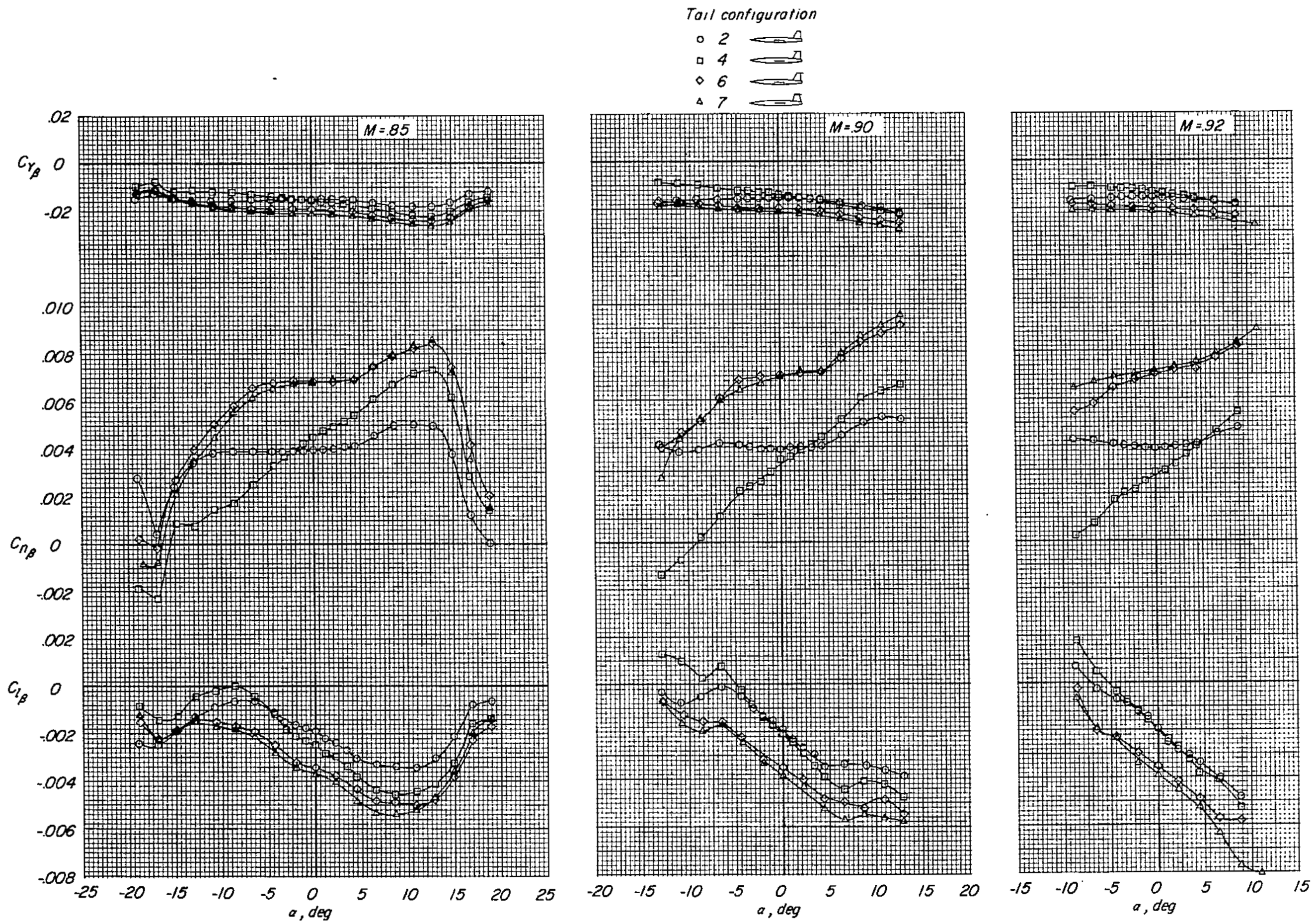

(b) M = 0.85, 0.90, and 0.92.

Figure 5.- Concluded.

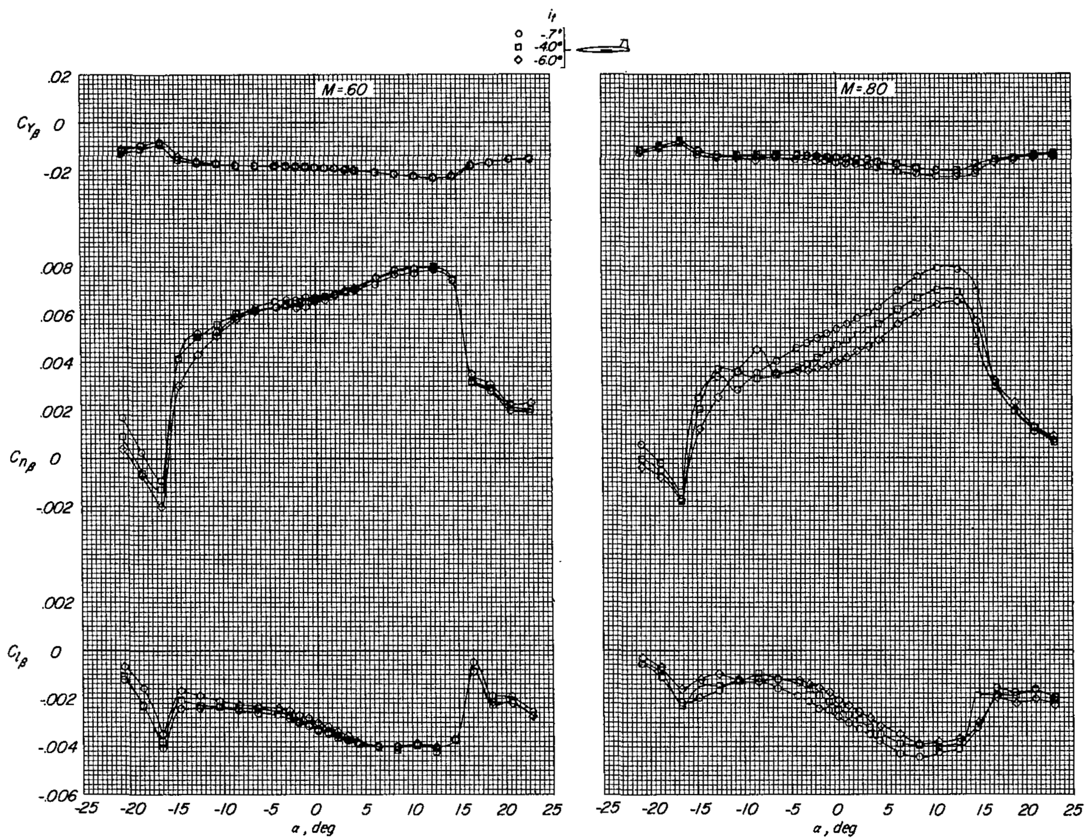

(a) M = 0.60 and 0.80.

Figure 6.- Effect of stabilizer deflection on lateral derivatives for the T-tail configuration with leading-edge overhang. Tail configuration 4; wing aspect ratio, 3.50.

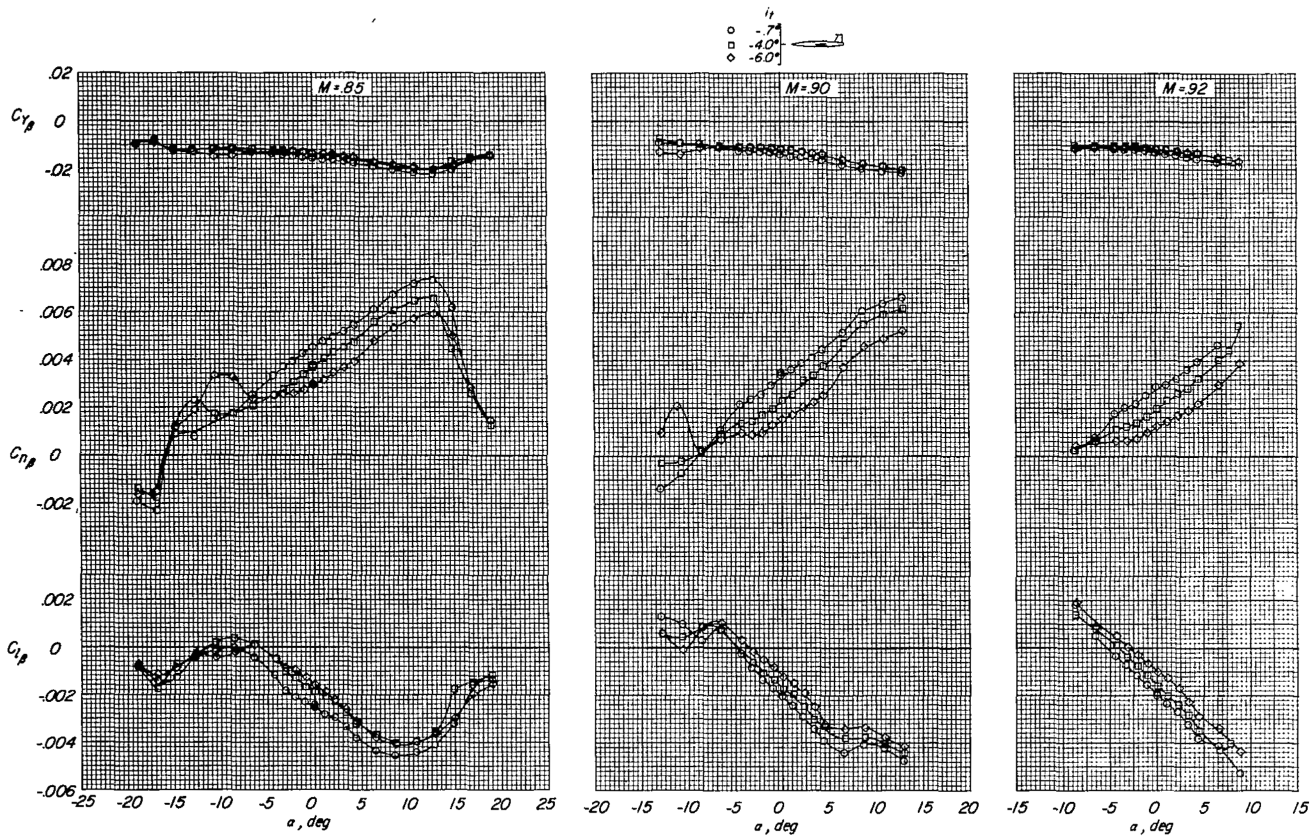

(b) M = 0.85, 0.90, and 0.92.

Figure 6.- Concluded.

~~CONFIDENTIAL~~

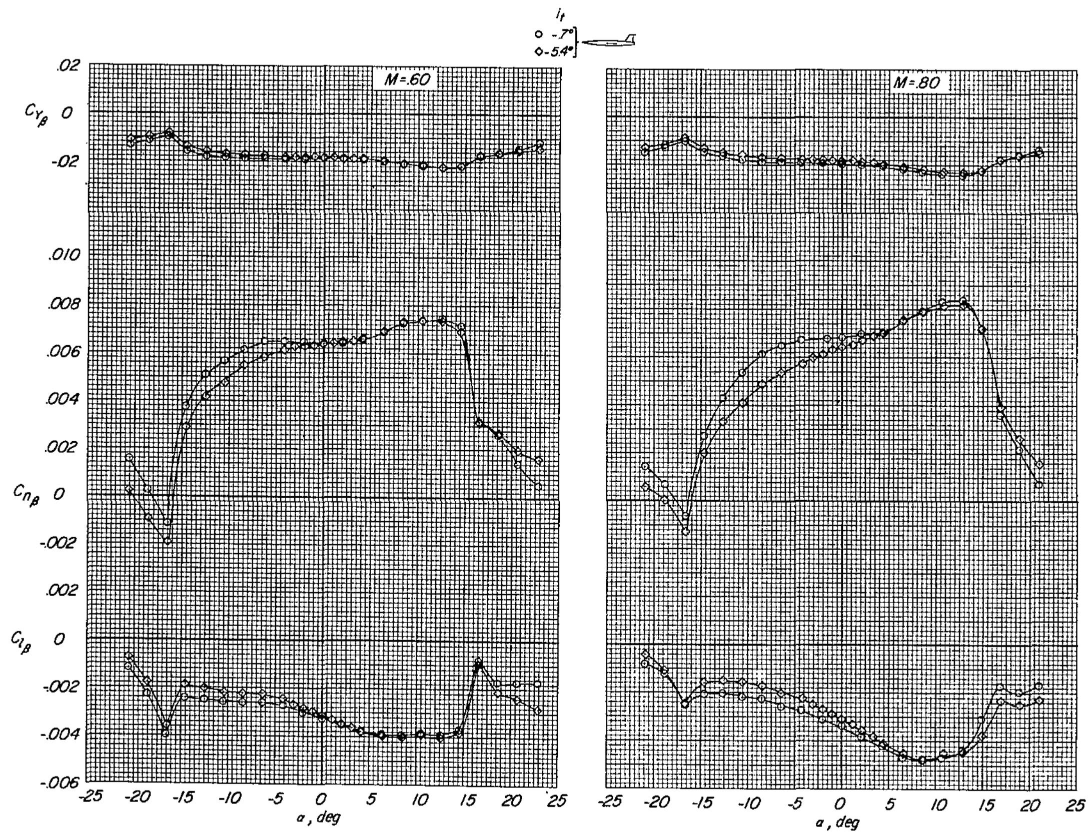

(a) M = 0.60 and 0.80.

Figure 7.- Effect of stabilizer deflection on lateral derivatives for the T-tail configuration with zero leading-edge overhang. Tail configuration 6; wing aspect ratio 3.50.

~~CONFIDENTIAL~~

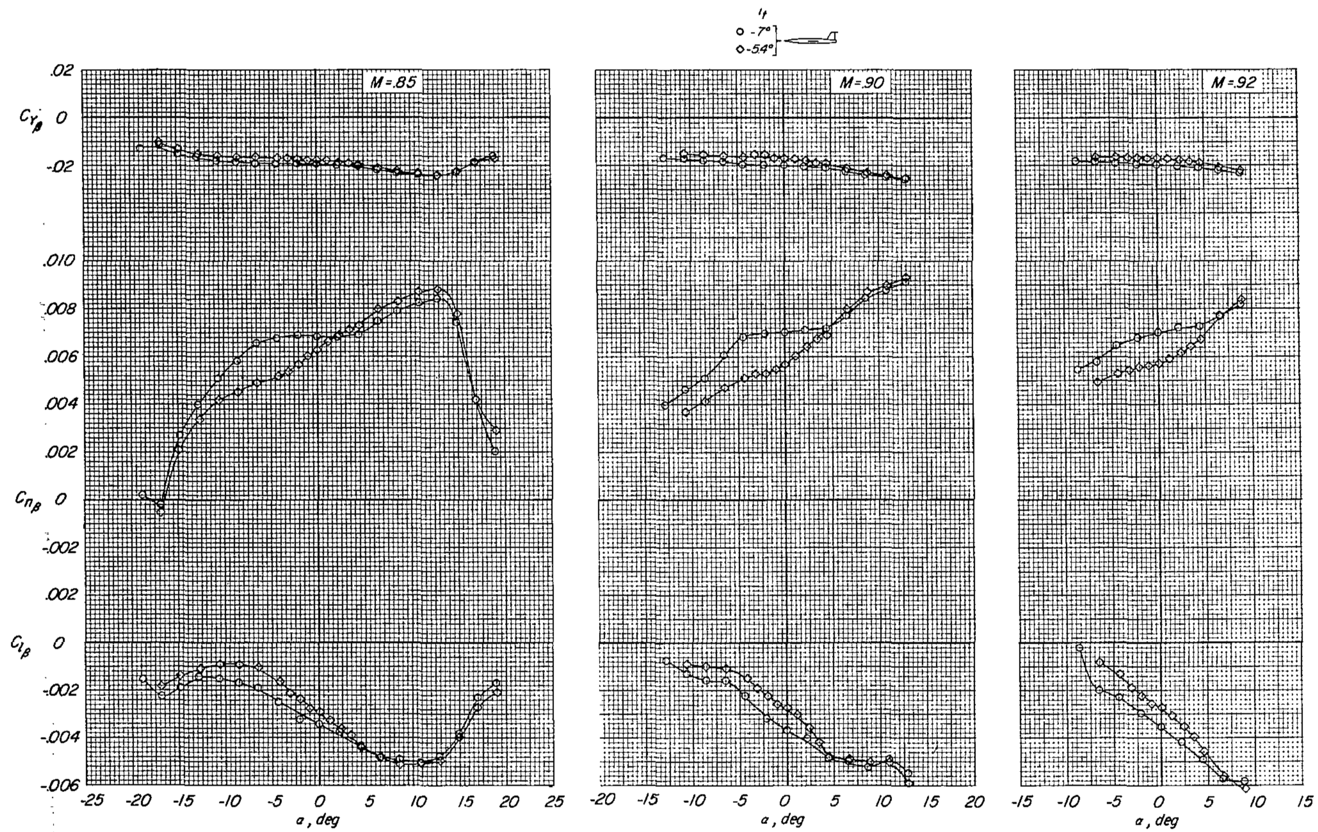

(b) M = 0.85, 0.90, and 0.92.

Figure 7.- Concluded.

~~CONFIDENTIAL~~

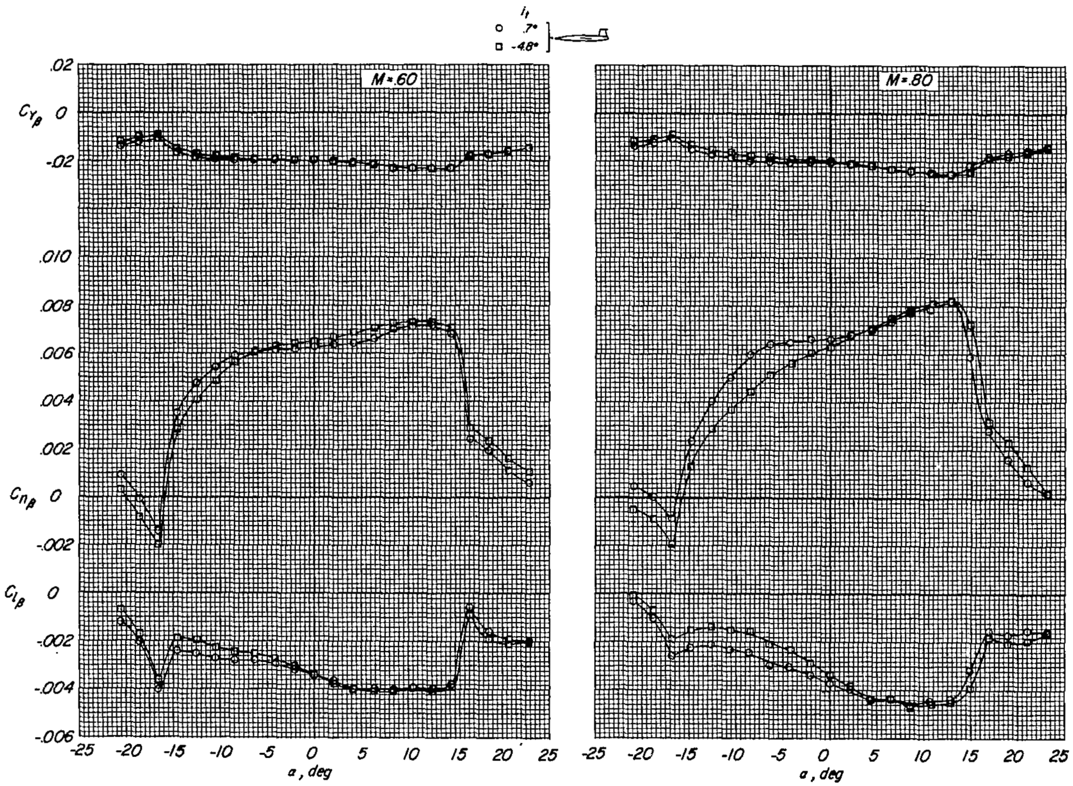

(a) M = 0.60 and 0.80.

Figure 8.- Effect of stabilizer deflection on lateral derivatives for the T-tail with zero leading-edge overhang and mounted on a reduced-sweep vertical tail. Tail configuration 7; wing aspect ratio, 3.50.

~~CONFIDENTIAL~~

[redacted]

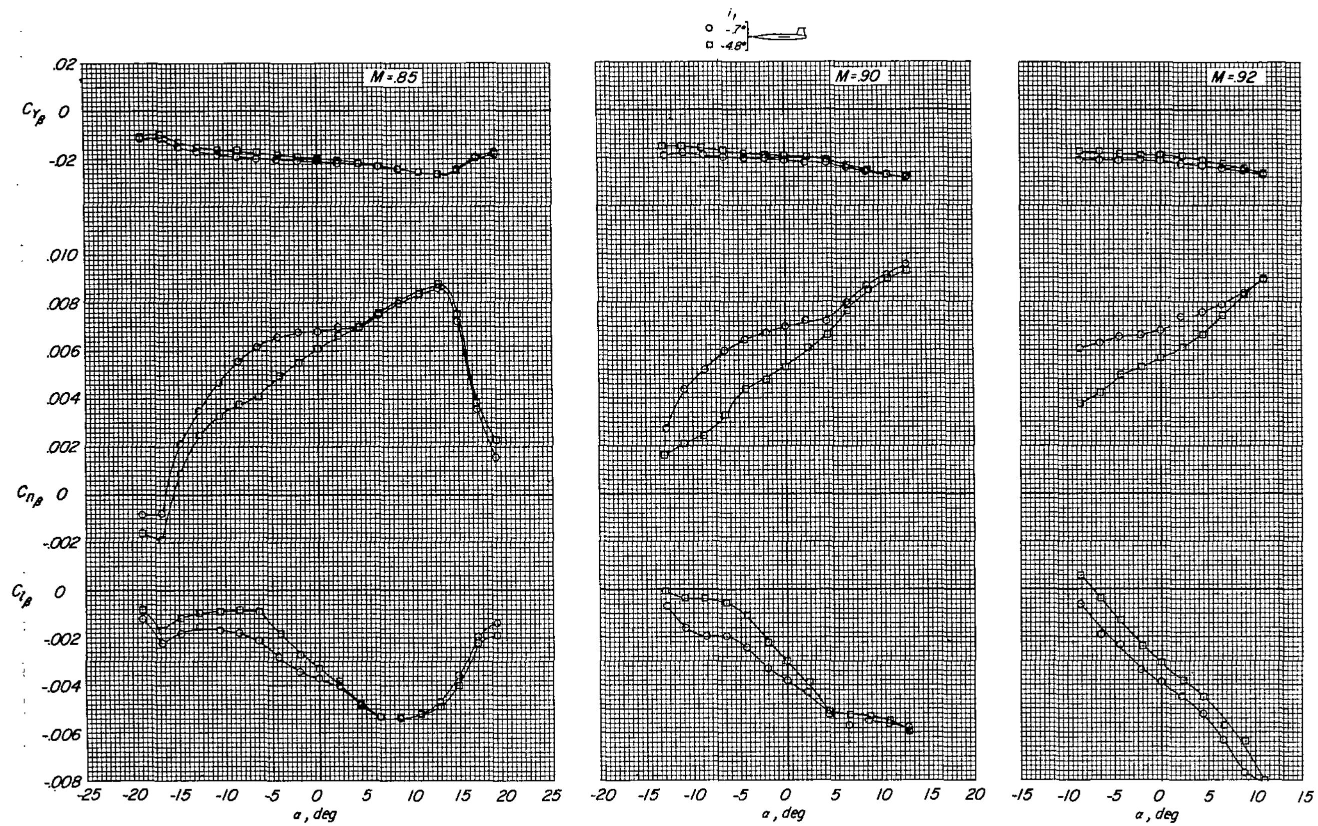

(b) M = 0.85, 0.90, and 0.92.

Figure 8.- Concluded.

[redacted]

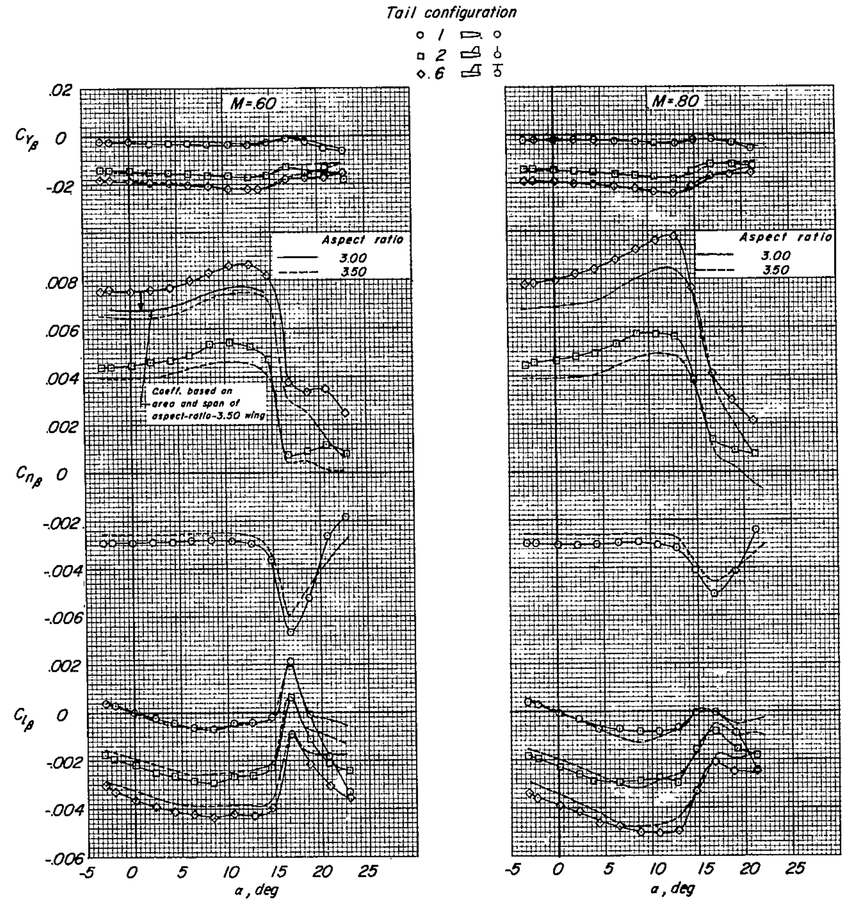

(a) M = 0.60 and 0.80.

Figure 9.- Effect of aspect ratio on lateral derivatives of the model for several tail configurations. $i_t = 0^{\circ}$.

[redacted]

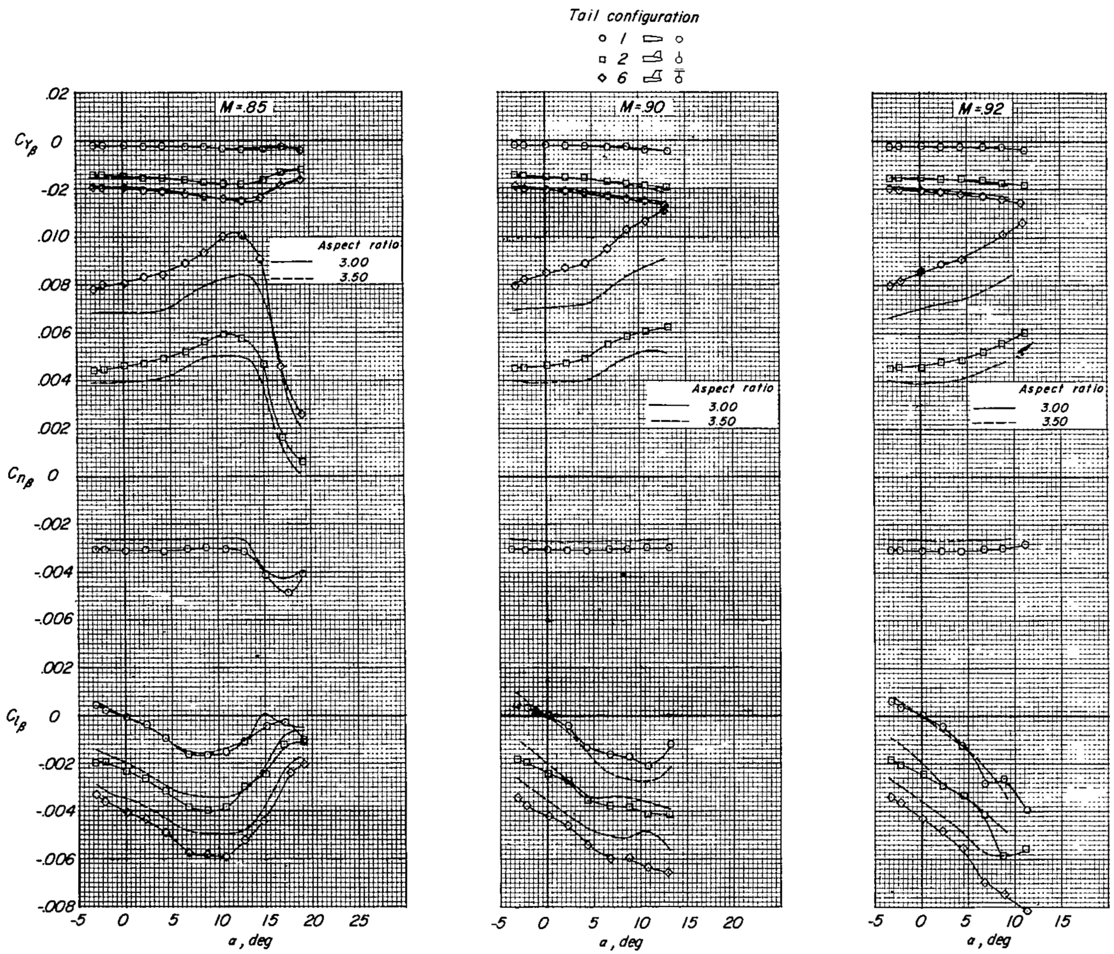

(b) M = 0.85, 0.90, and 0.92.

Figure 9.- Concluded.

[redacted]

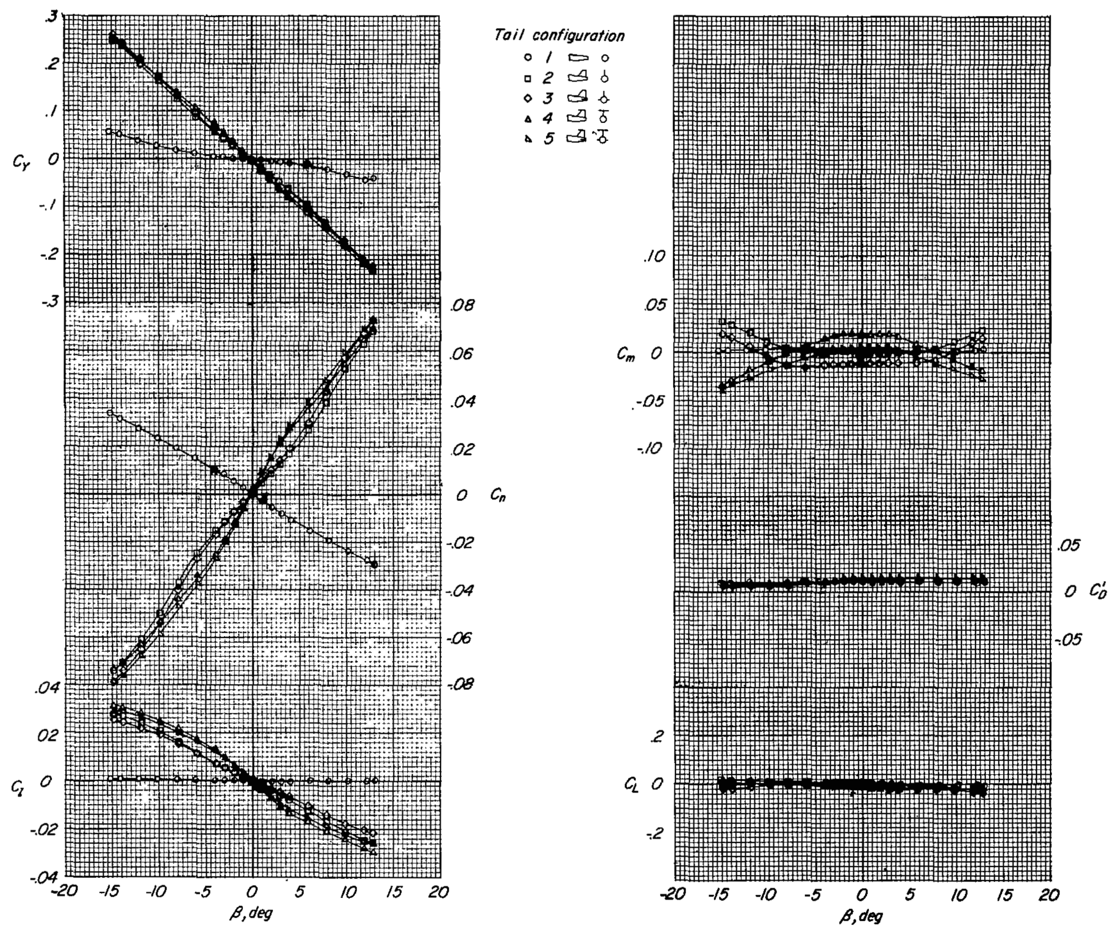

(a) M = 0.60.

Figure 10.- Aerodynamic characteristics of sideslipped model for several tail configurations. Wing aspect ratio, 3.50; $i_t = 0^{\circ}$; $\alpha = 0^{\circ}$.

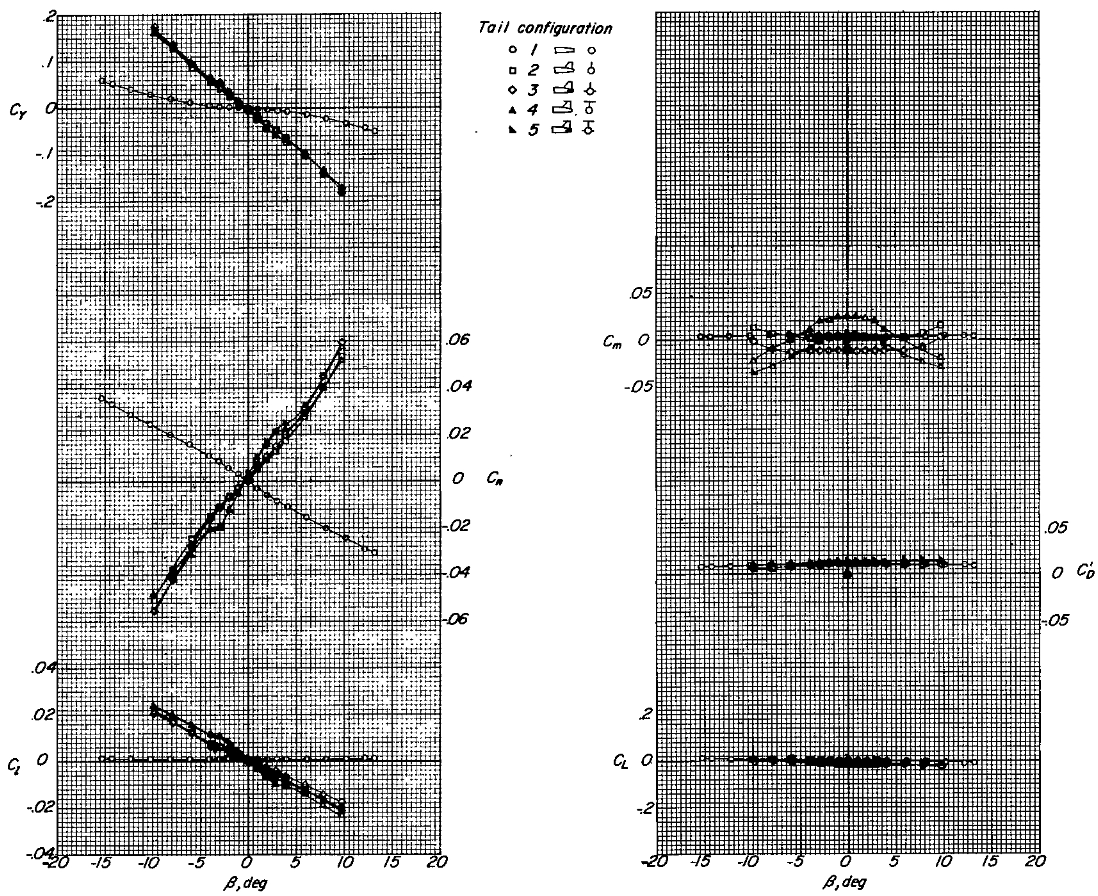

(b) M = 0.80.

Figure 10.- Continued.

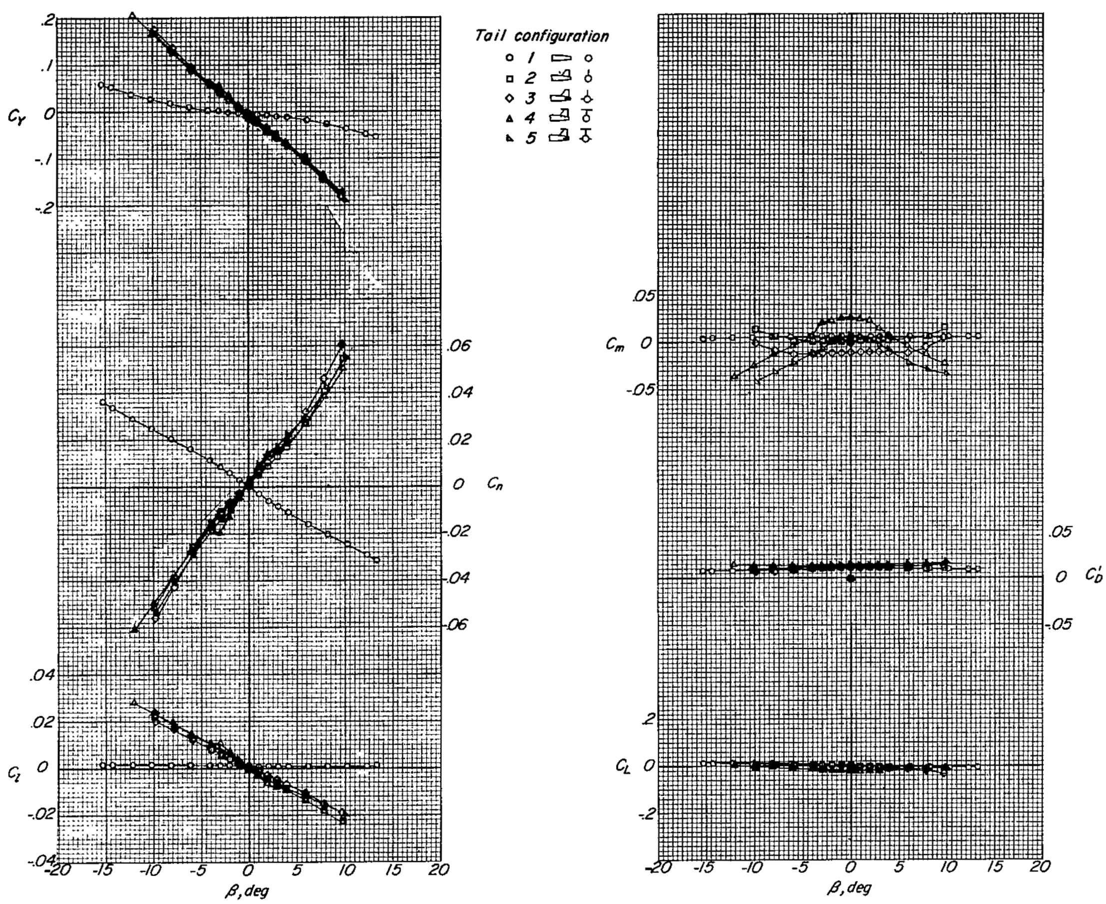

(c) M = 0.85.

Figure 10.- Continued.

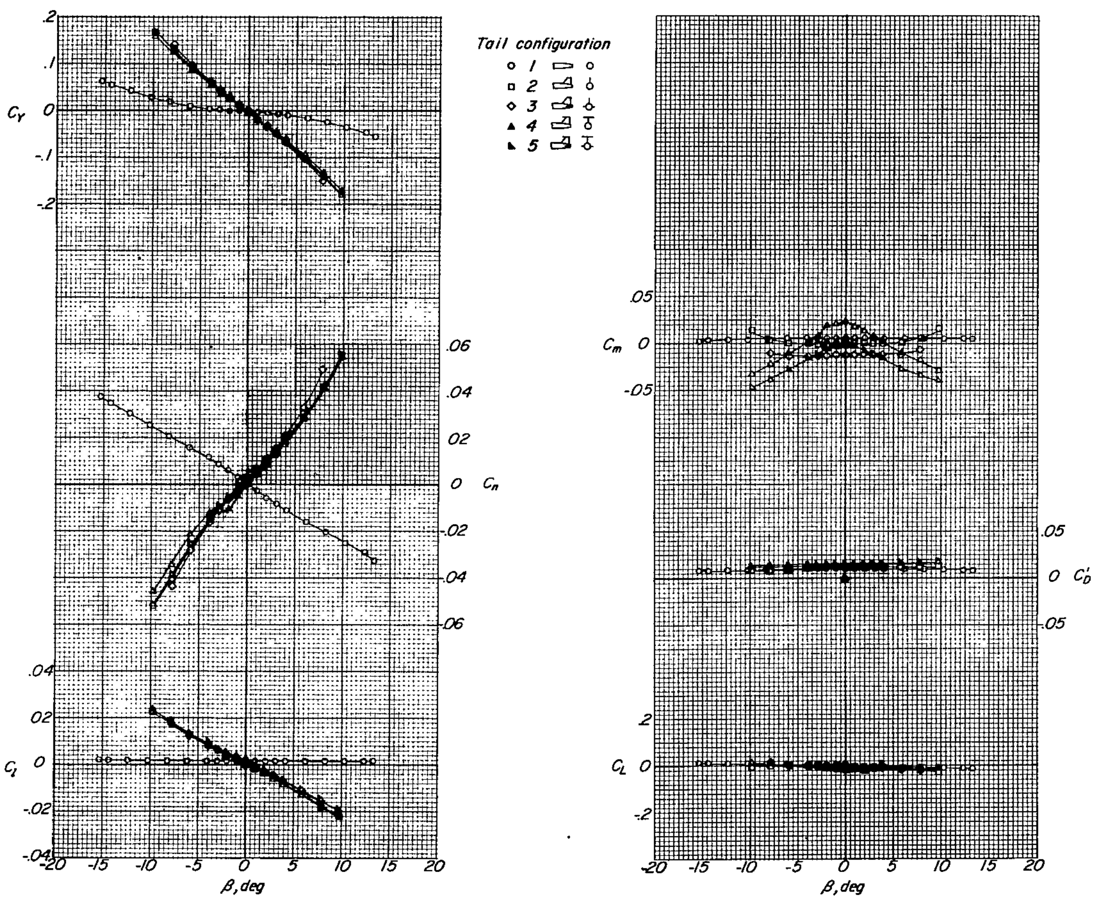

(d) M = 0.90.

Figure 10.- Continued.

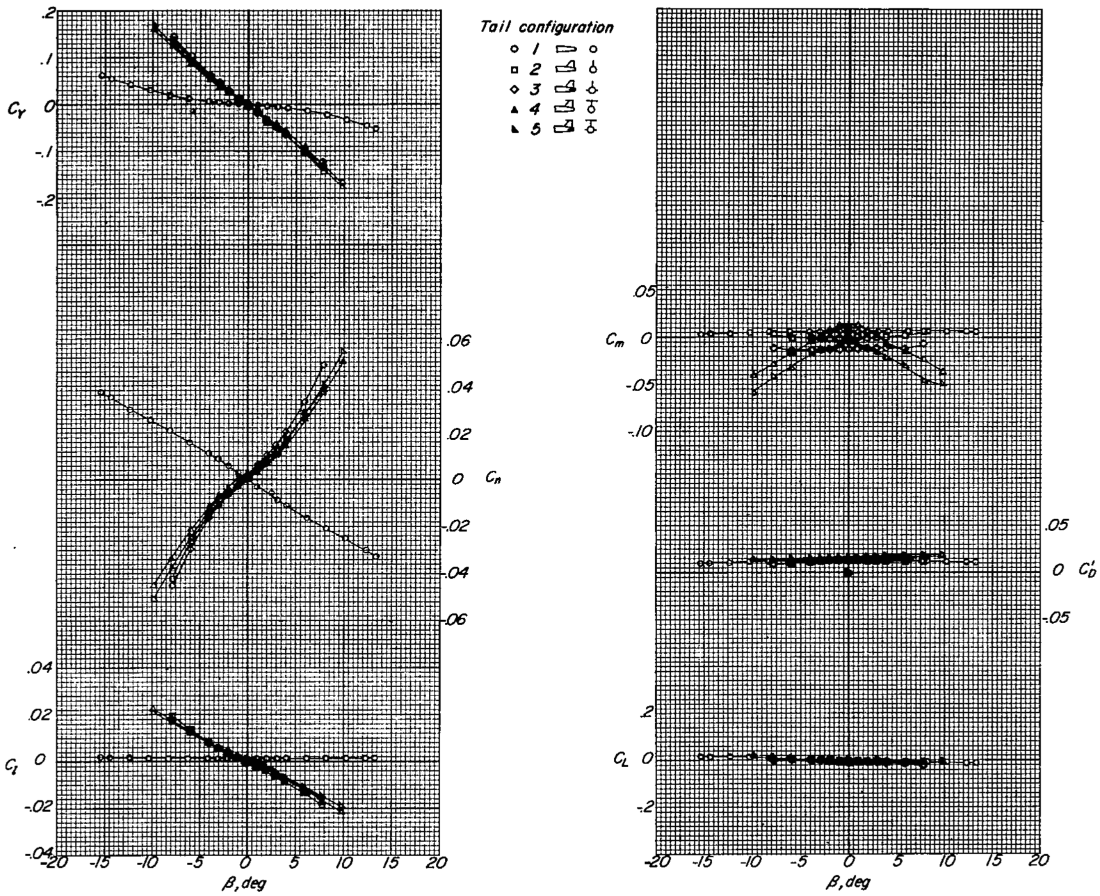

(e) M = 0.92.

Figure 10.- Concluded.

[redacted]

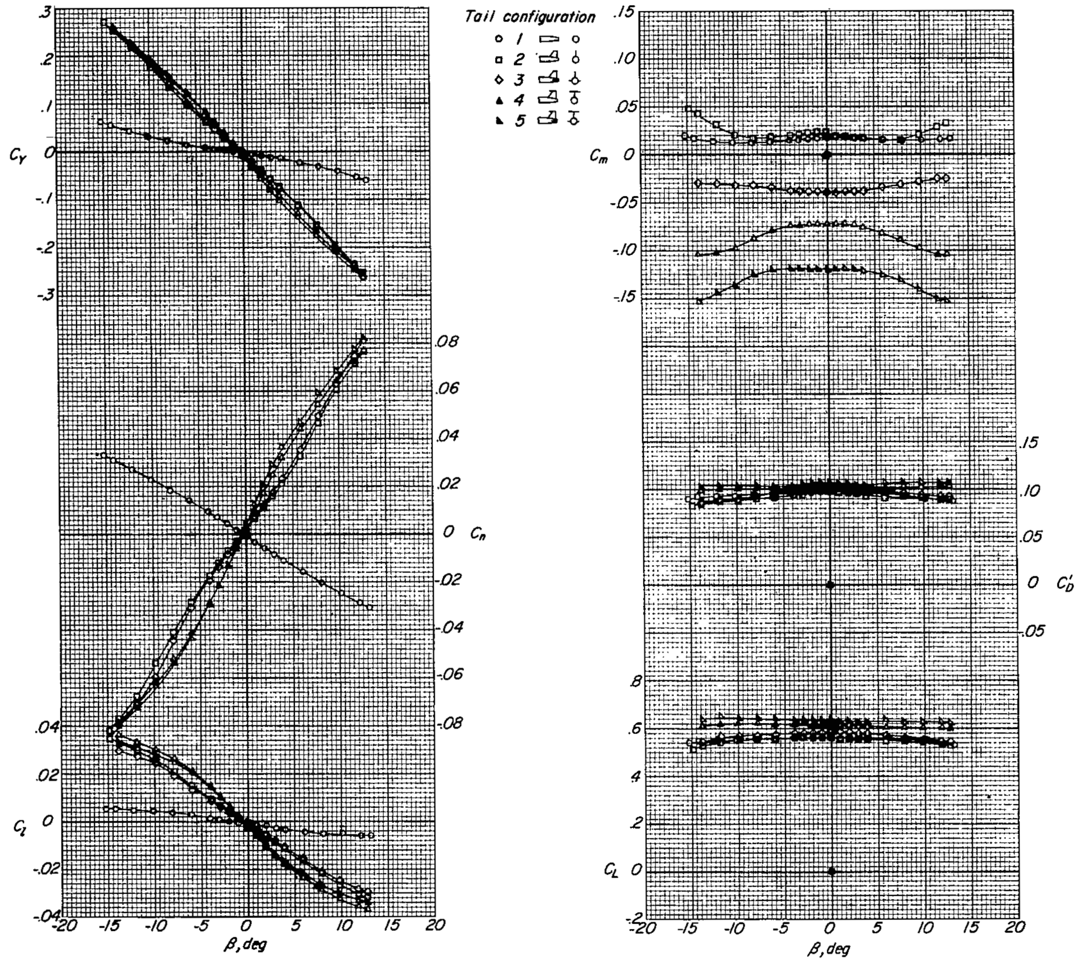

(a) M = 0.60.

Figure 11.- Aerodynamic characteristics of sideslipped model for several tail configurations. Wing aspect ratio, 3.50; $i_t = 0^{\circ}$; $\alpha = 9.5^{\circ}$.

[redacted]

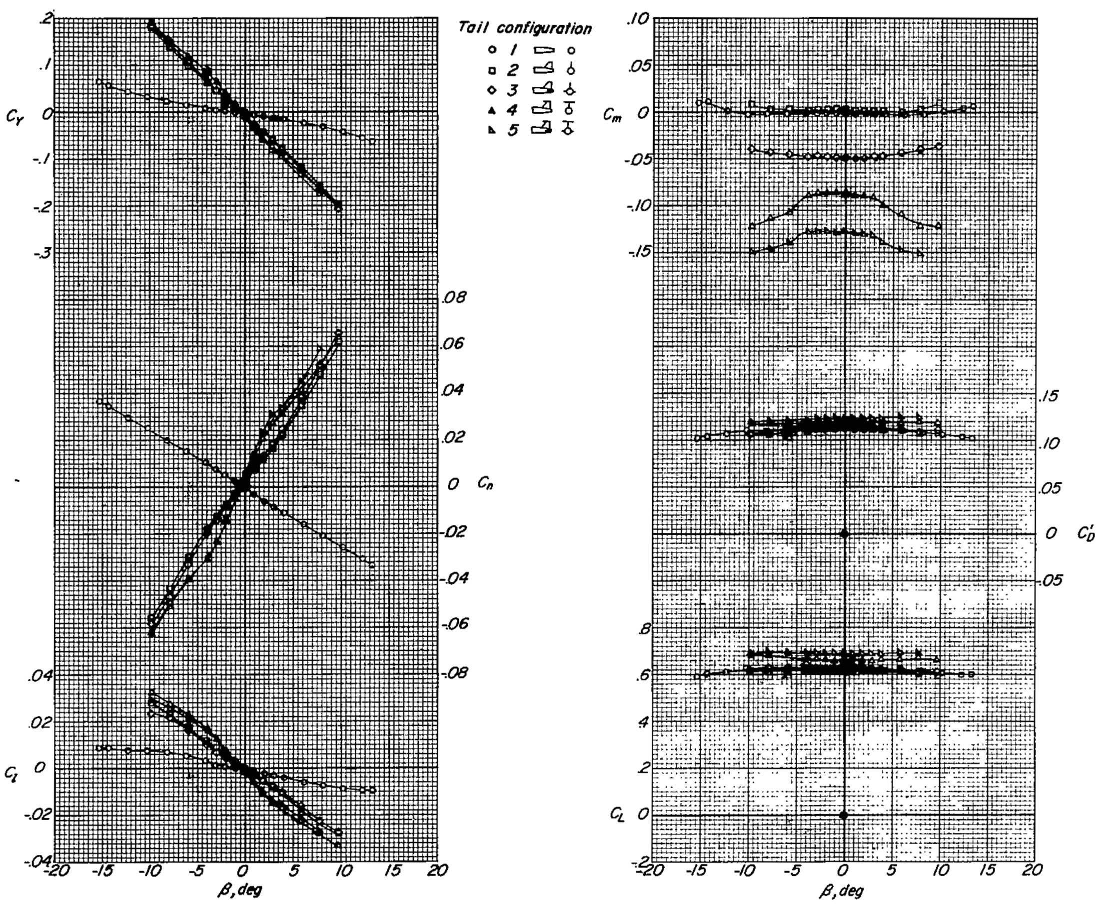

(b) M = 0.80.

Figure 11.- Continued.

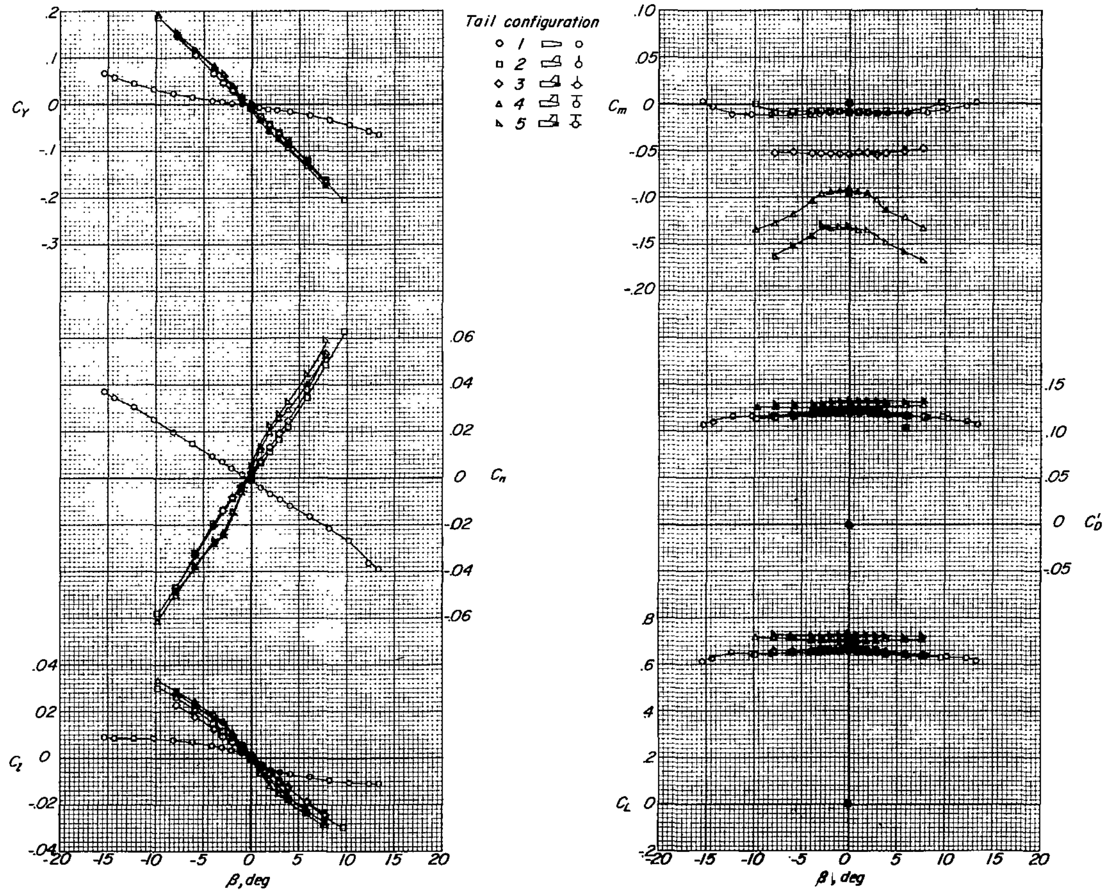

(c) M = 0.85.

Figure 11.- Continued.

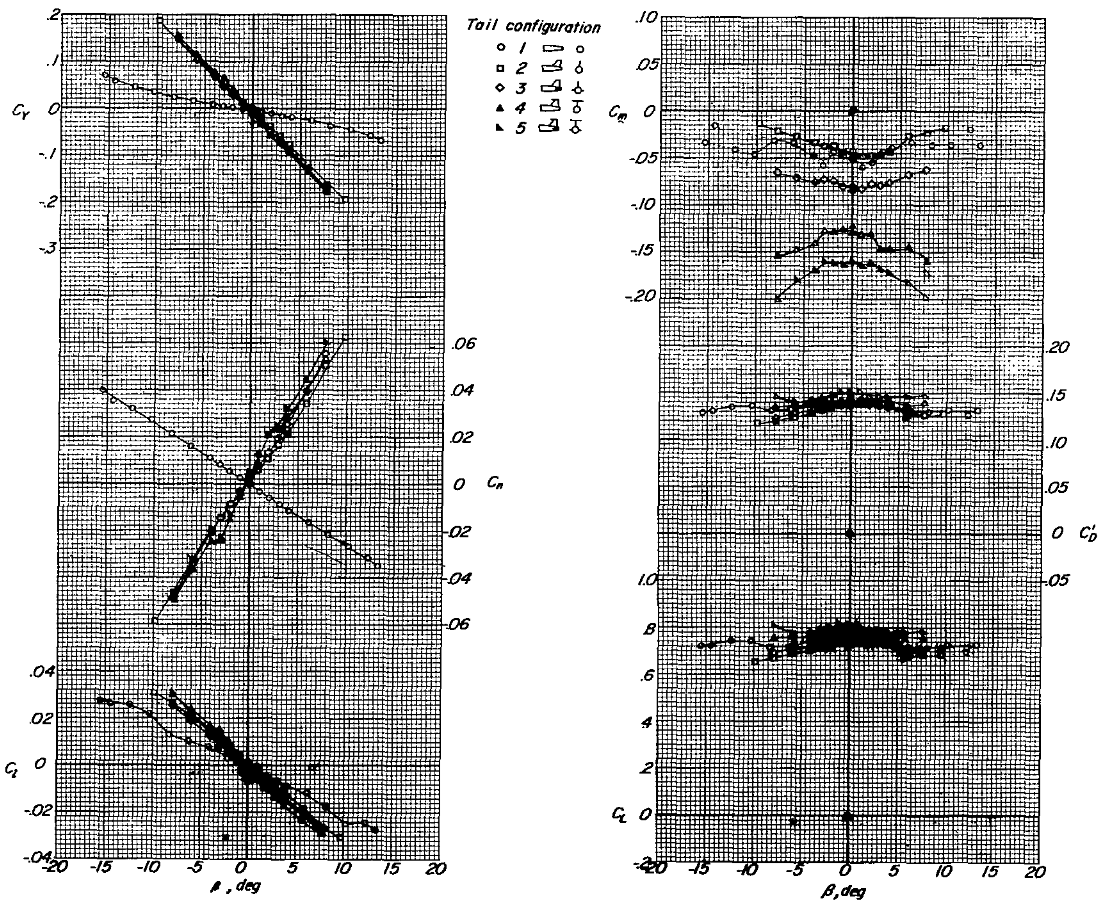

(d) M = 0.90.

Figure 11.- Continued.

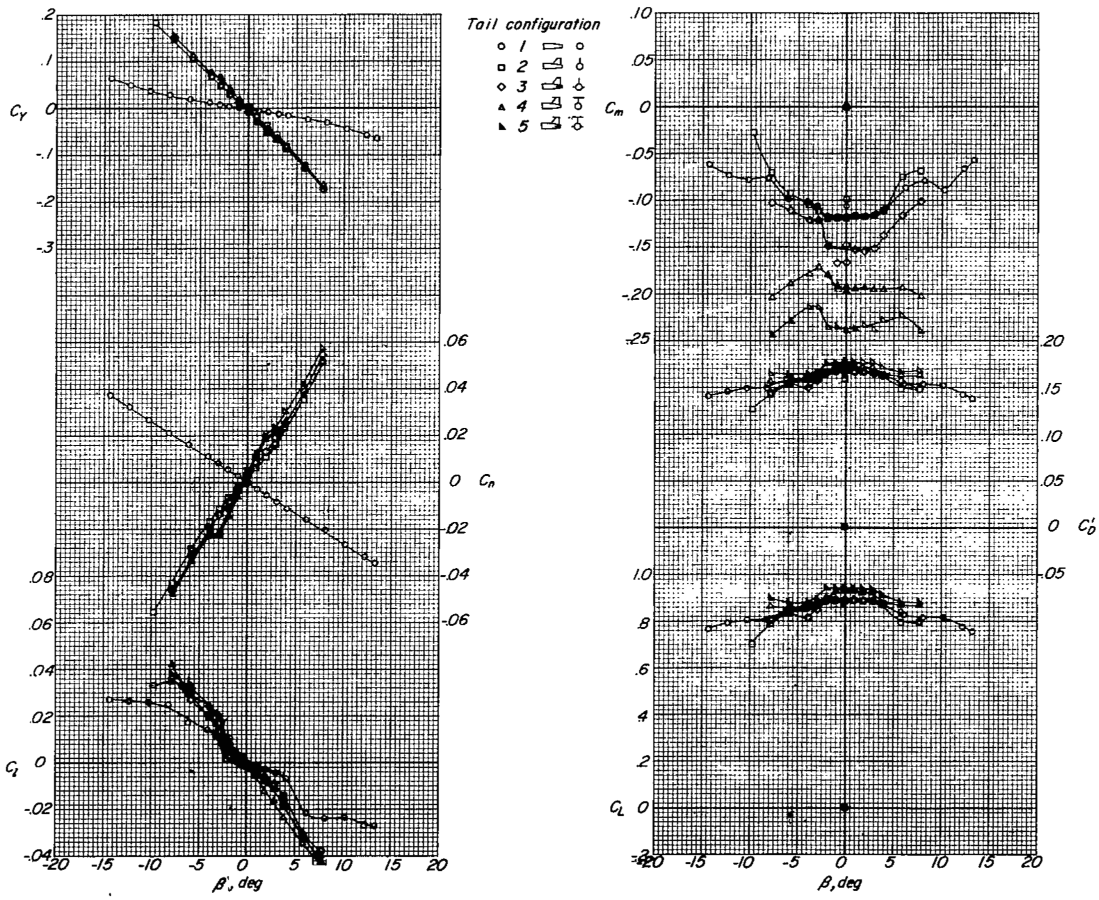

(e) M = 0.92.

Figure 11.- Concluded.

[redacted]

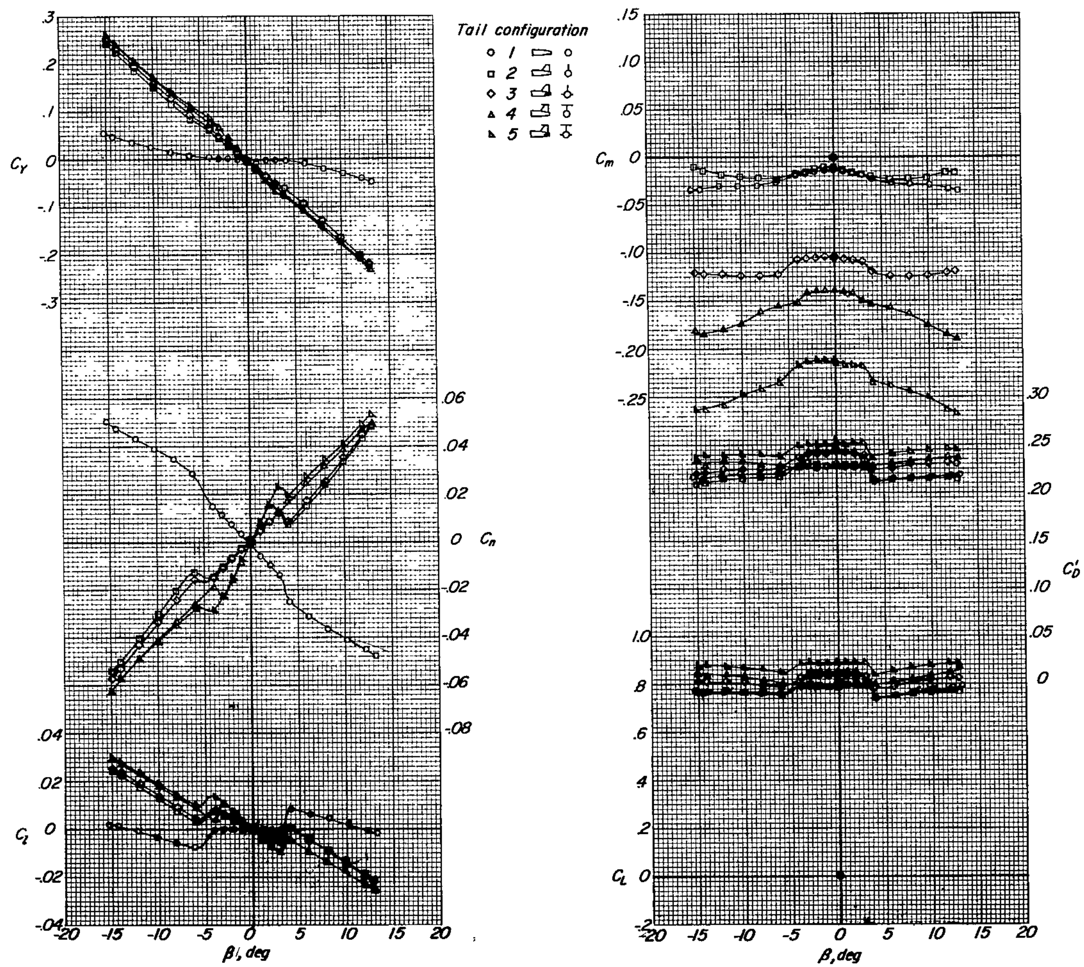

(a) M = 0.60.

Figure 12.- Aerodynamic characteristics of sideslipped model for several tail configurations. Wing aspect ratio, 3.50; $i_t = 0^{\circ}$; $\alpha = 15.6^{\circ}$.

[redacted]

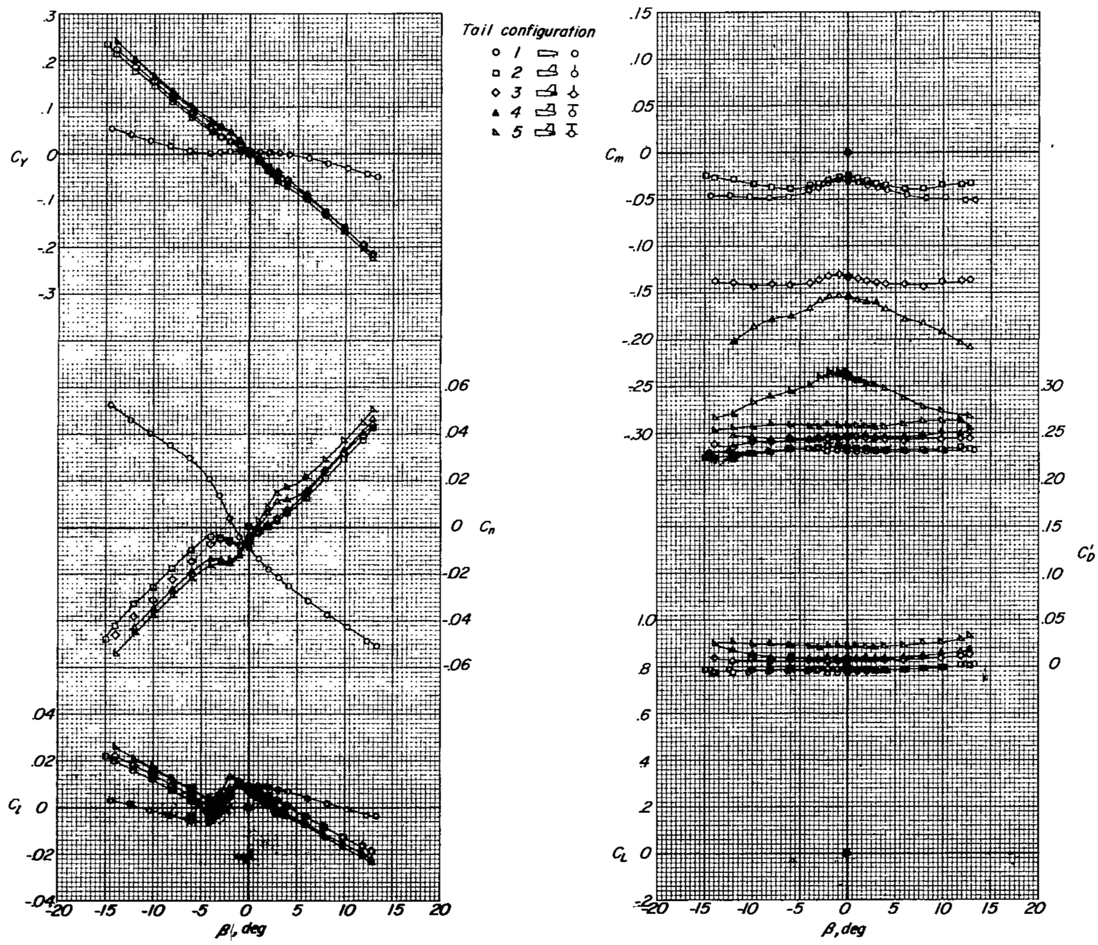

(b) M = 0.80.

Figure 12.- Continued.

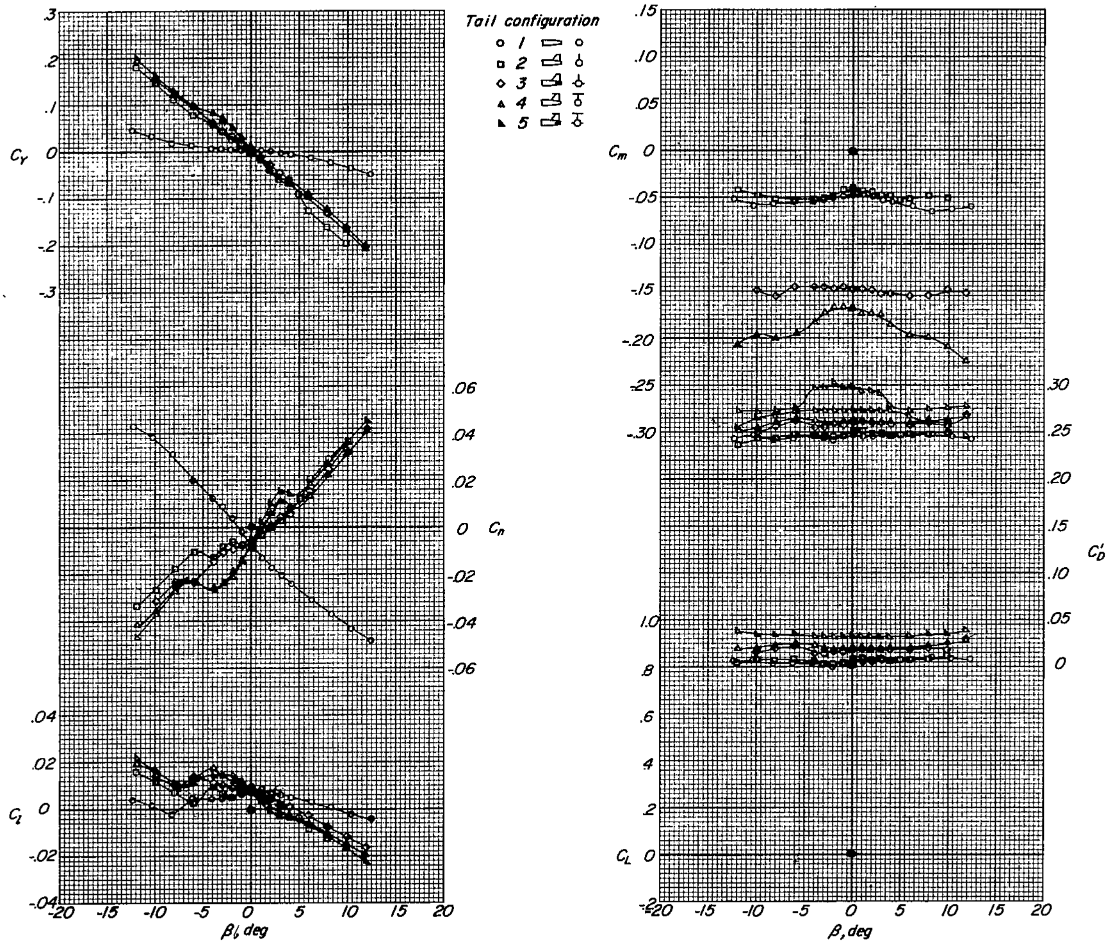

(c) M = 0.85.

Figure 12.- Concluded.

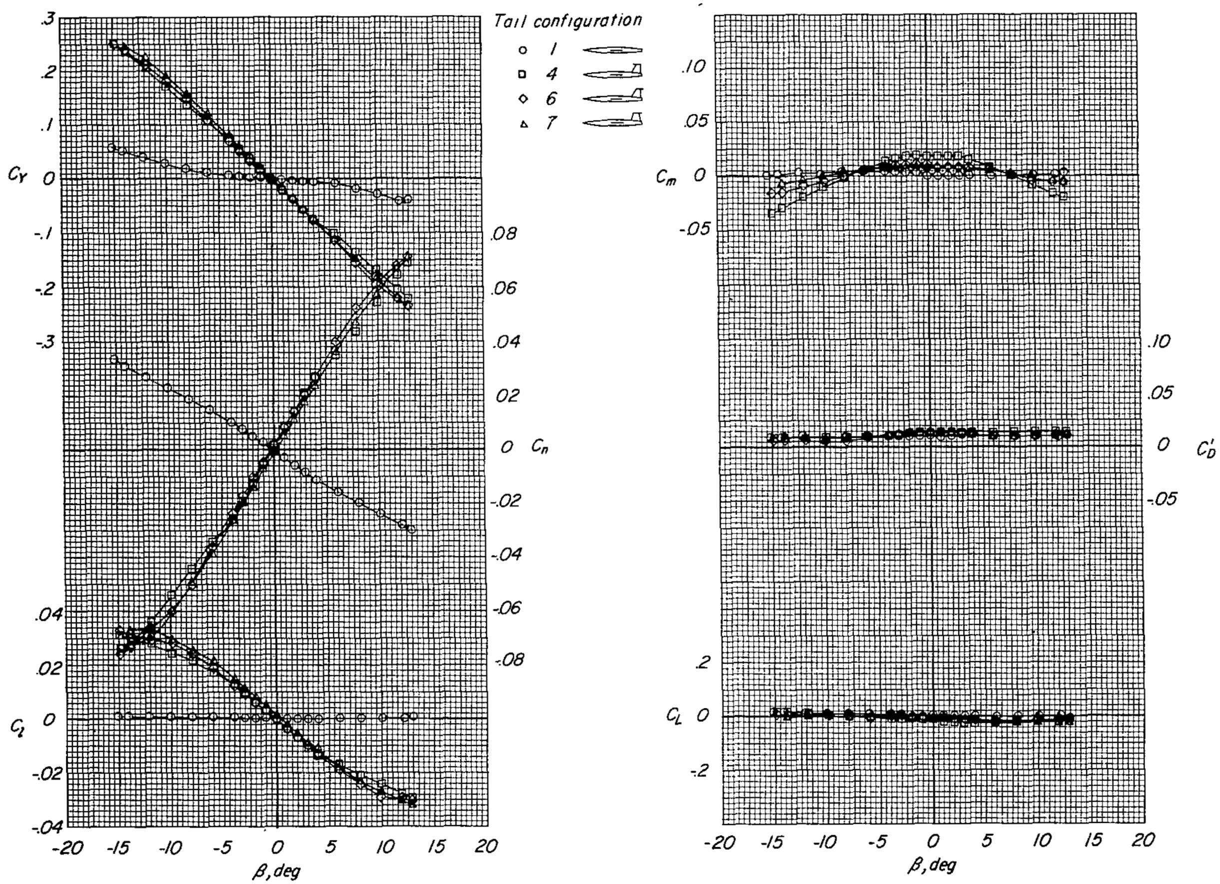

(a) M = 0.60.

Figure 13.- Aerodynamic characteristics of sideslipped model for several variations of the T-tail arrangement. Wing aspect ratio, 3.50; $i_t = 0^{\circ}$; $\alpha = 0^{\circ}$.

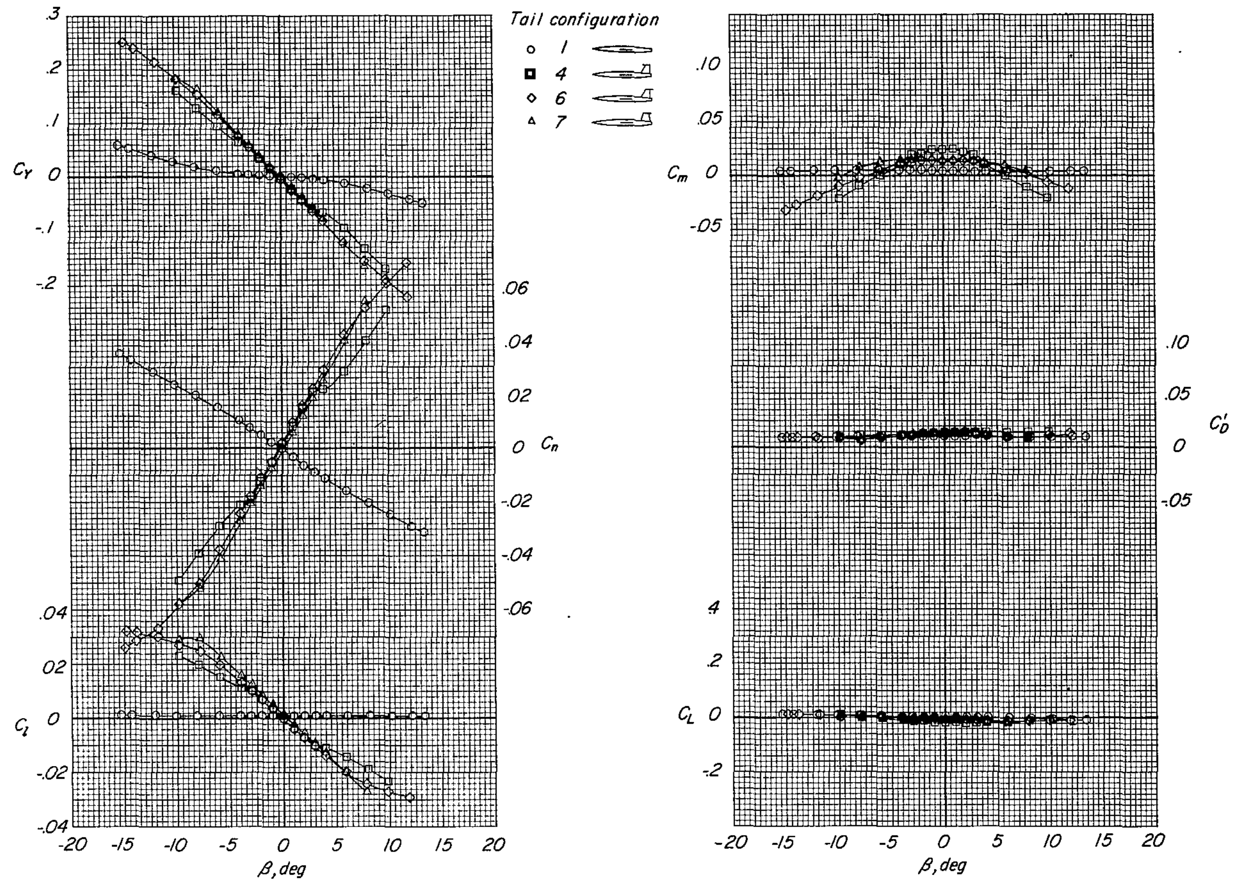

(b) M = 0.80.

Figure 13.- Continued.

~~CONFIDENTIAL~~

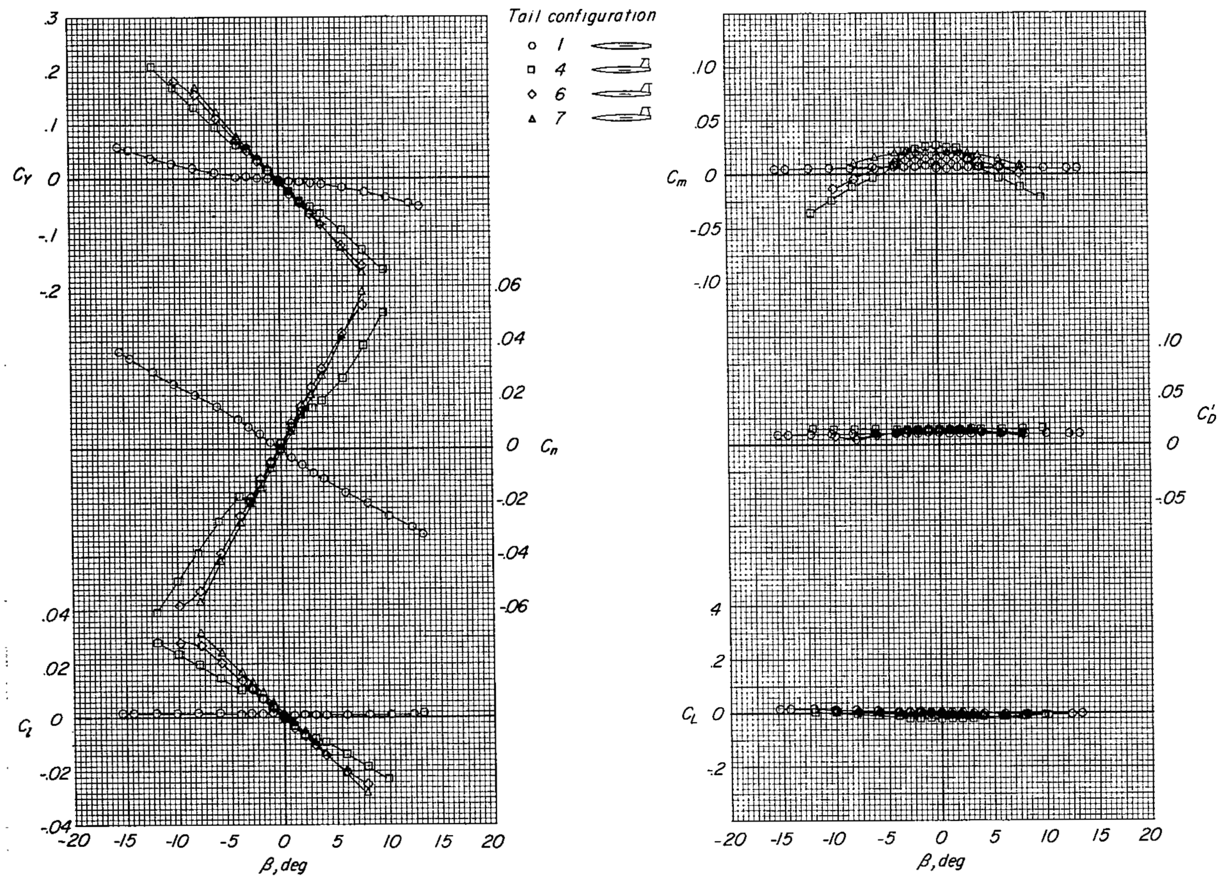

(c) M = 0.85.

Figure 13.- Continued.

~~CONFIDENTIAL~~

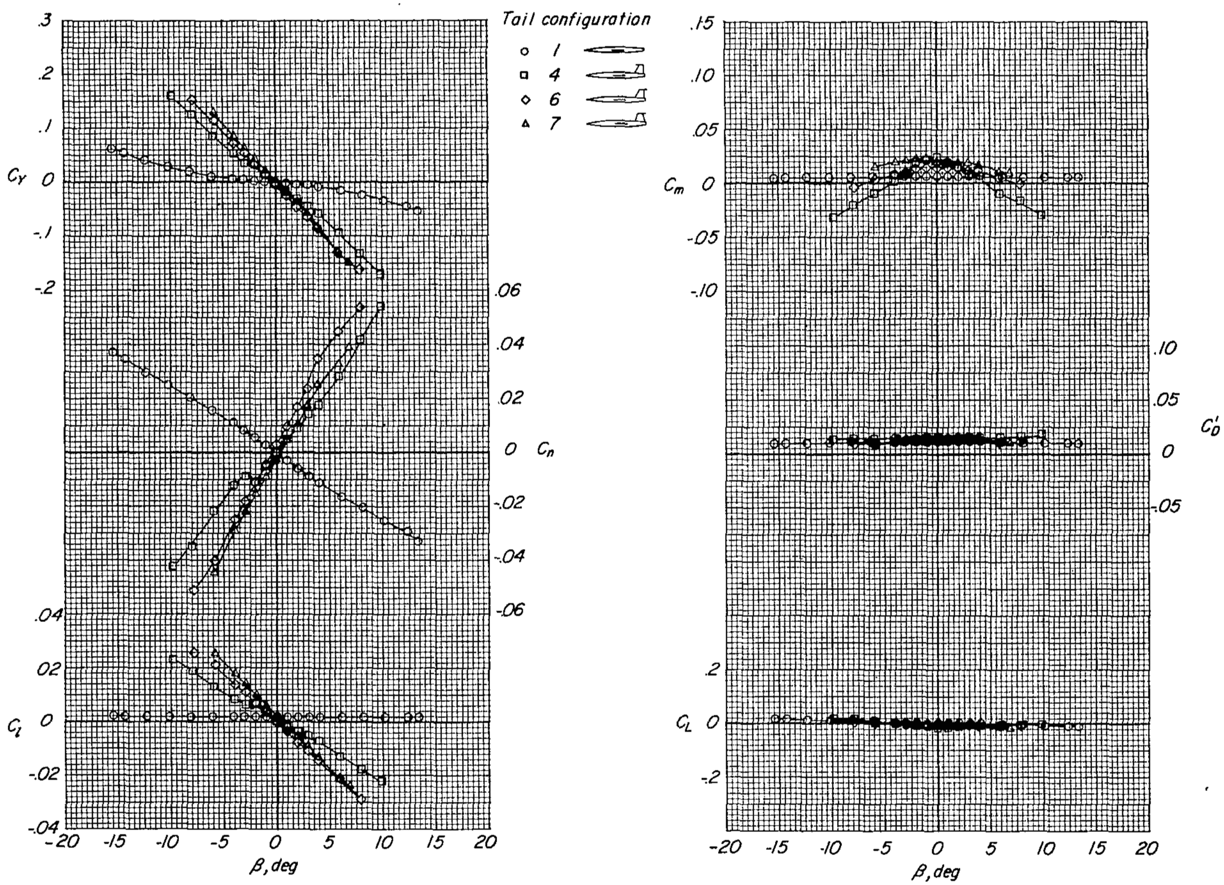

(d) M = 0.90.

Figure 13.- Continued.

[redacted]

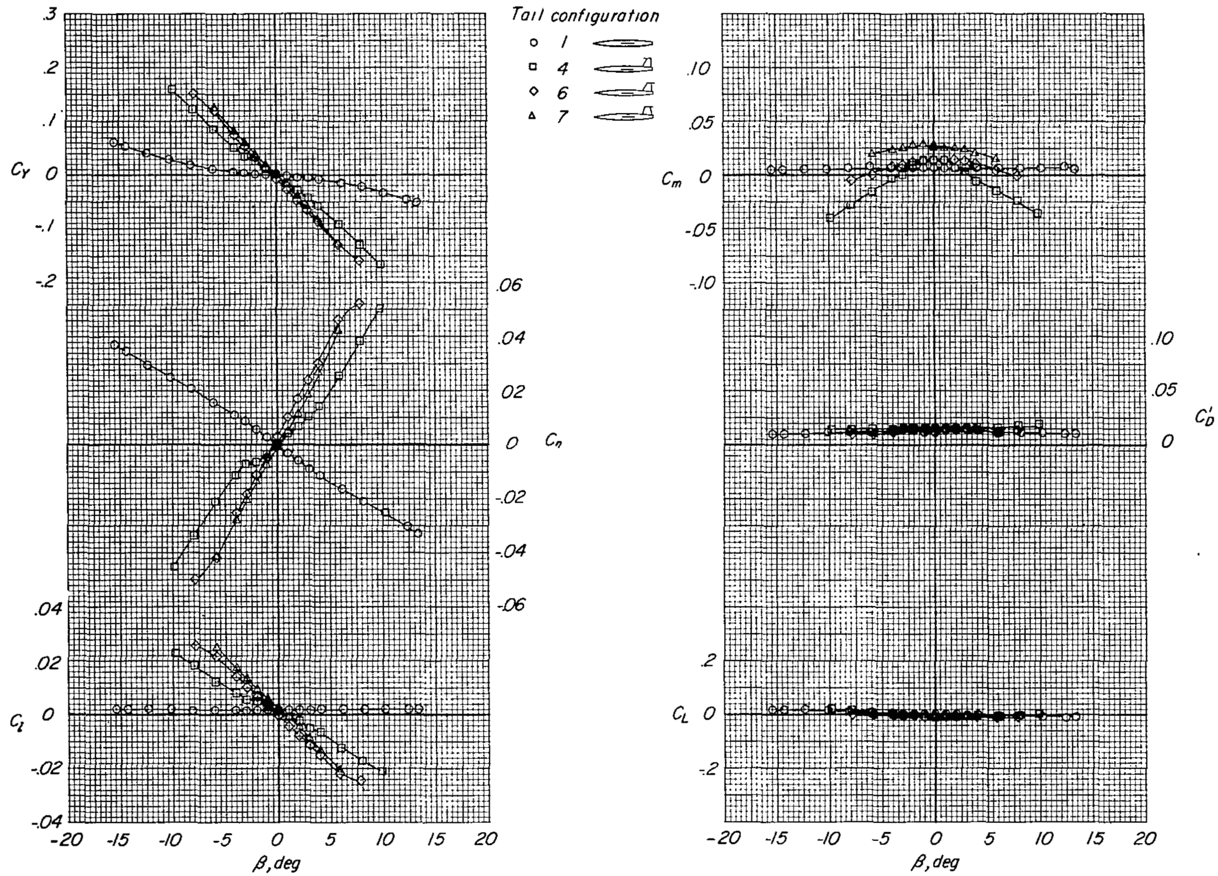

(e) M = 0.92.

Figure 13.- Concluded.

[redacted]

[redacted]

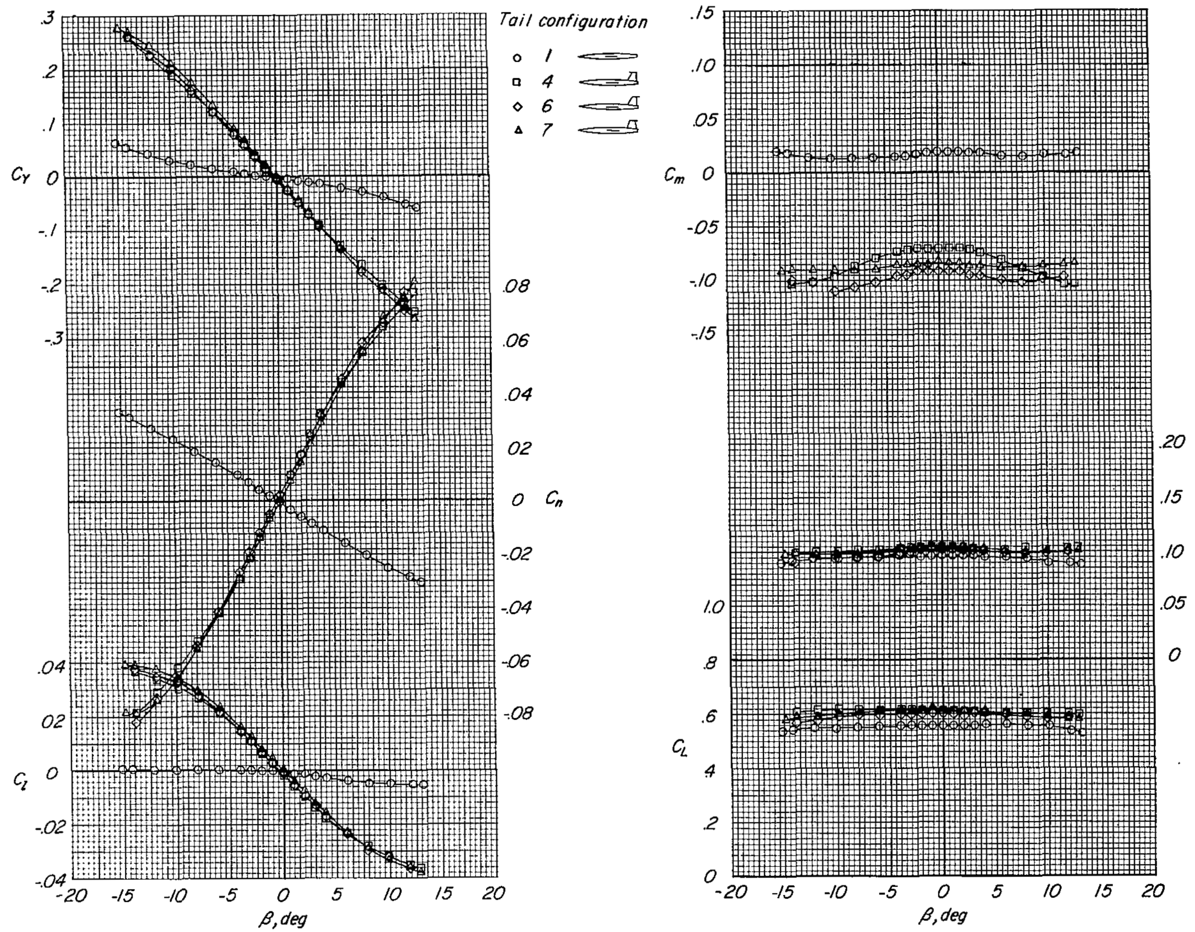

(a) M = 0.60.

Figure 14.- Aerodynamic characteristics of sideslipped model for several variations of the T-tail arrangement. Wing aspect ratio, 3.50; $i_t = 0^{\circ}$; $\alpha = 9.5^{\circ}$.

~~CONFIDENTIAL~~

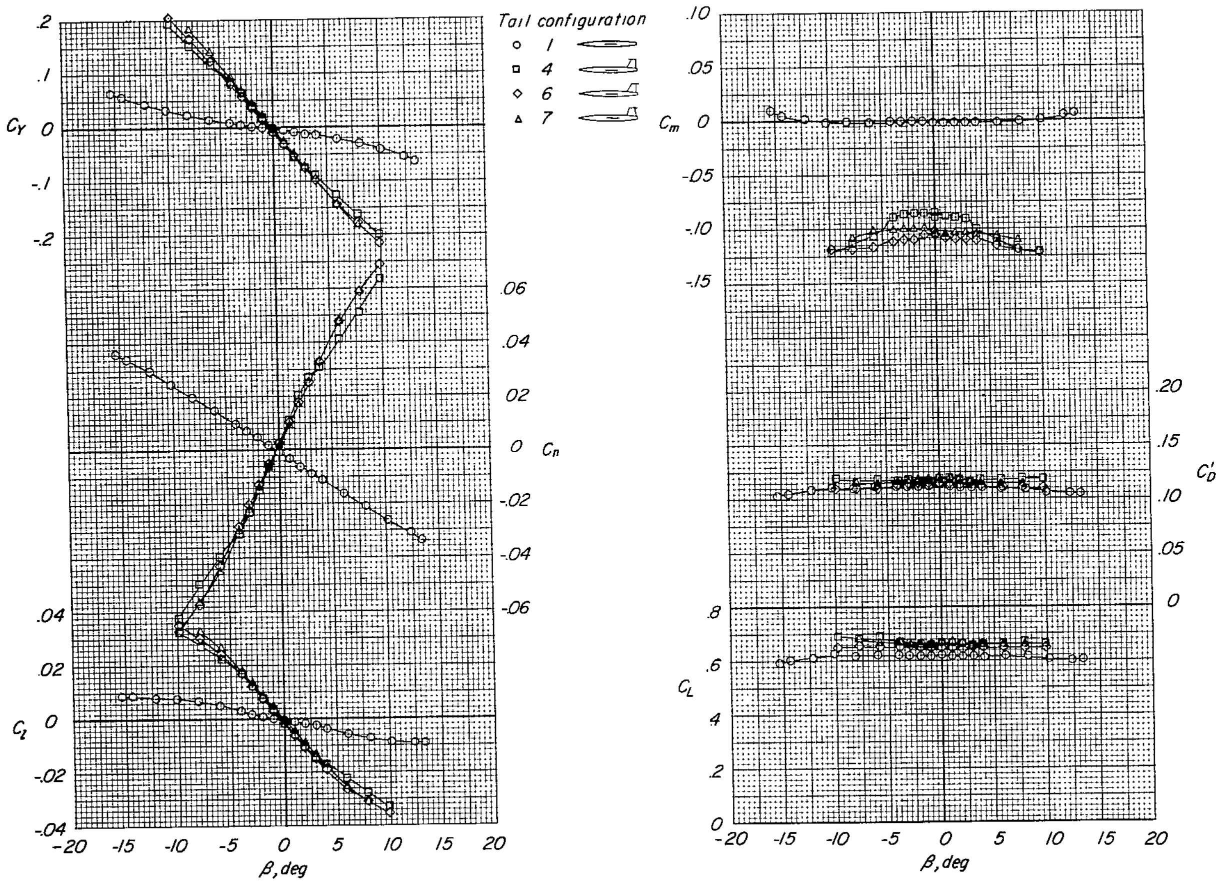

(b) M = 0.80.

Figure 14.- Continued.

~~CONFIDENTIAL~~

[redacted]

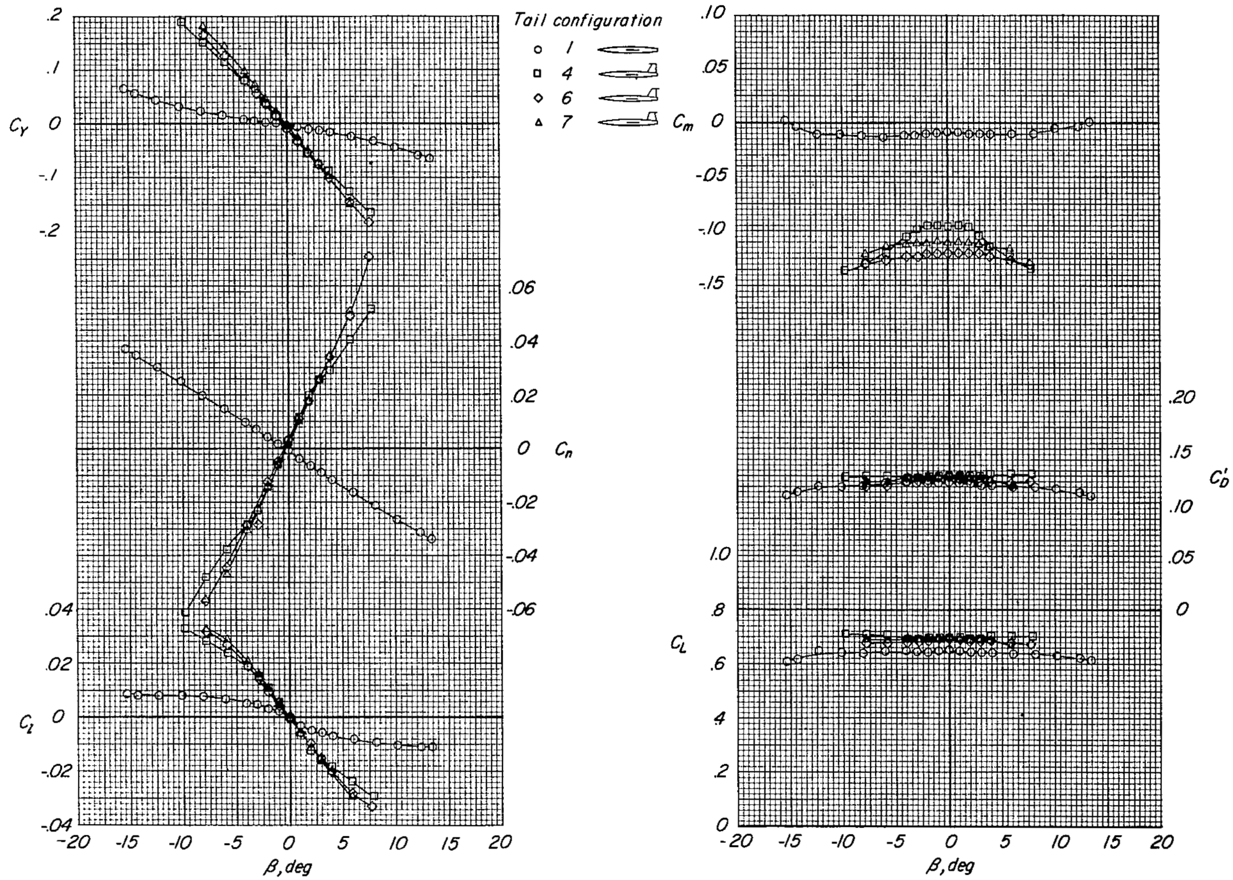

(c) M = 0.85.

Figure 14.- Continued.

[redacted]

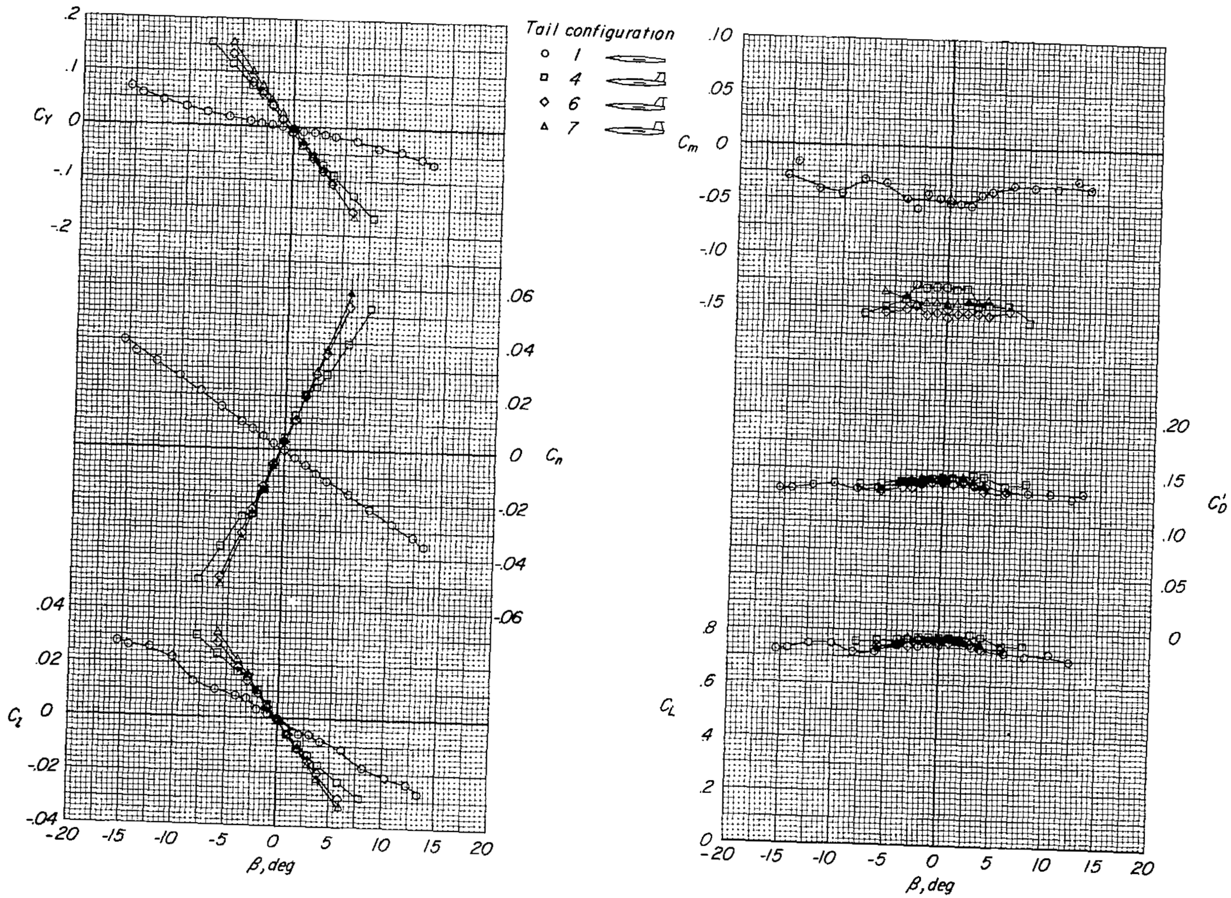

(d) M = 0.90.

Figure 14.- Continued.

[redacted]

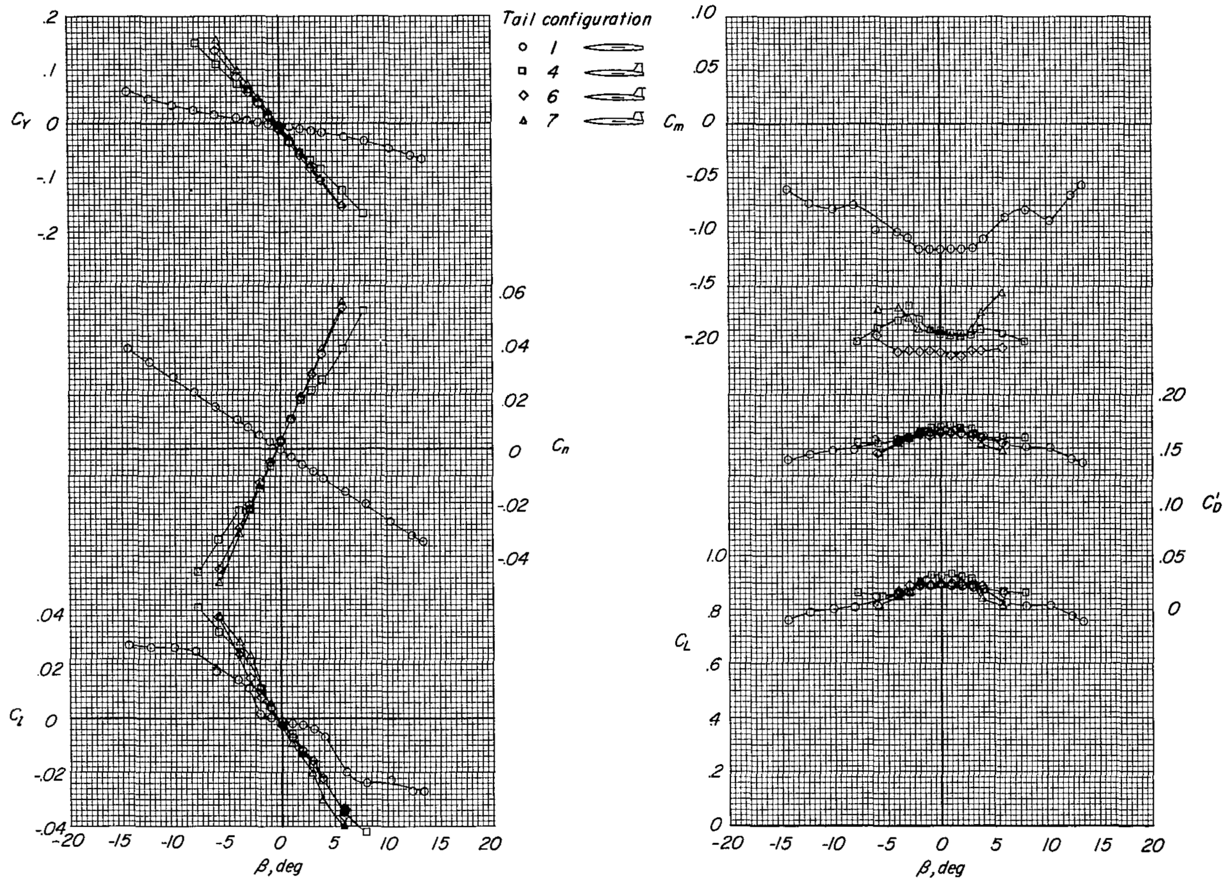

(e) M = 0.92.

Figure 14.- Concluded.

[redacted]

[redacted]

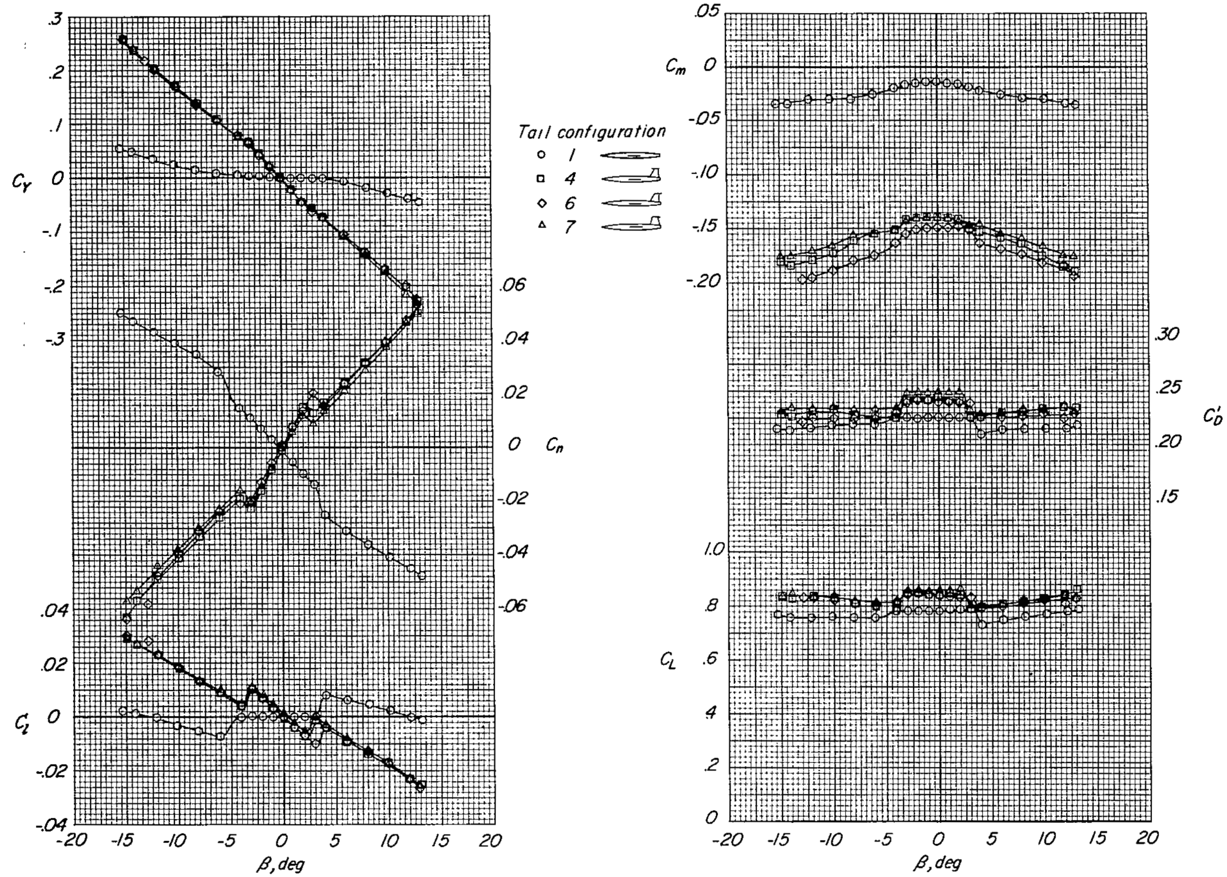

(a) M = 0.60.

Figure 15.- Aerodynamic characteristics of sideslipped model for several variations of the T-tail arrangement. Wing aspect ratio, 3.50; $i_t = 0^{\circ}$; $\alpha = 15.6^{\circ}$.

[redacted]

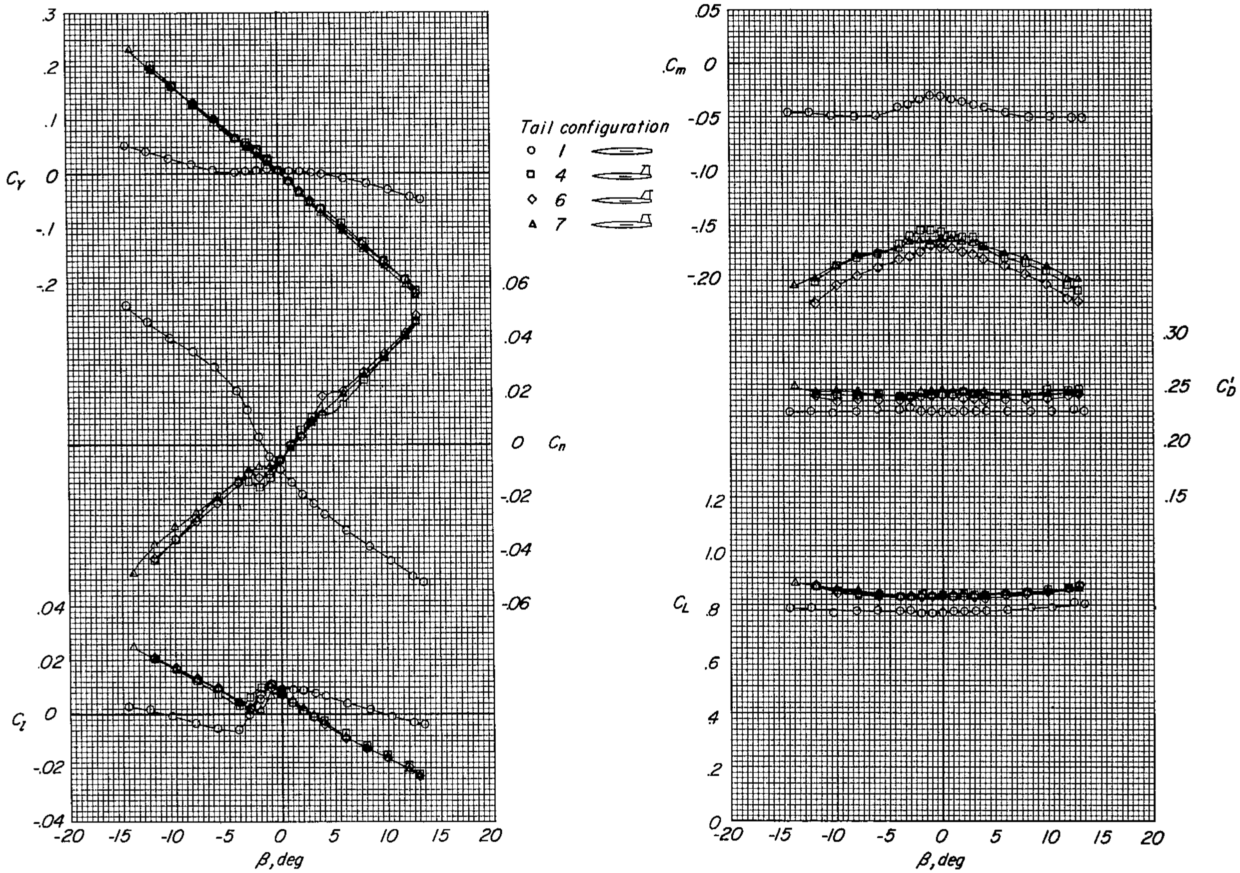

(b) M = 0.80.

Figure 15.- Continued.

[redacted]

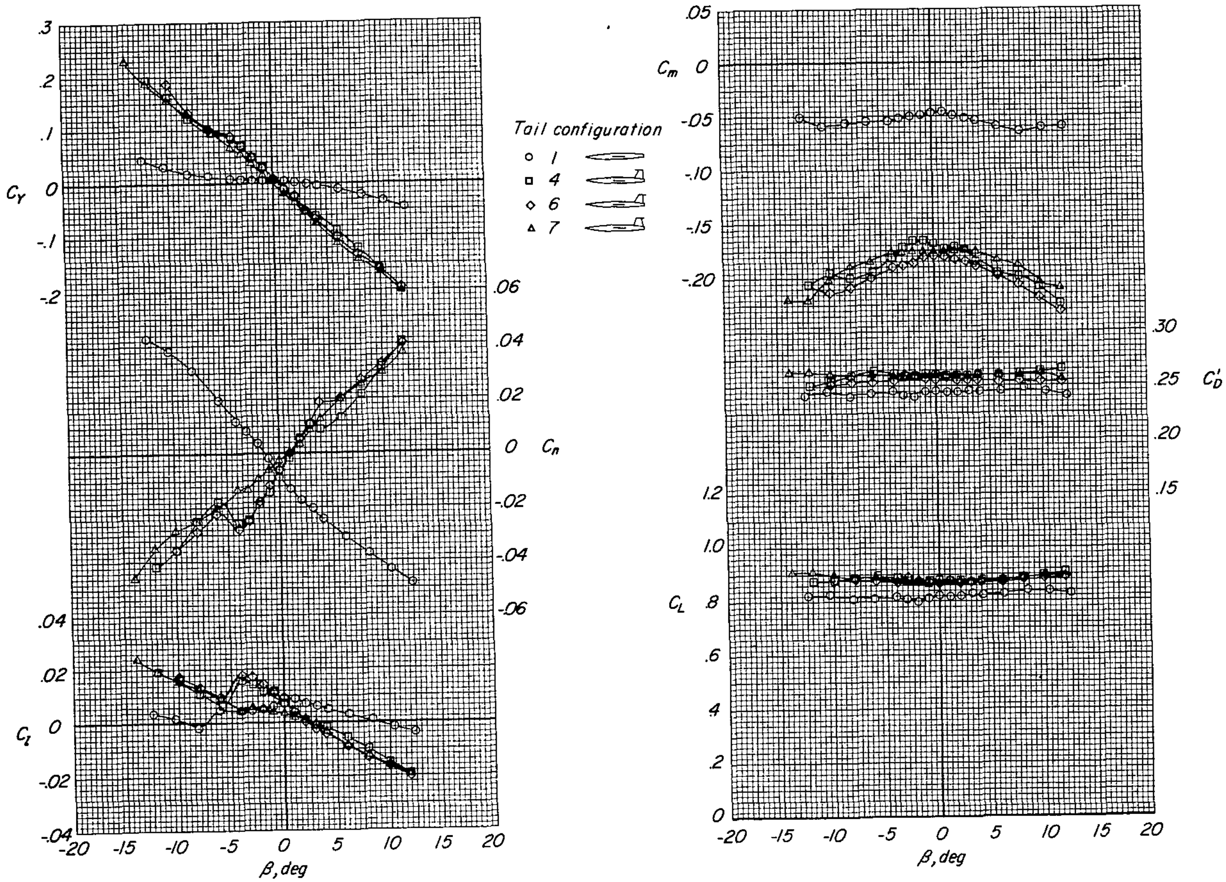

(c) M = 0.85.

Figure 15.- Concluded.

[redacted]

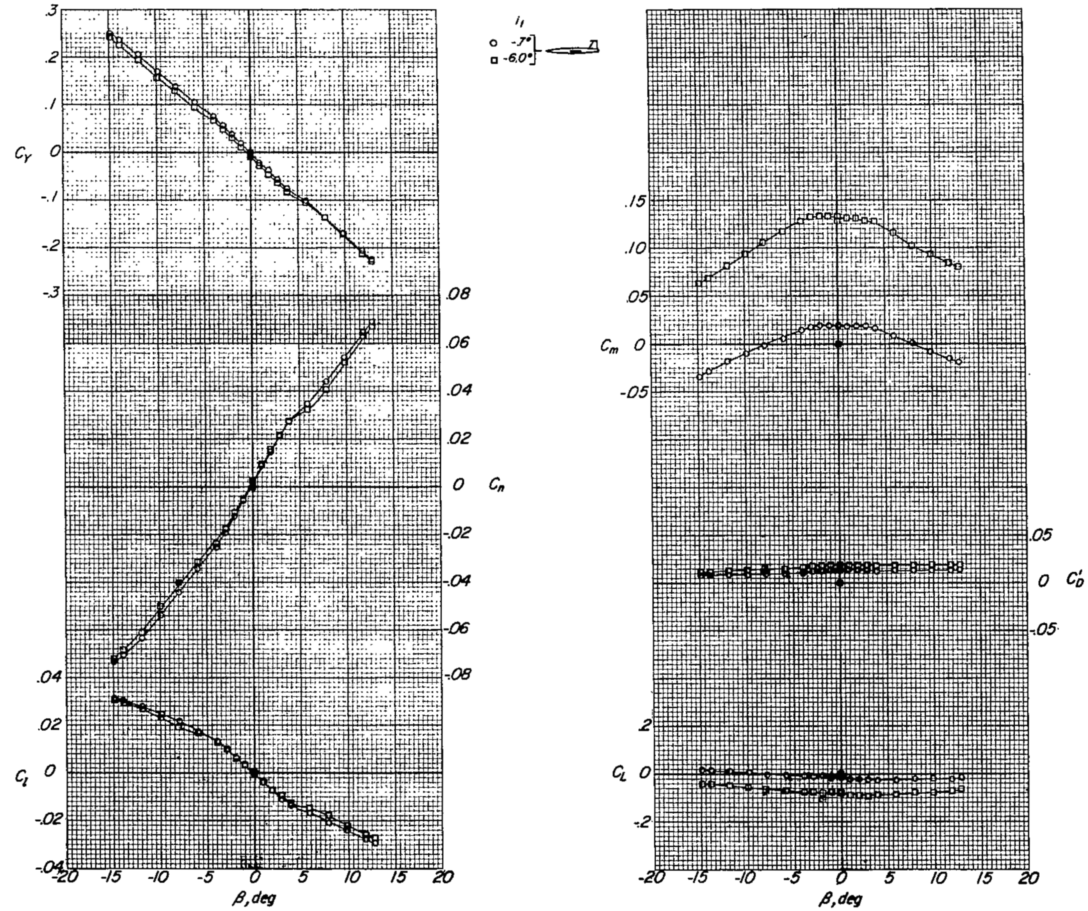

(a) M = 0.60.

Figure 16.- Effects of stabilizer deflection on aerodynamic characteristics of sideslipped model with the T-tail configuration having leading-edge overhang. Tail configuration 4; wing aspect ratio, 3.50; $\alpha = 0^{\circ}$.

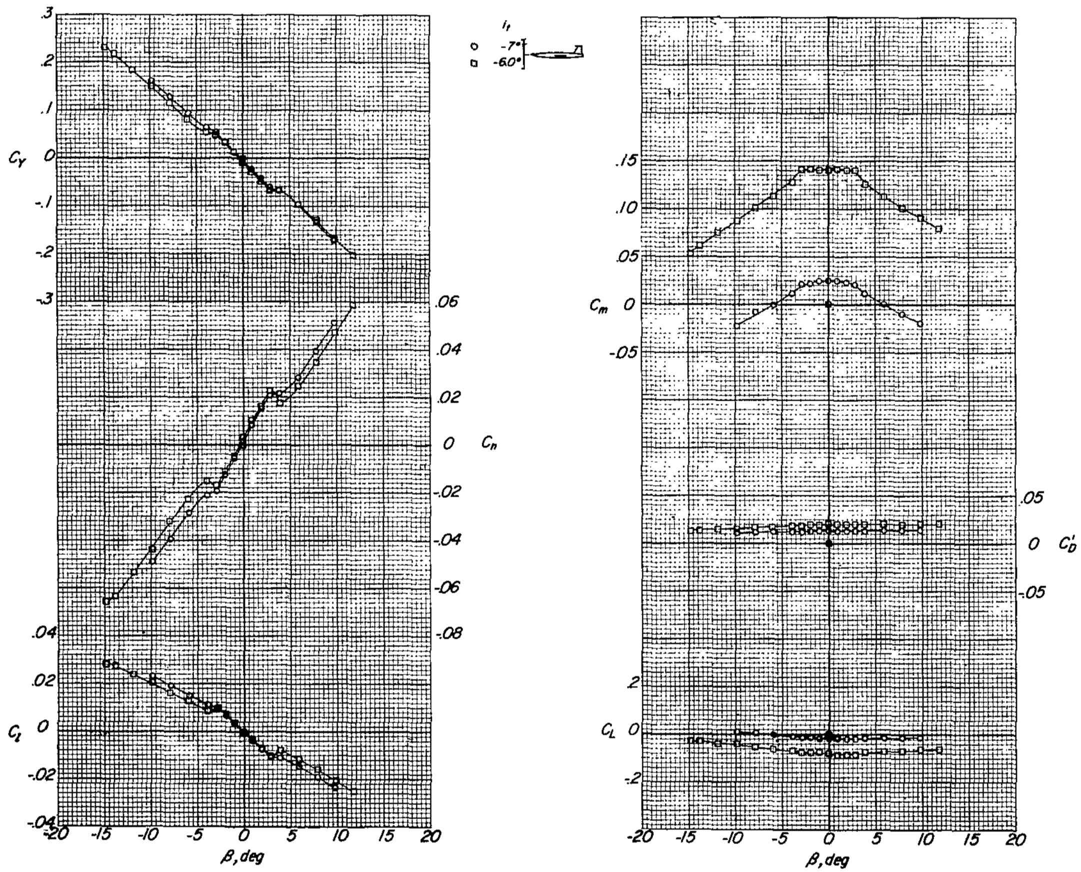

(b) M = 0.80.

Figure 16.- Continued.

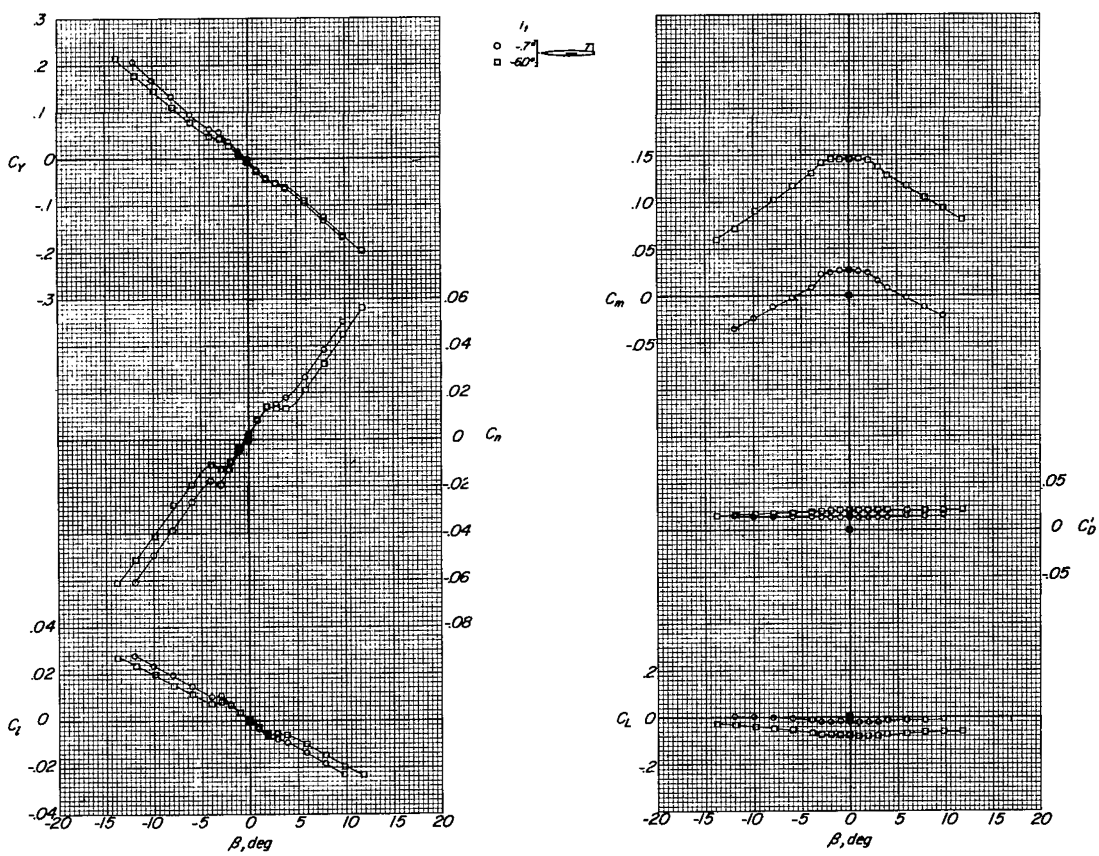

(c) M = 0.85.

Figure 16.- Continued.

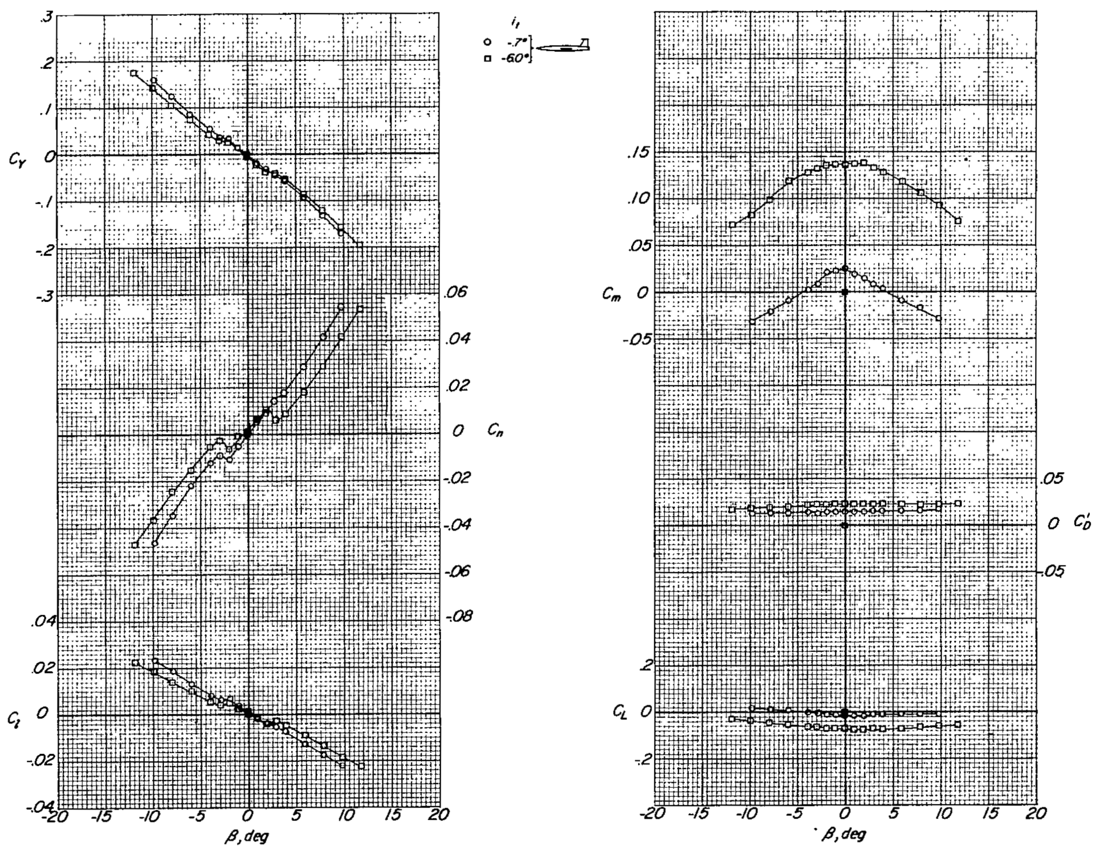

(d) M = 0.90.

Figure 16.- Continued.

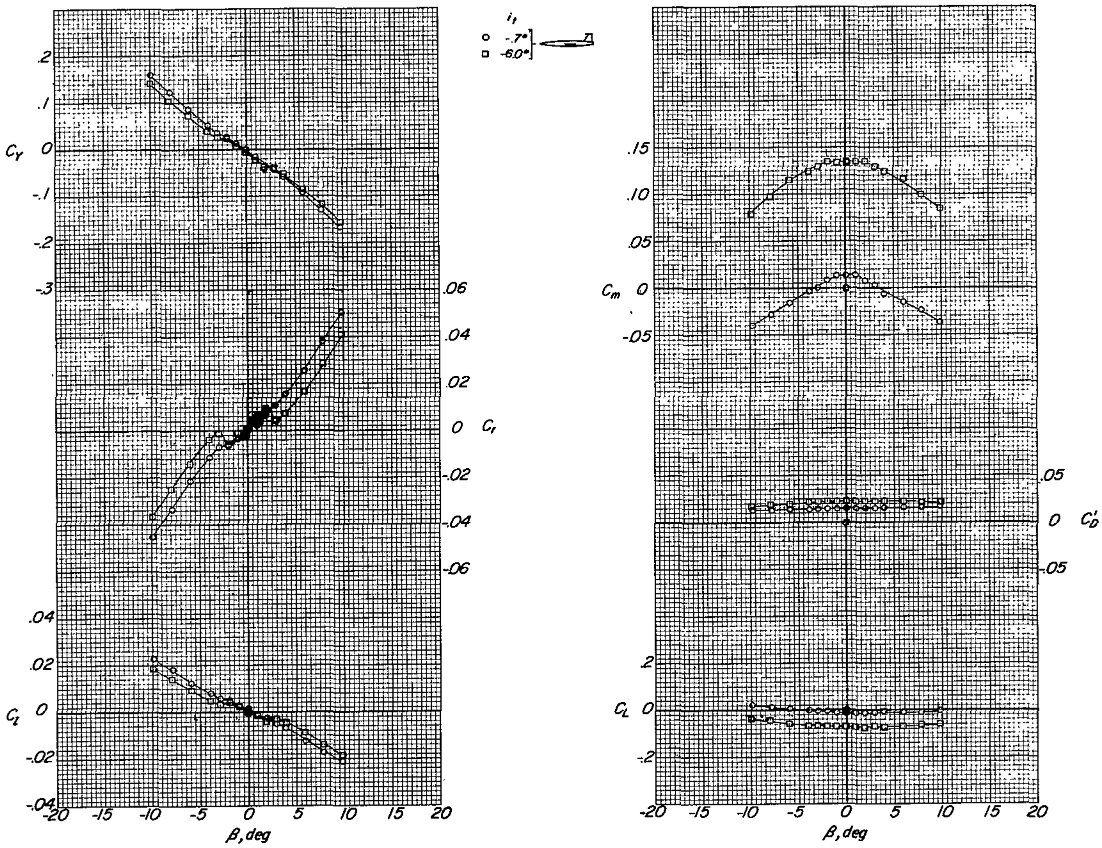

(e) M = 0.92.

Figure 16.- Concluded.

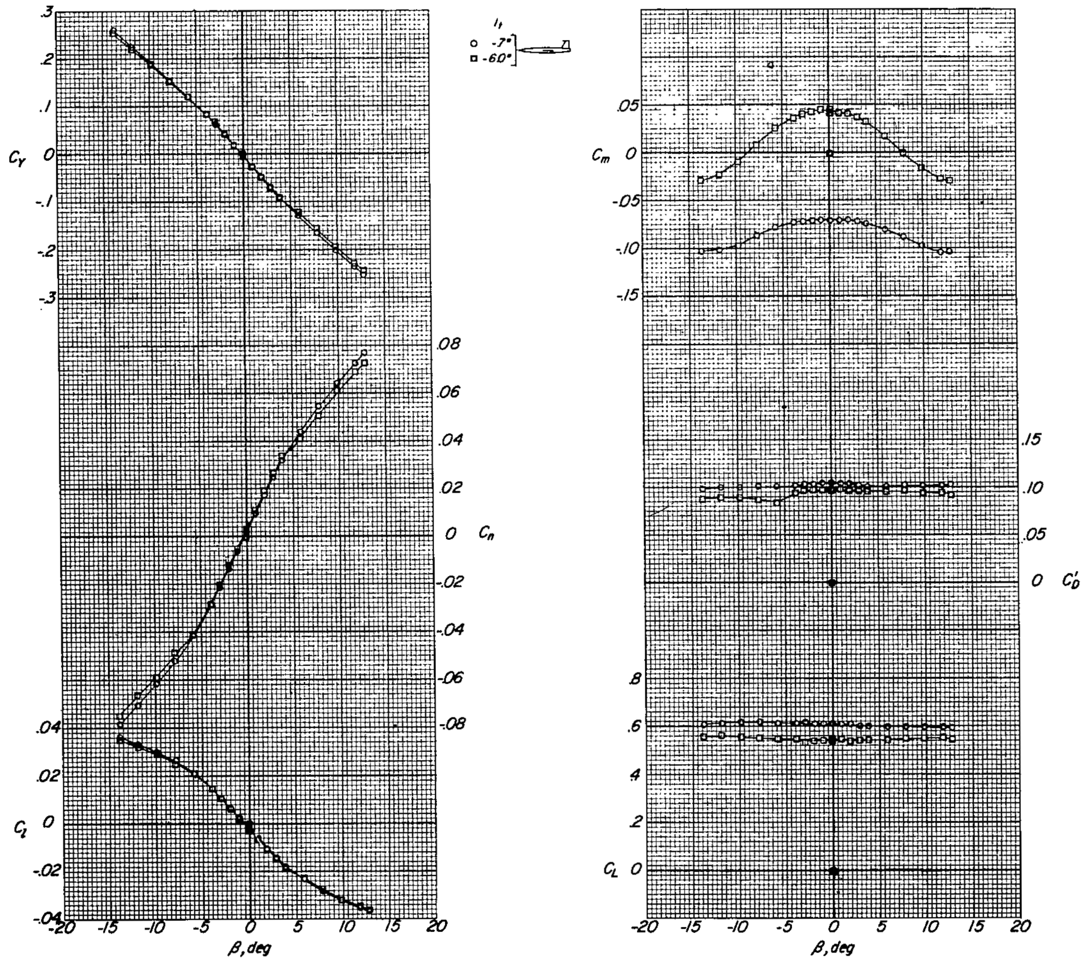

(a) M = 0.60.

Figure 17.- Effect of stabilizer deflection on aerodynamic characteristics of sideslipped model with the T-tail configuration having leading-edge overhang. Tail configuration 4; wing aspect ratio, 3.50; $\alpha = 9.5^{\circ}$.

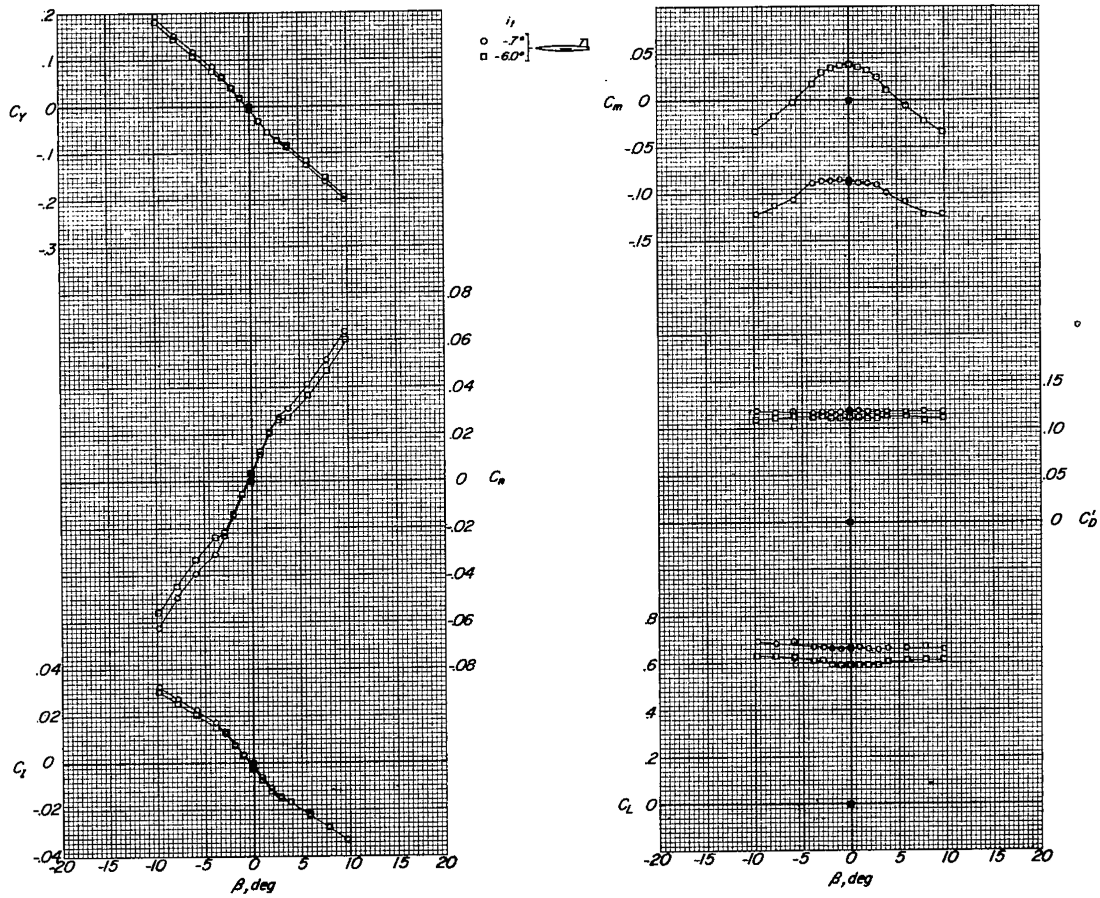

(b) M = 0.80.

Figure 17.- Continued.

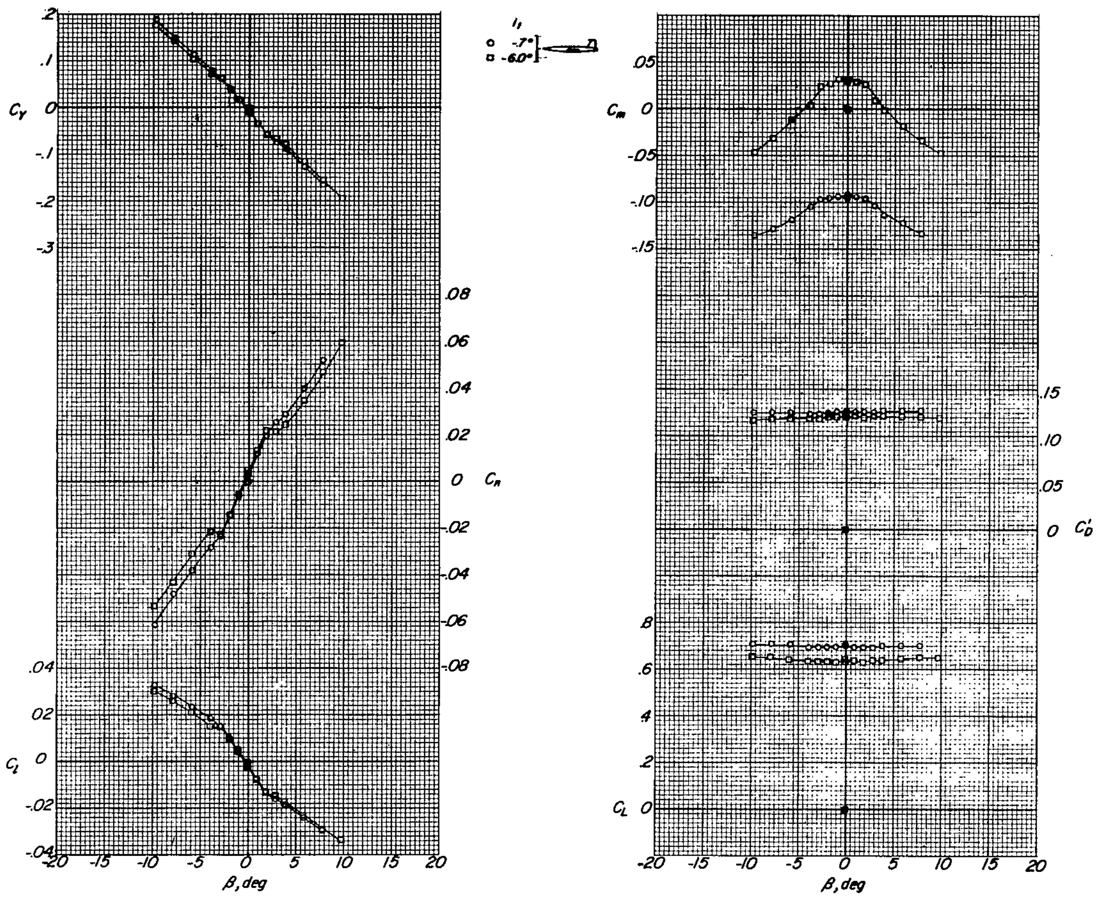

(c) M = 0.85.

Figure 17.- Continued.

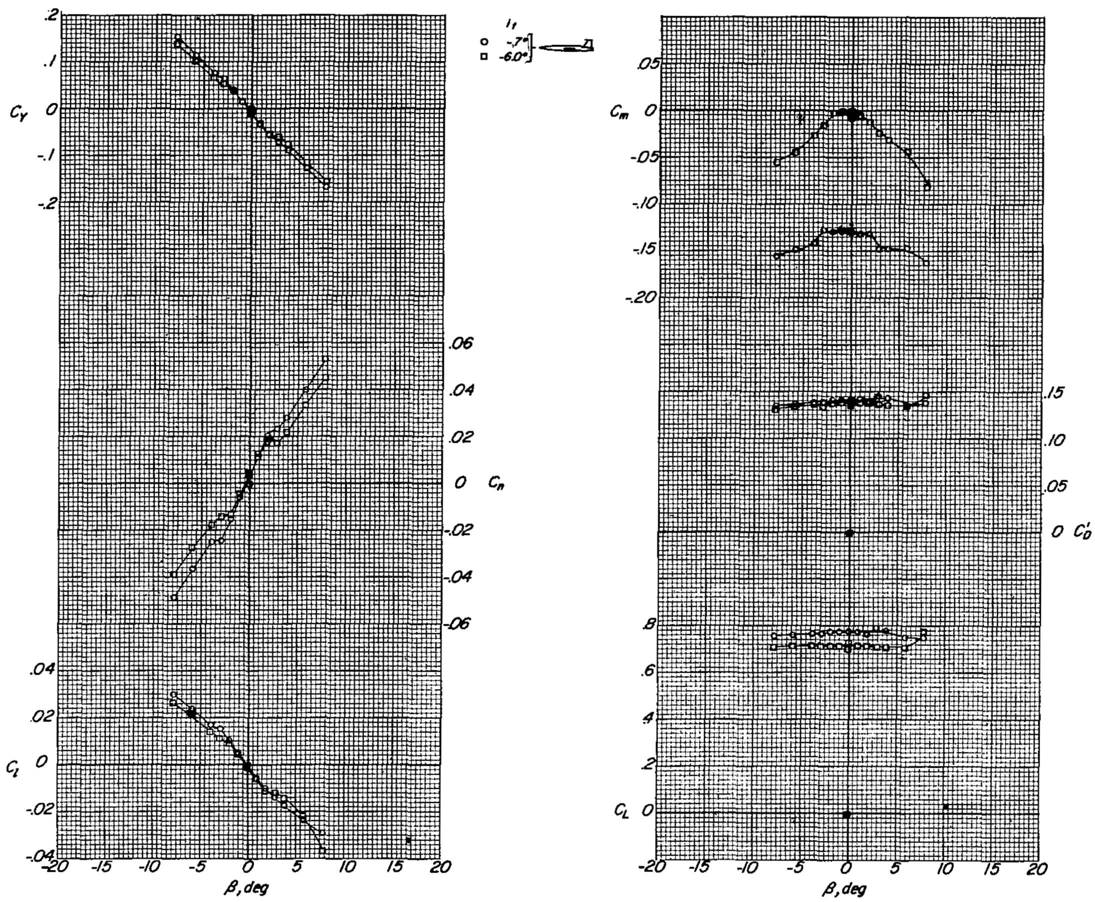

(d) M = 0.90.

Figure 17.- Continued.

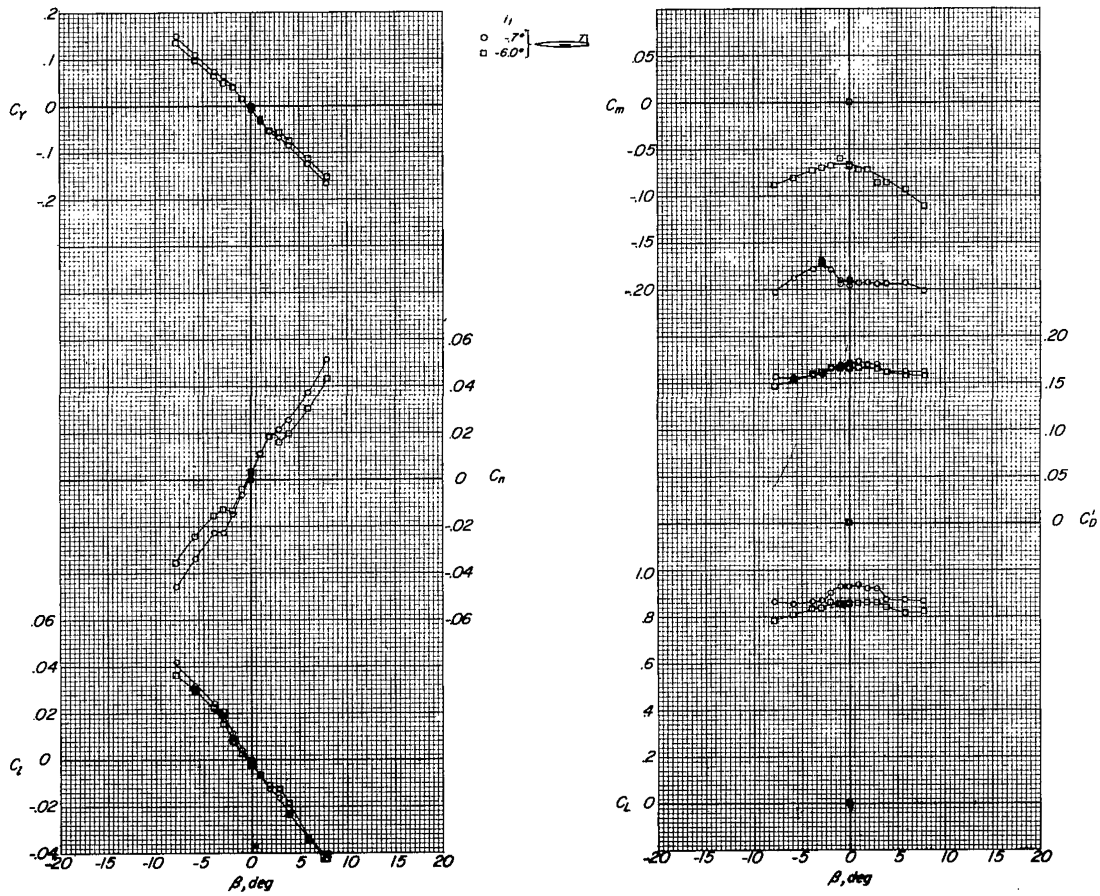

(e) M = 0.92.

Figure 17.- Concluded.

[redacted]

[redacted]

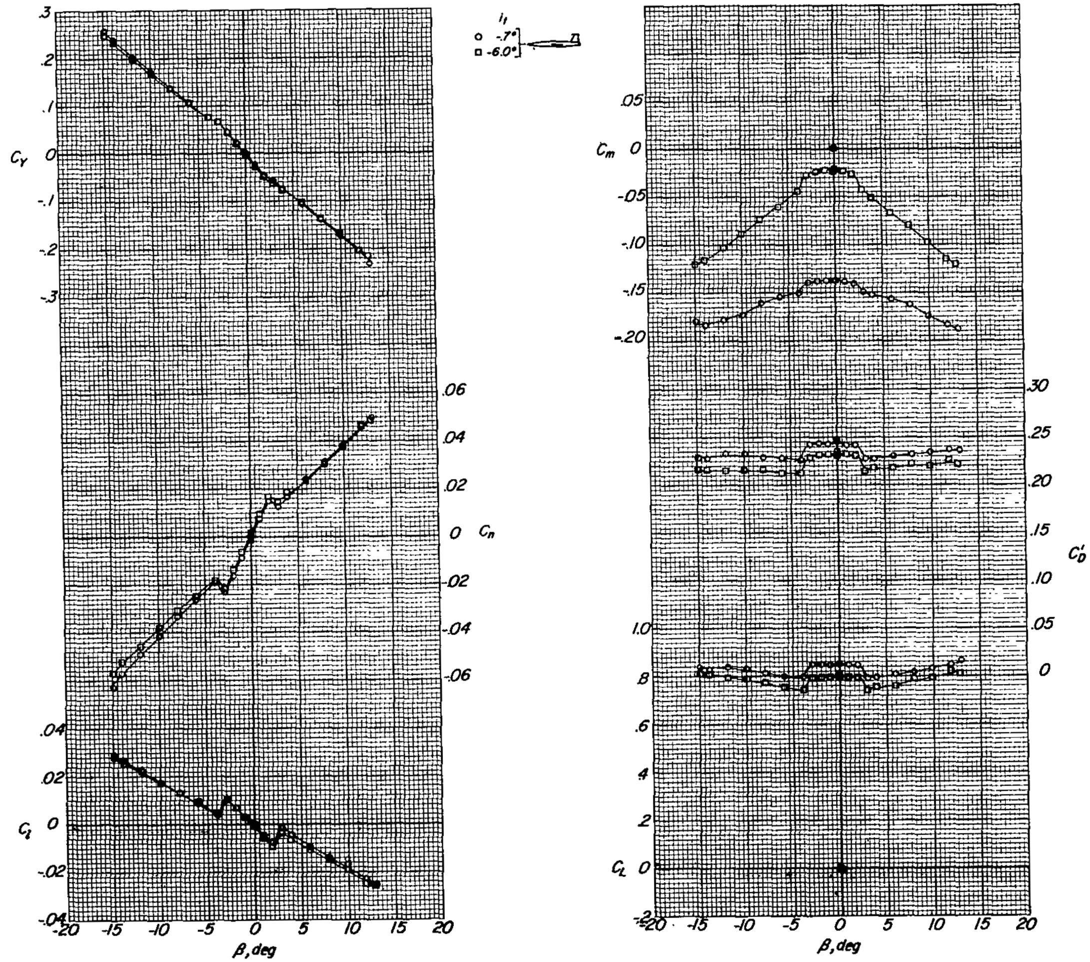

(a) M = 0.60.

Figure 18.- Effect of stabilizer deflection on aerodynamic characteristics of sideslipped model with the T-tail configuration having leading-edge overhang. Tail configuration 4; wing aspect ratio, 3.50; α = 15.6°.

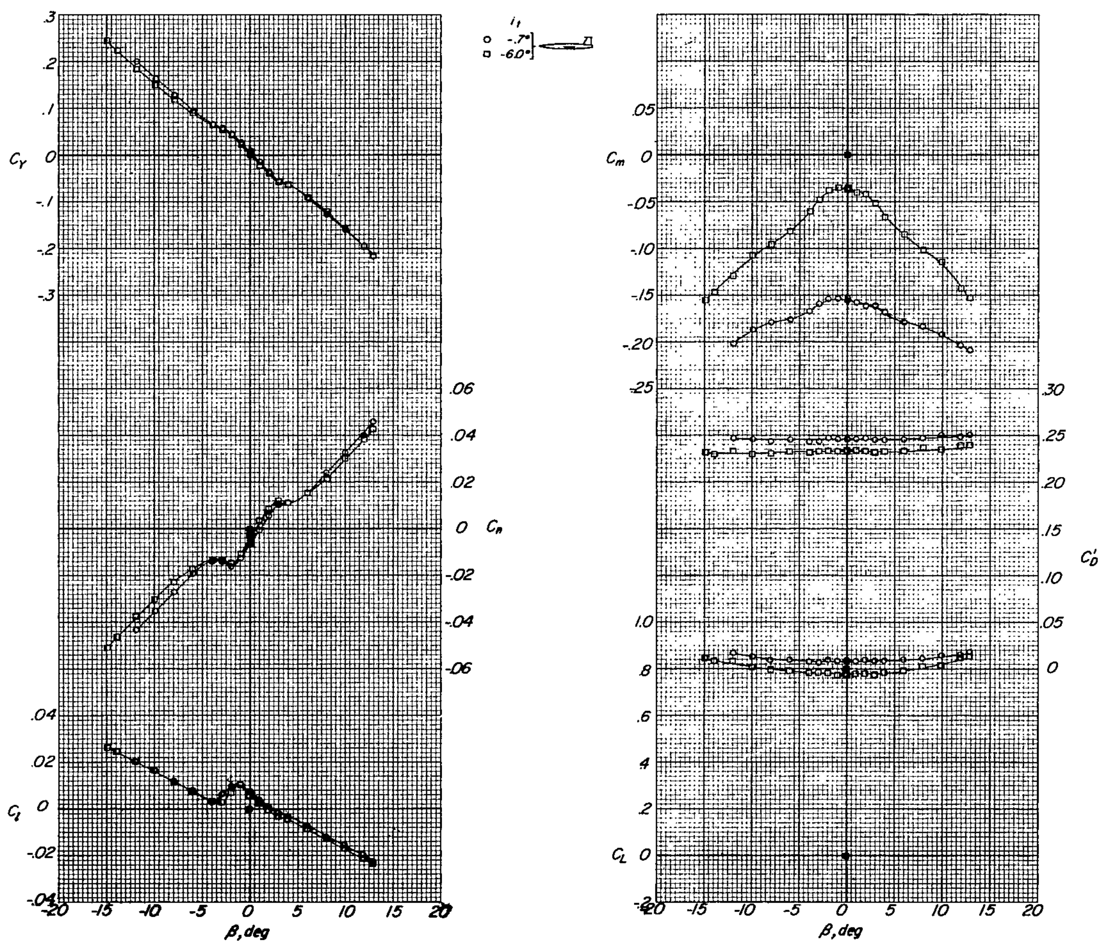

(b) M = 0.80.

Figure 18.- Continued.

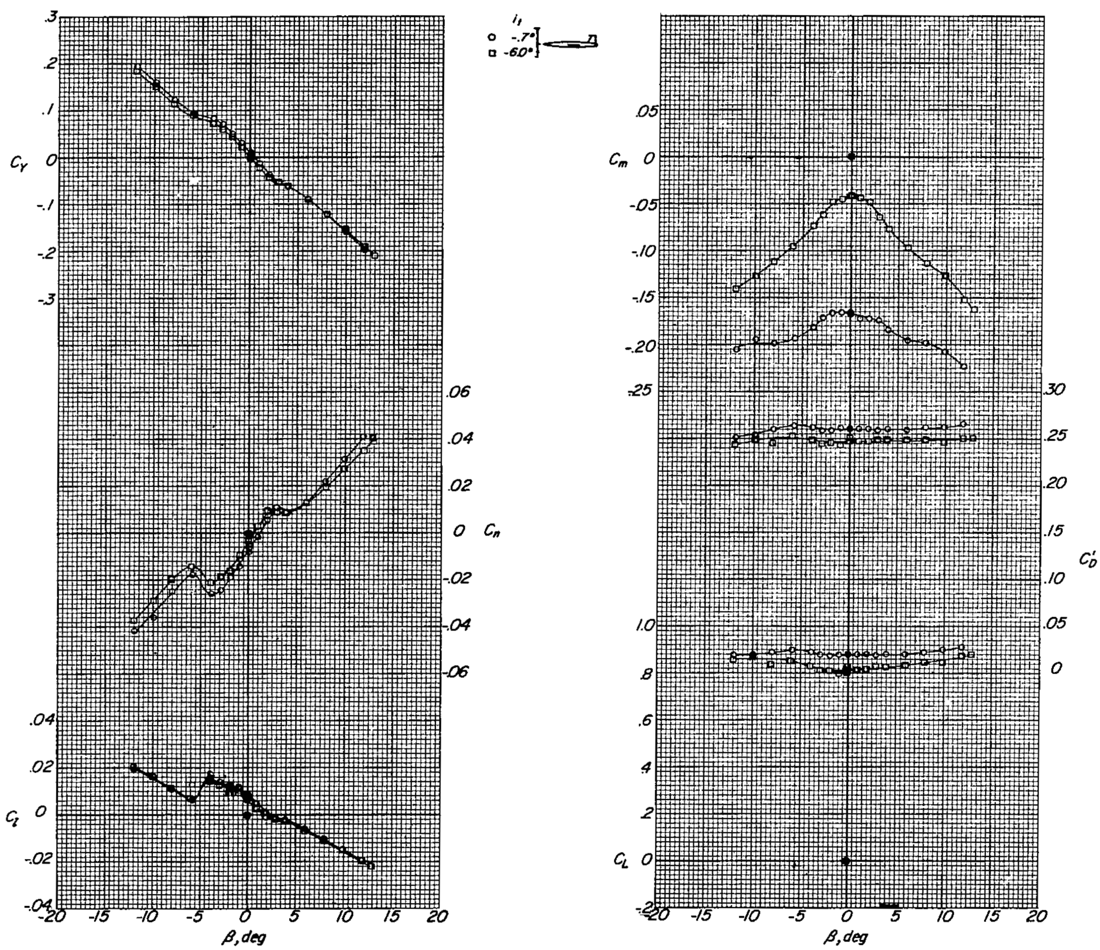

(c) M = 0.85.

Figure 18.- Concluded.

[redacted]

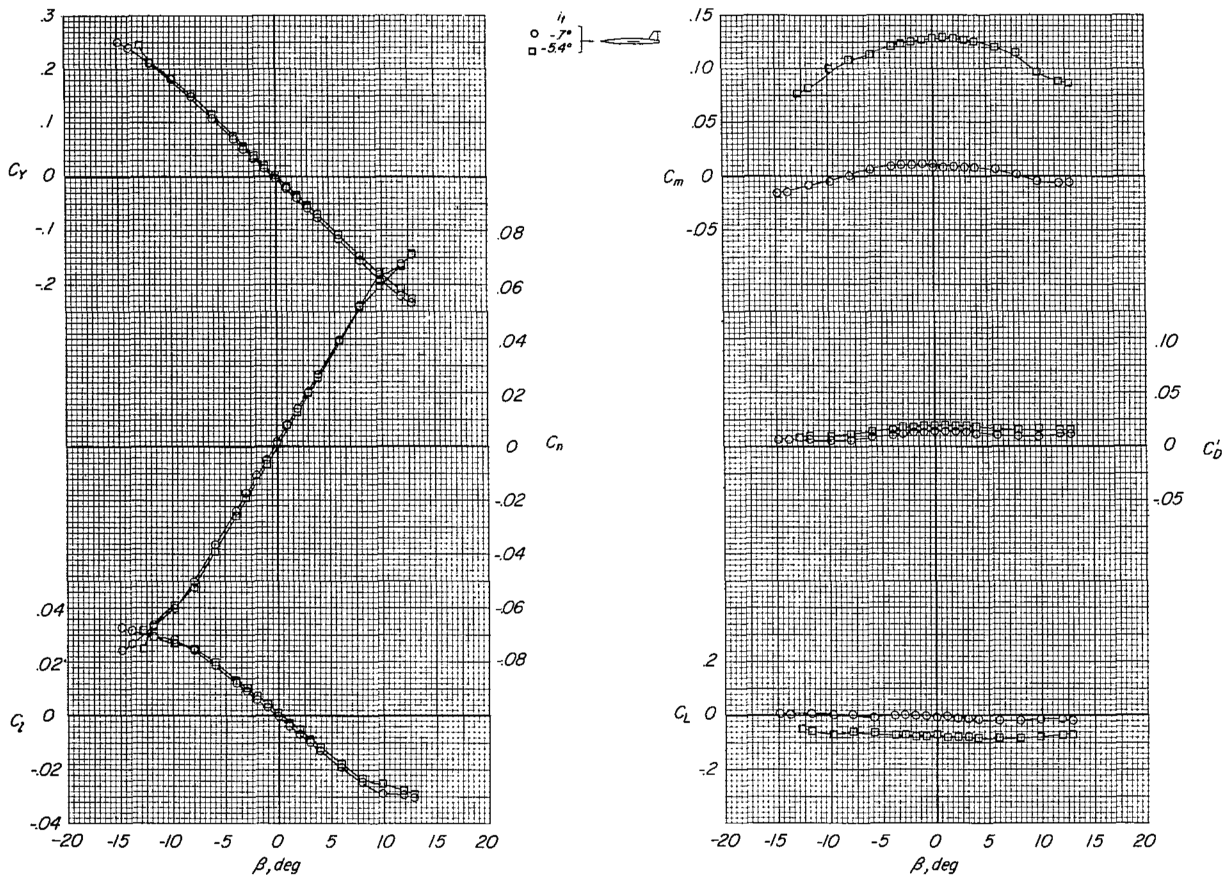

(a) M = 0.60.

Figure 19.- Effects of stabilizer deflection on aerodynamic characteristics of sideslipped model with the T-tail configuration having zero leading-edge overhang. Tail configuration 6; wing aspect ratio, 3.50; $\alpha = 0^{\circ}$.

[redacted]

[redacted]

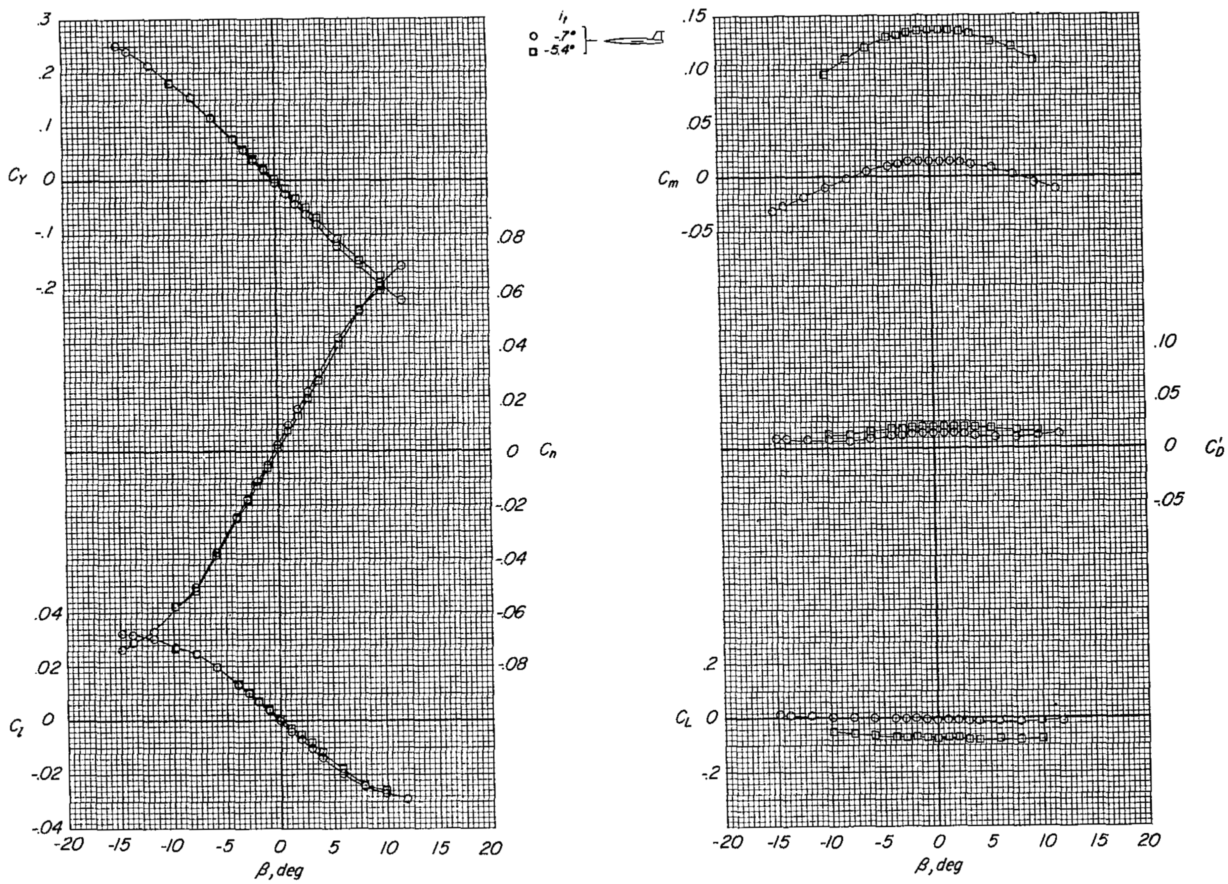

(b) M = 0.80.

Figure 19.- Continued.

[redacted]

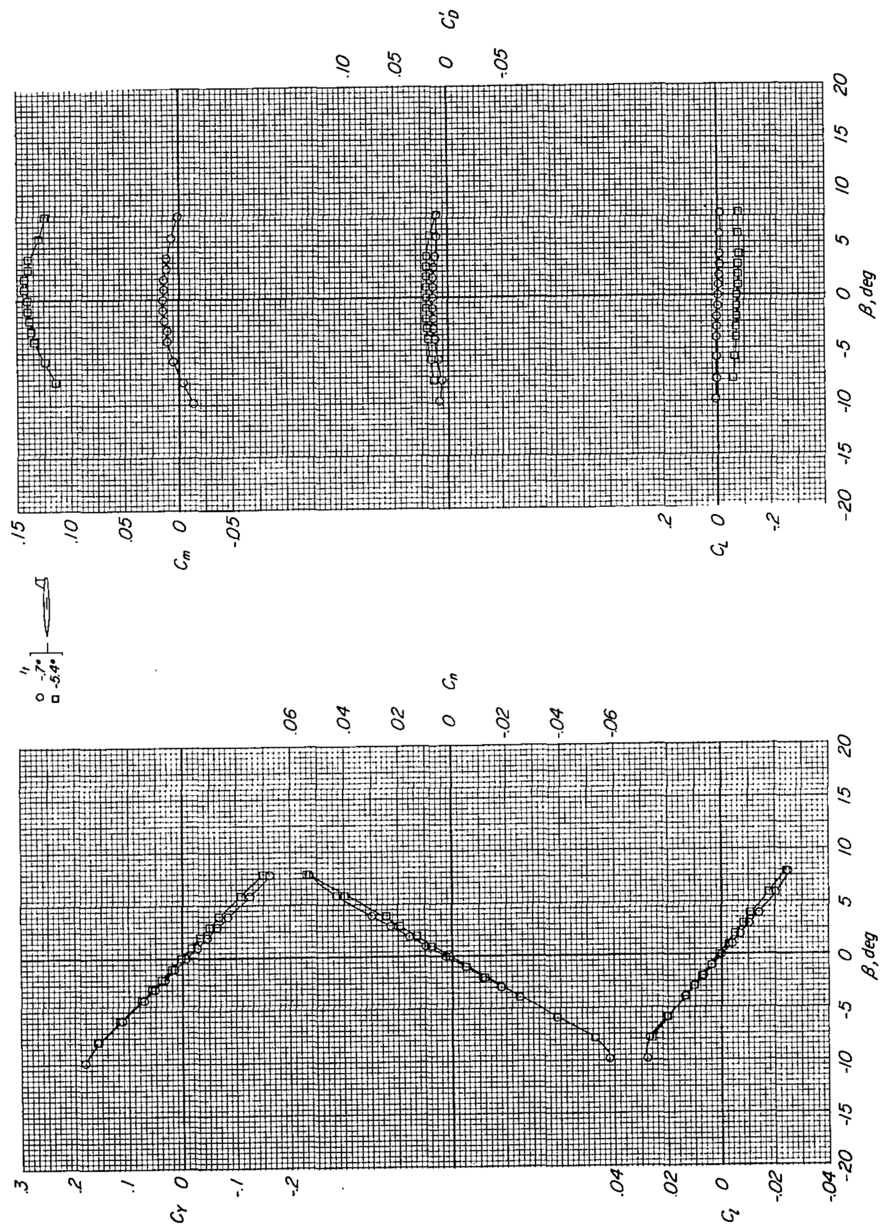

(c) M = 0.85.

Figure 19.- Continued.

[redacted]

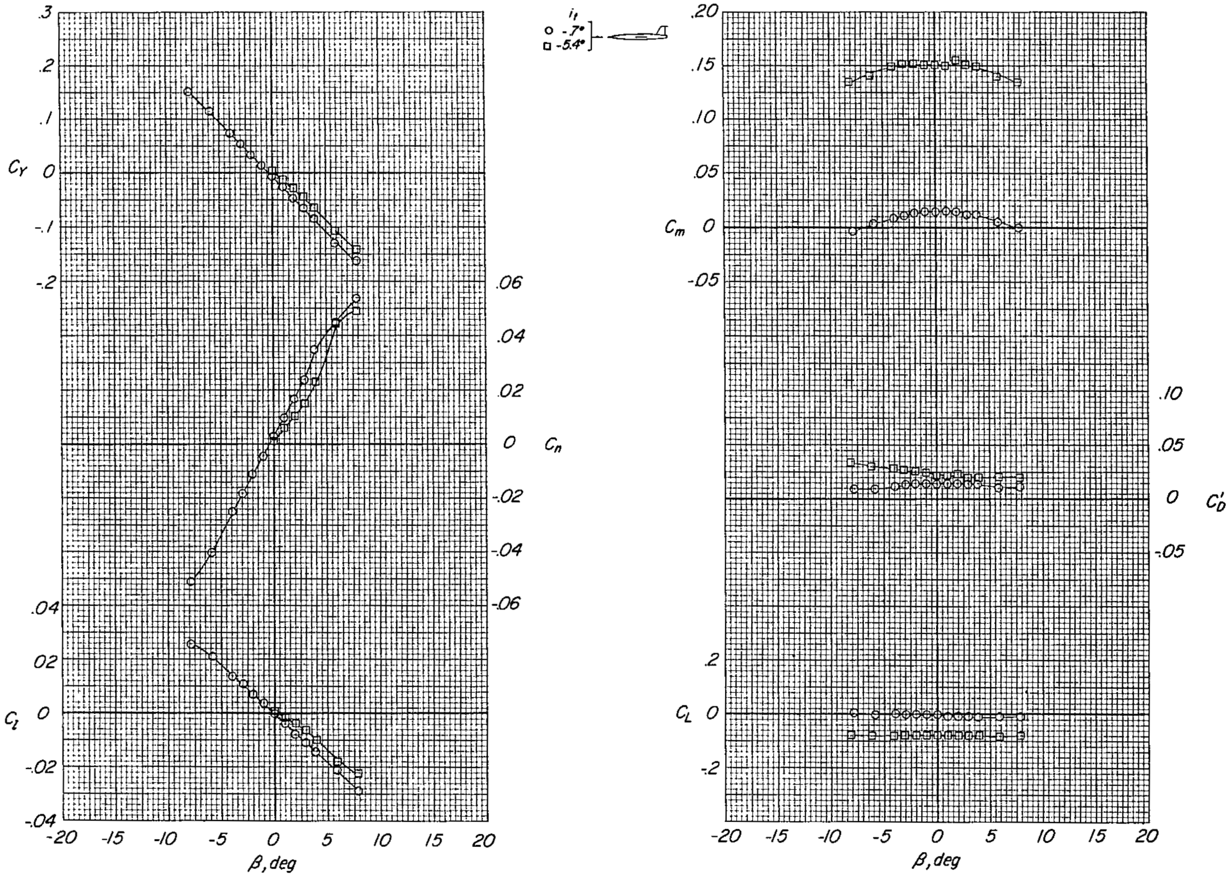

(d) M = 0.90.

Figure 19.- Continued.

[redacted]

~~CONFIDENTIAL~~

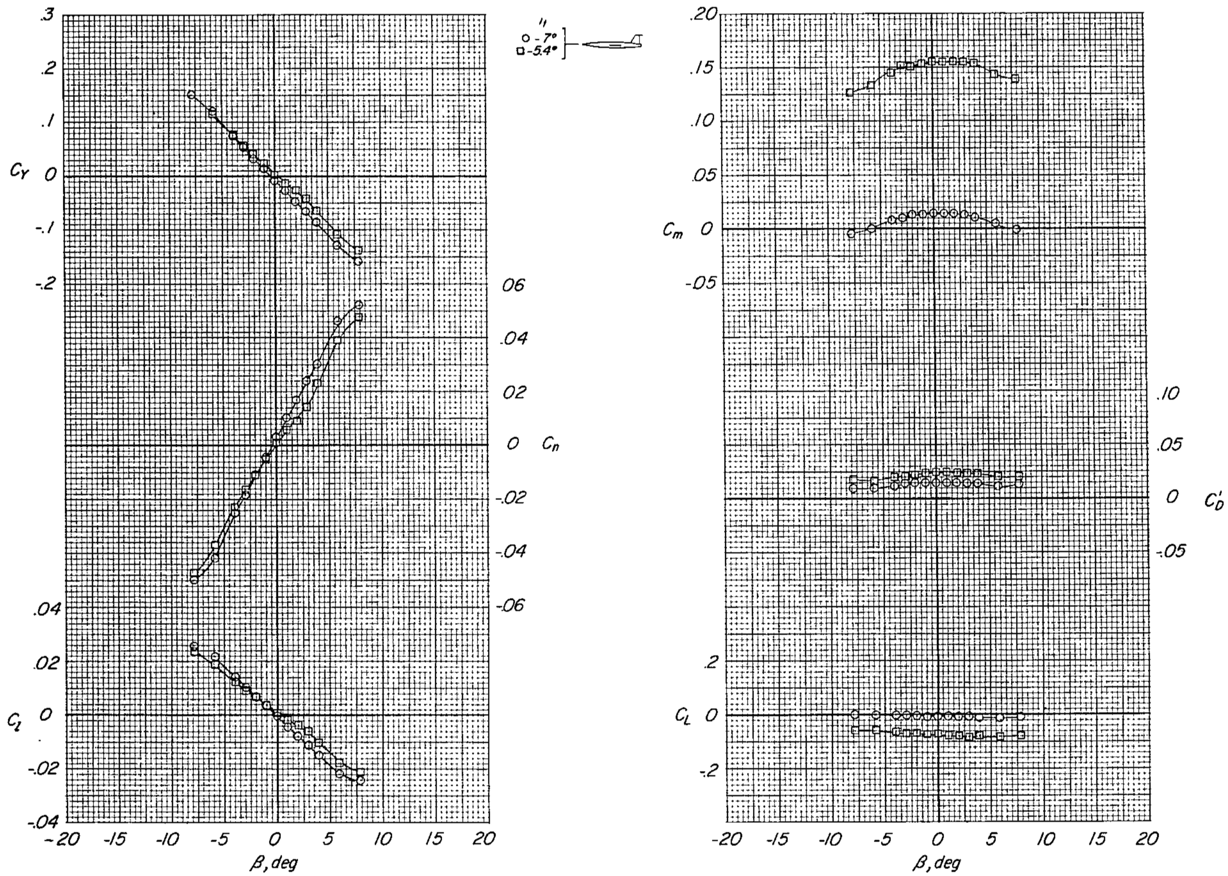

(e) M = 0.92.

Figure 19.- Concluded.

~~CONFIDENTIAL~~

[redacted]

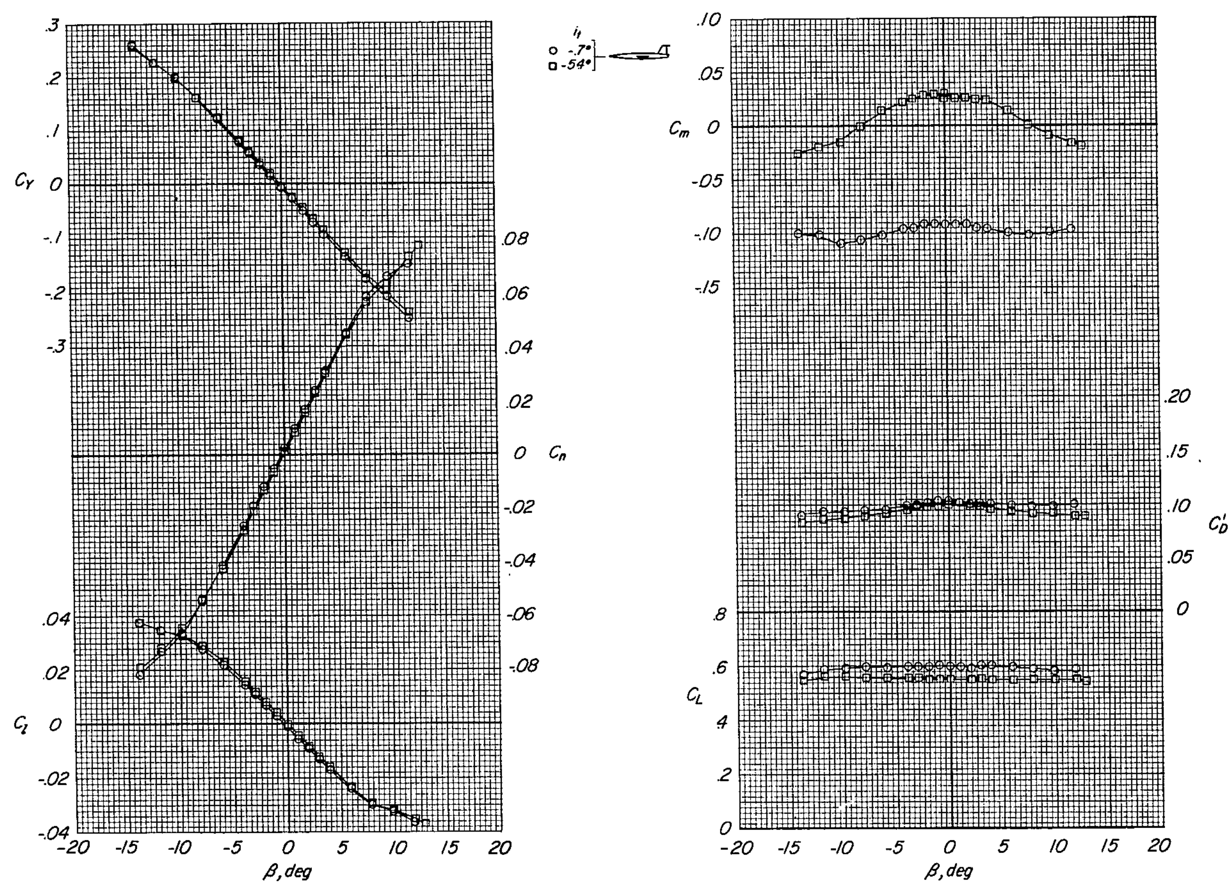

(a) M = 0.60.

Figure 20.- Effects of stabilizer deflection on aerodynamic characteristics of sideslipped model with the T-tail configuration having zero leading-edge overhang. Tail configuration 6; wing aspect ratio, 3.50; $\alpha = 9.5^{\circ}$.

[redacted]

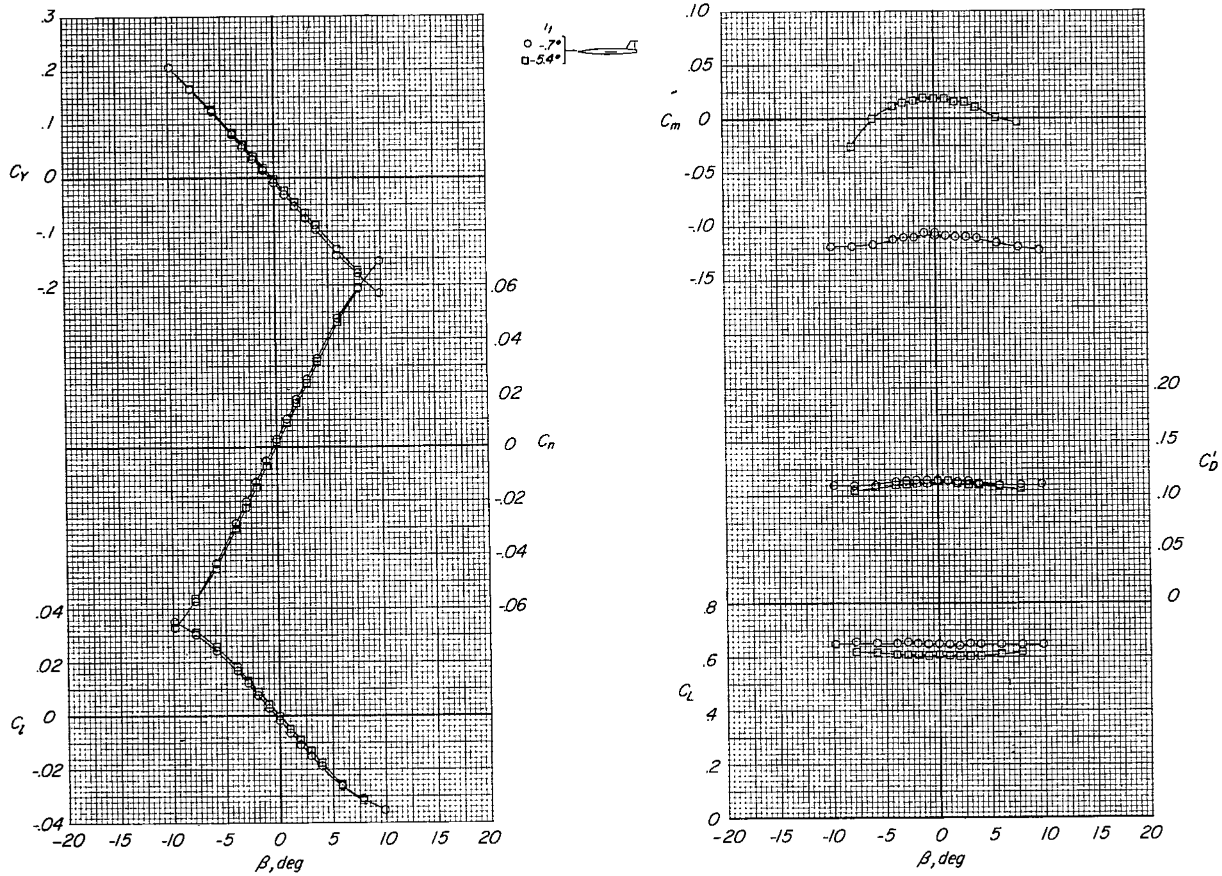

(b) M = 0.80.

Figure 20.- Continued.

[redacted]

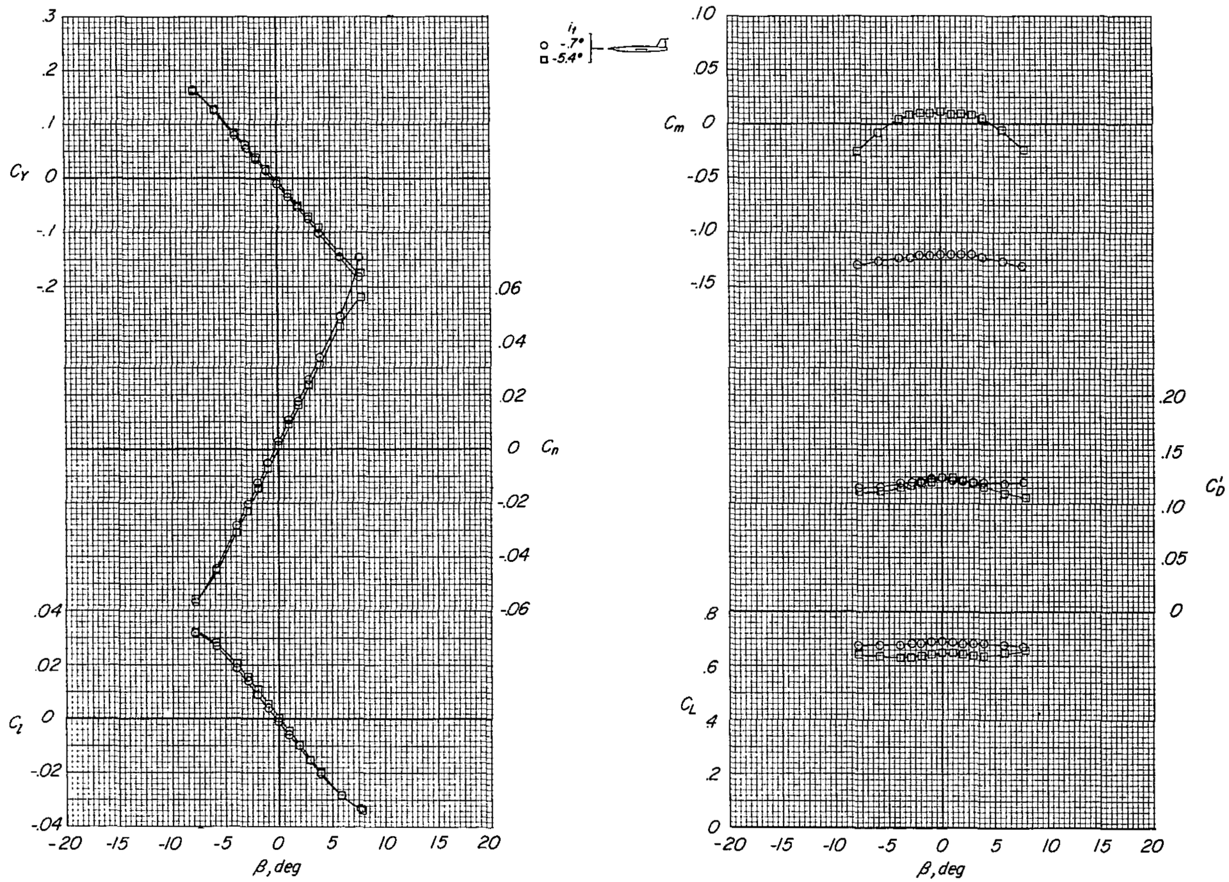

(c) M = 0.85.

Figure 20.- Continued.

[redacted]

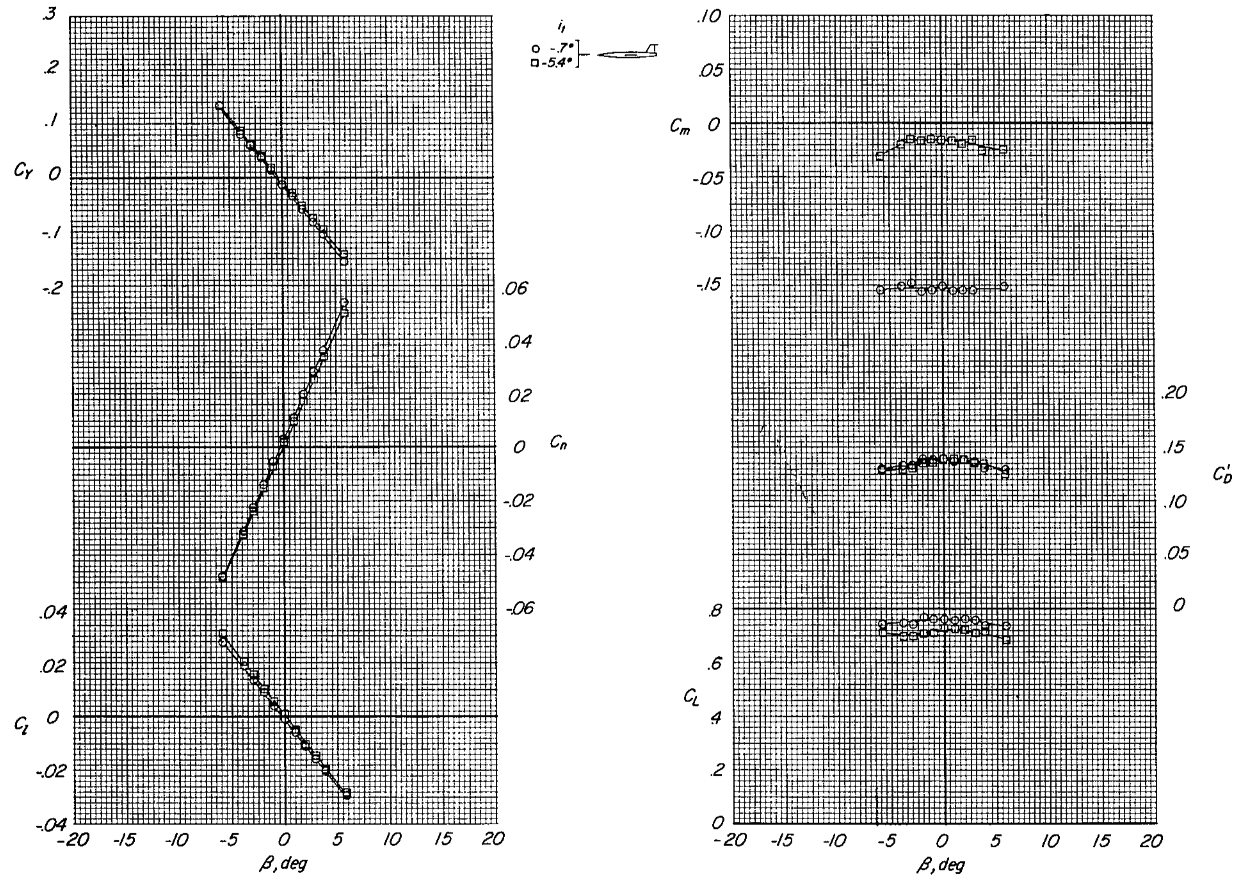

(d) M = 0.90.

Figure 20.- Continued.

[redacted]

[redacted]

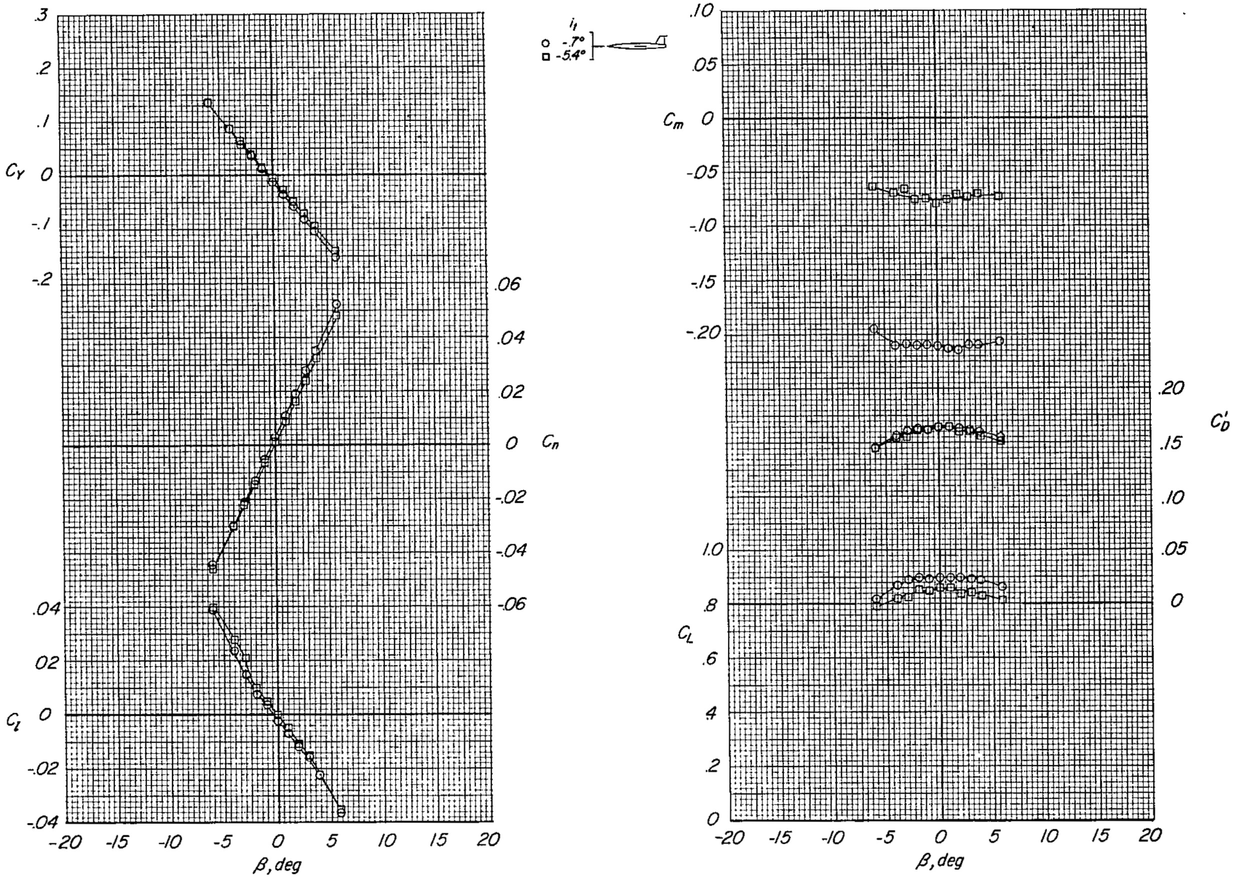

(e) M = 0.92.

Figure 20.- Concluded.

[redacted]

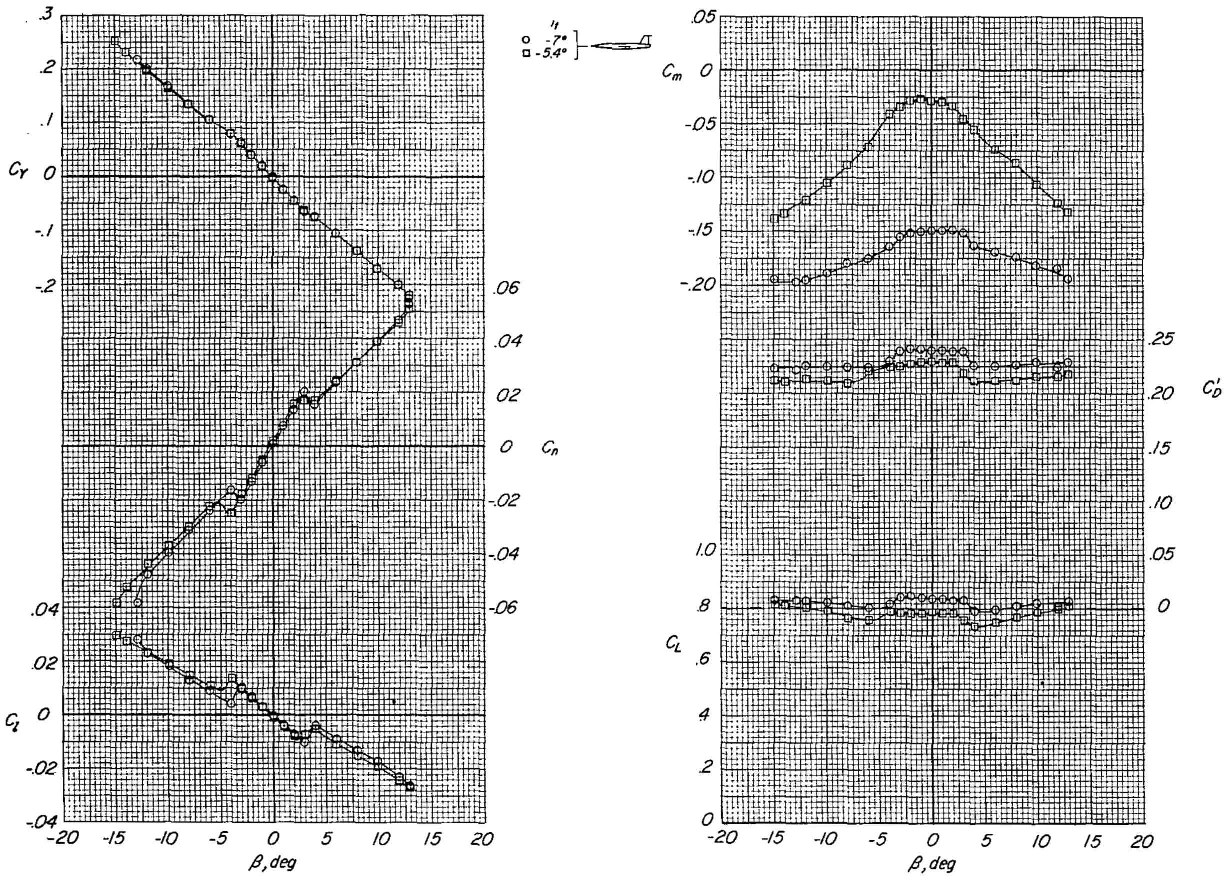

(a) M = 0.60.

Figure 21.- Effects of stabilizer deflection on aerodynamic characteristics of sideslipped model with the T-tail configuration having zero leading-edge overhang. Tail configuration 6; wing aspect ratio, 3.50; $\alpha = 15.6^{\circ}$.

[redacted]

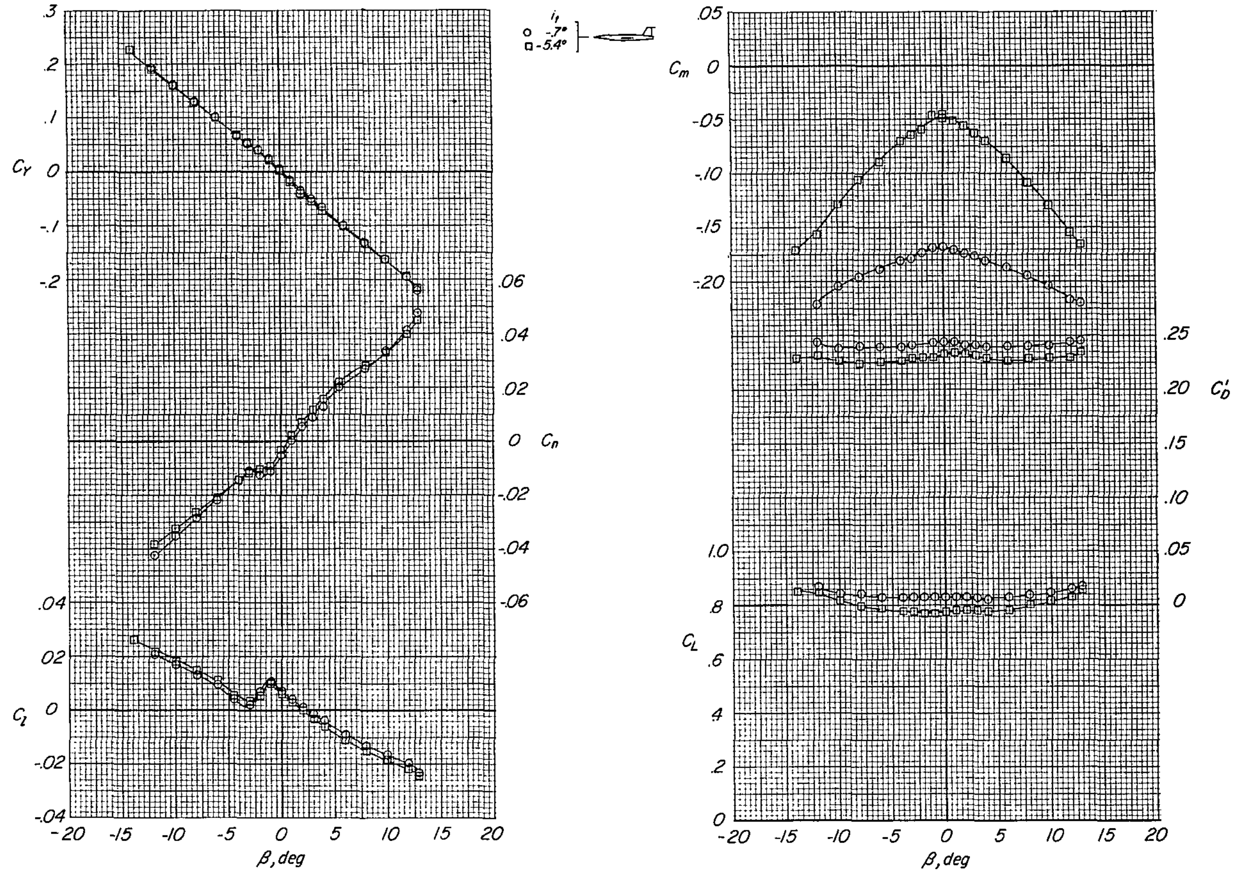

(b) M = 0.80.

Figure 21.- Continued.

[redacted]

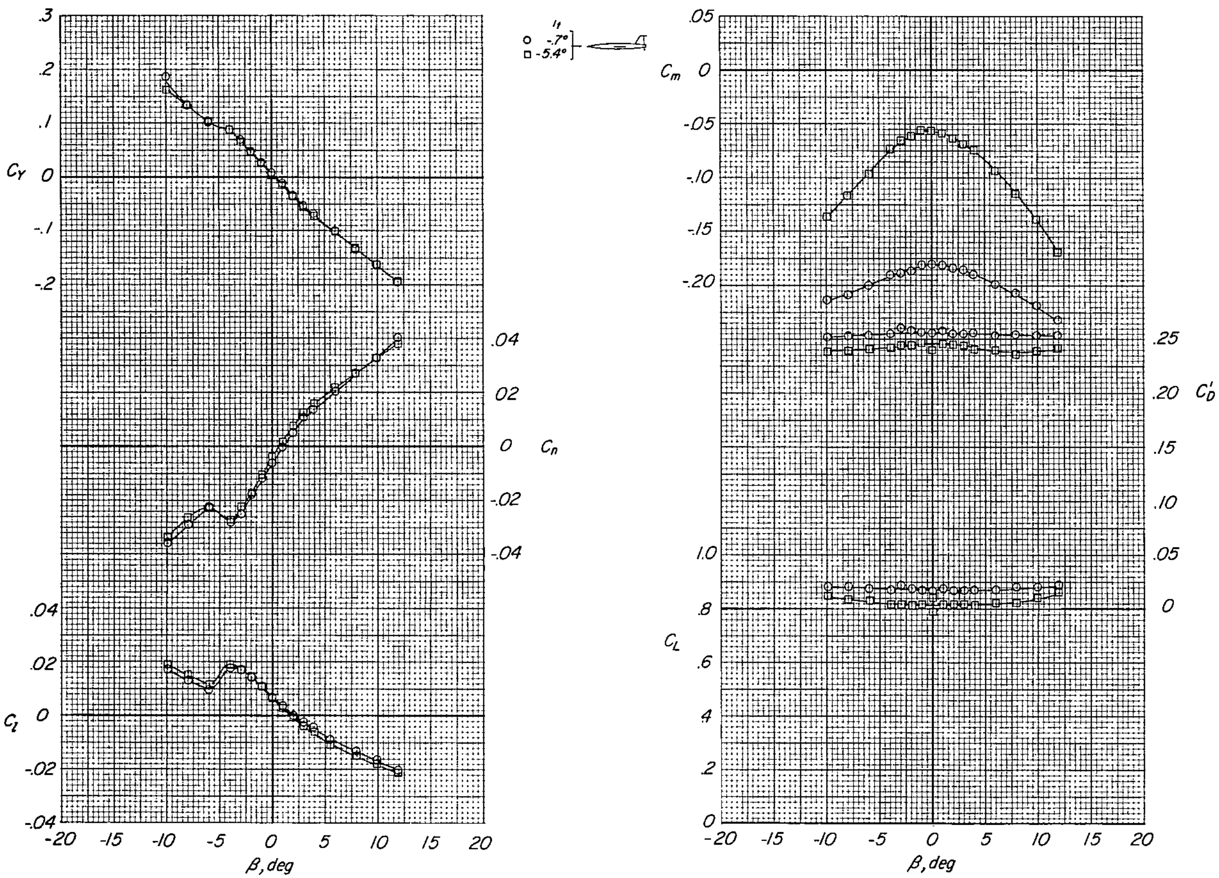

(c) M = 0.85.

Figure 21.- Concluded.

~~CONFIDENTIAL~~

[redacted]

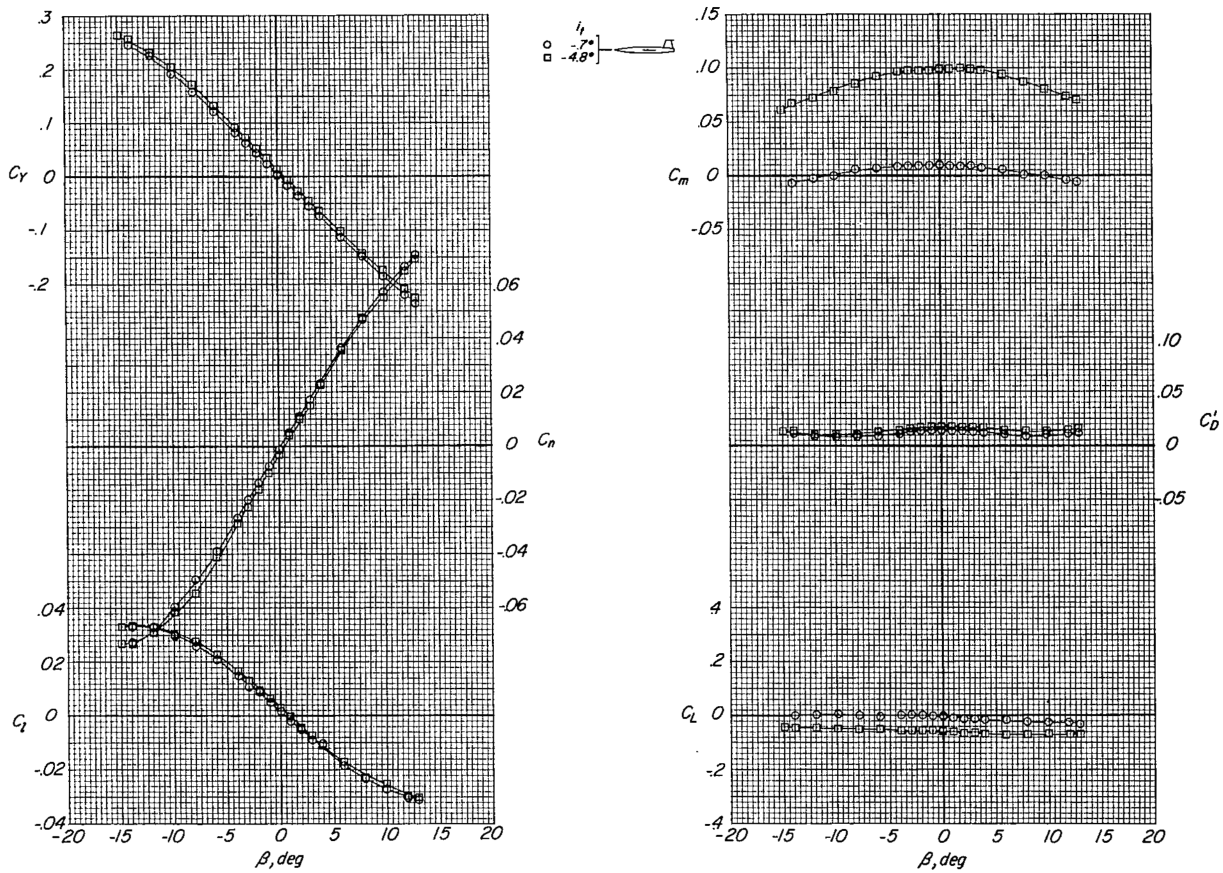

(a) M = 0.60.

Figure 22.- Effects of stabilizer deflection on aerodynamic characteristics of sideslipped model with the T-tail configuration with zero leading-edge overhang and mounted on a reduced-sweep vertical tail. Tail configuration 7; wing aspect ratio, 3.50; $\alpha = 0^{\circ}$.

[redacted]

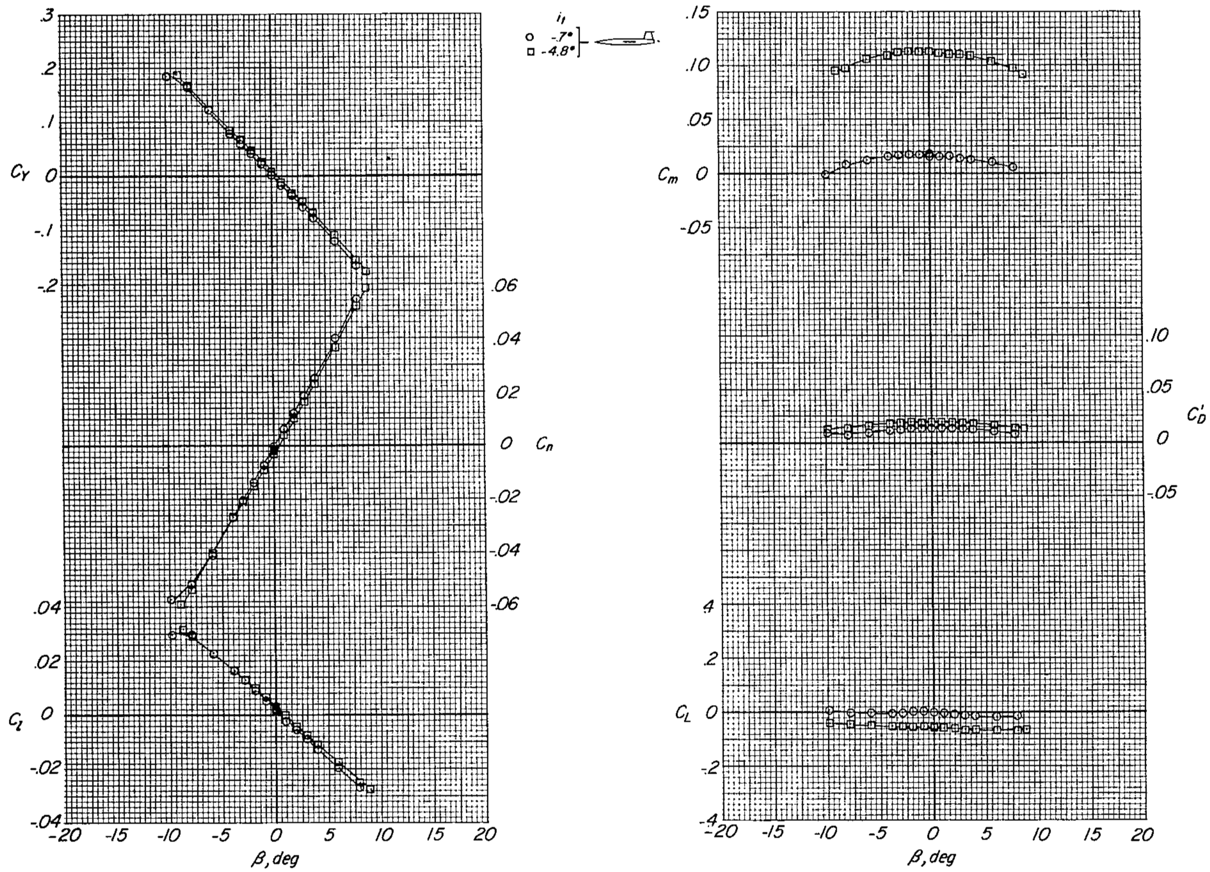

(b) M = 0.80.

Figure 22.- Continued.

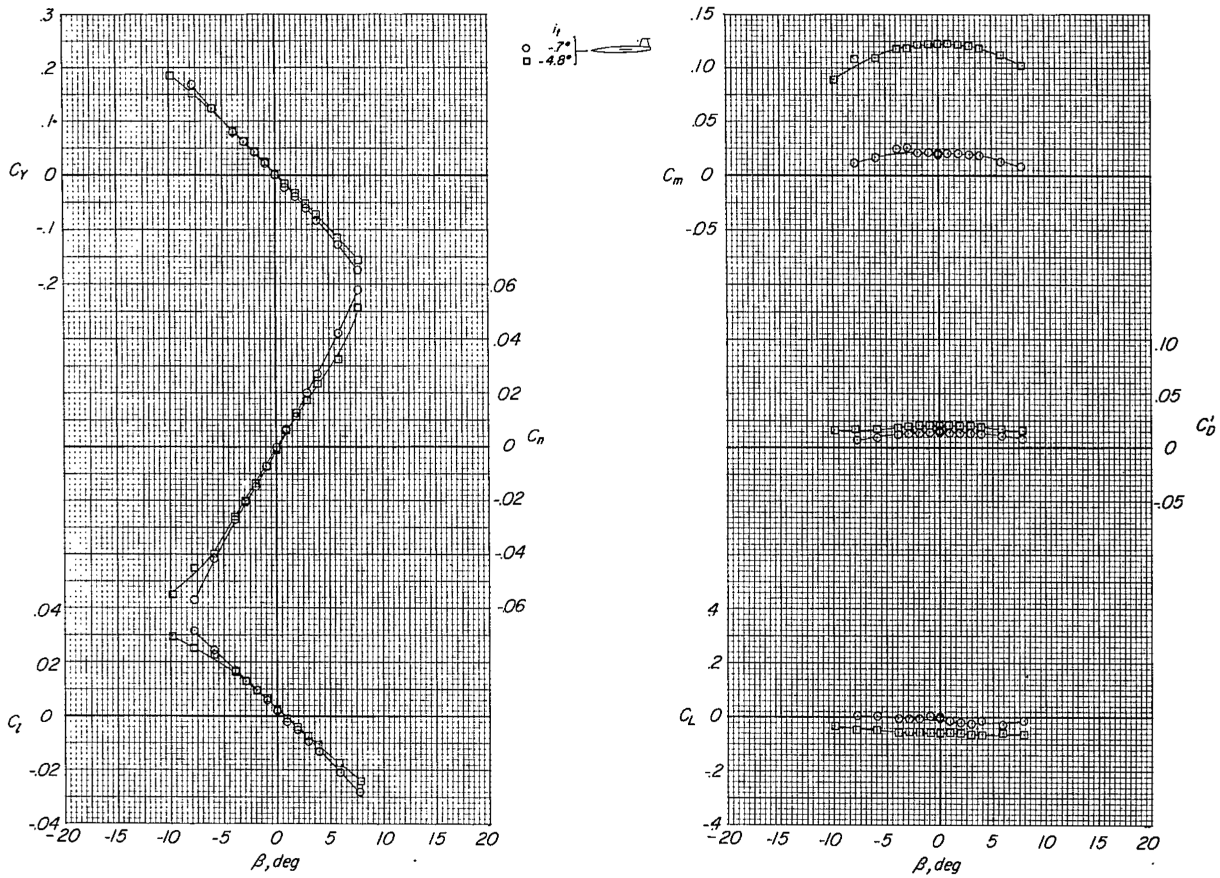

(c) M = 0.85.

Figure 22.- Continued.

[redacted]

[redacted]

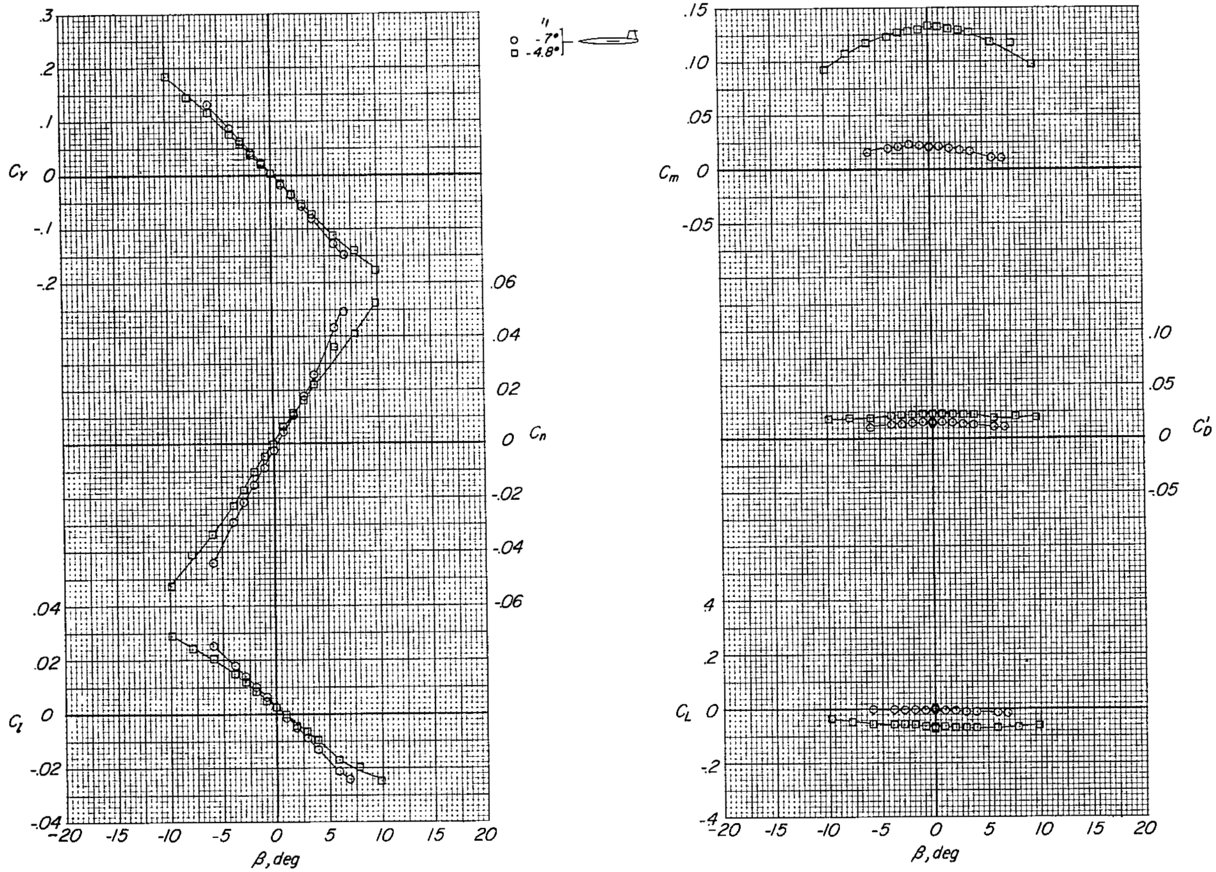

(d) M = 0.90.

Figure 22.- Continued.

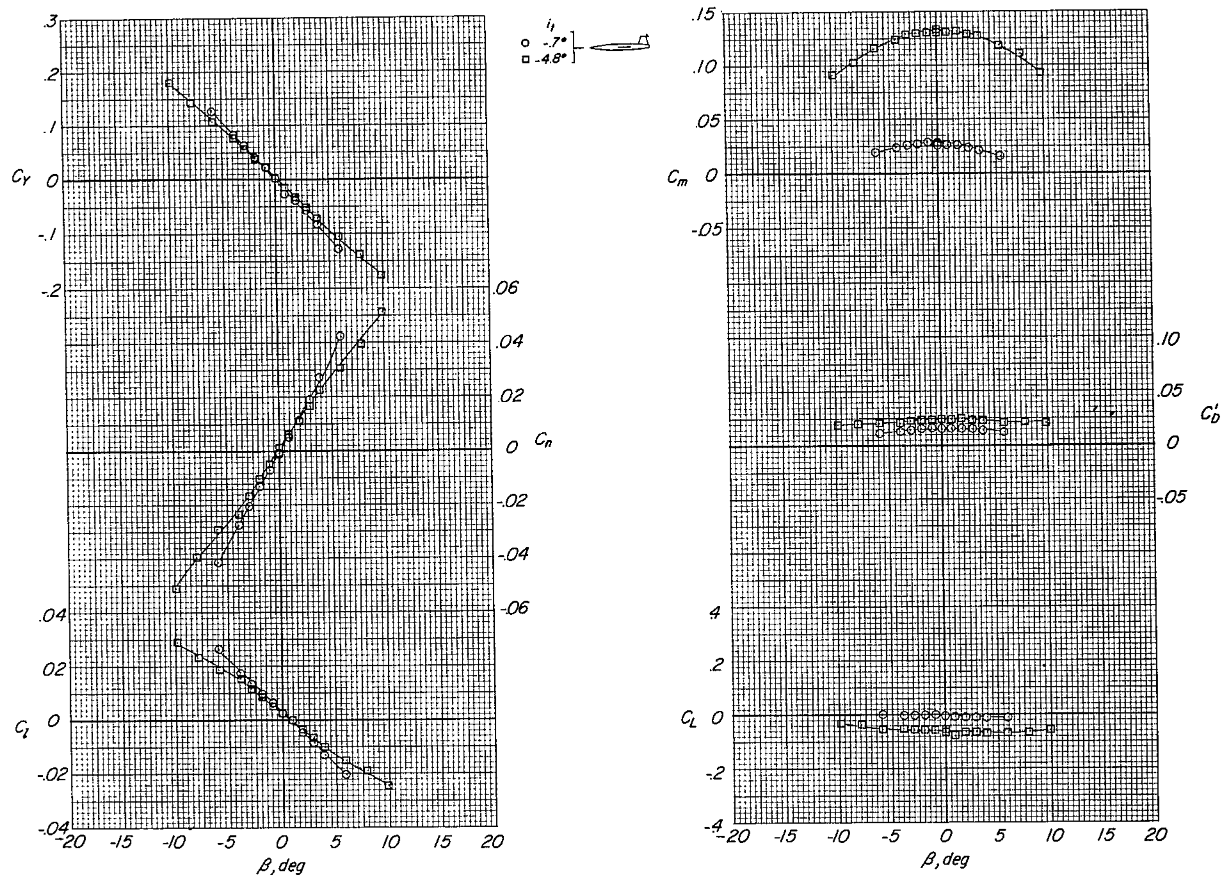

(e) M = 0.92.

Figure 22.- Concluded.

[redacted]

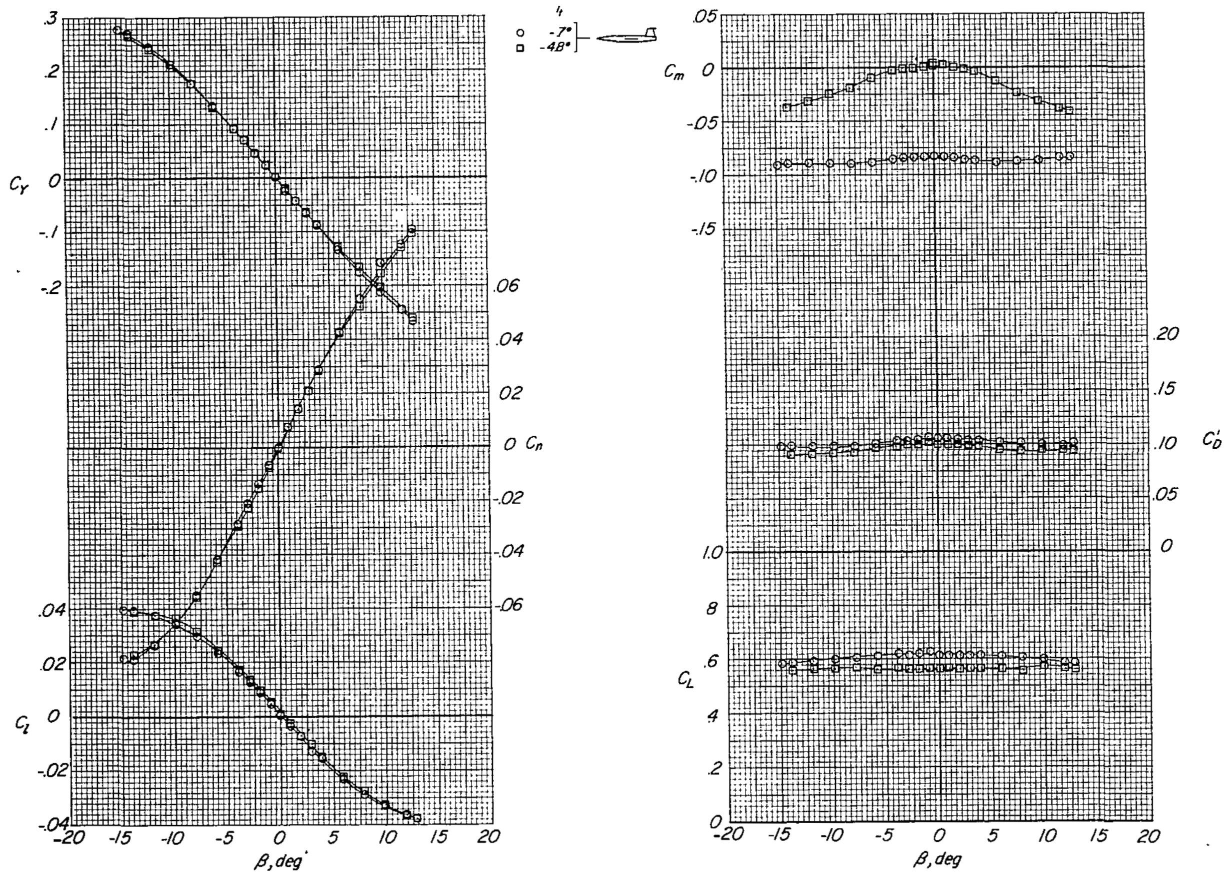

(a) M = 0.60.

Figure 23.- Effects of stabilizer deflection on aerodynamic characteristics of sideslipped model with the T-tail configuration with zero leading-edge overhang and mounted on a reduced-sweep vertical tail. Tail configuration 7; wing aspect ratio, 3.50; $\alpha = 9.5^{\circ}$.

[redacted]

[redacted]

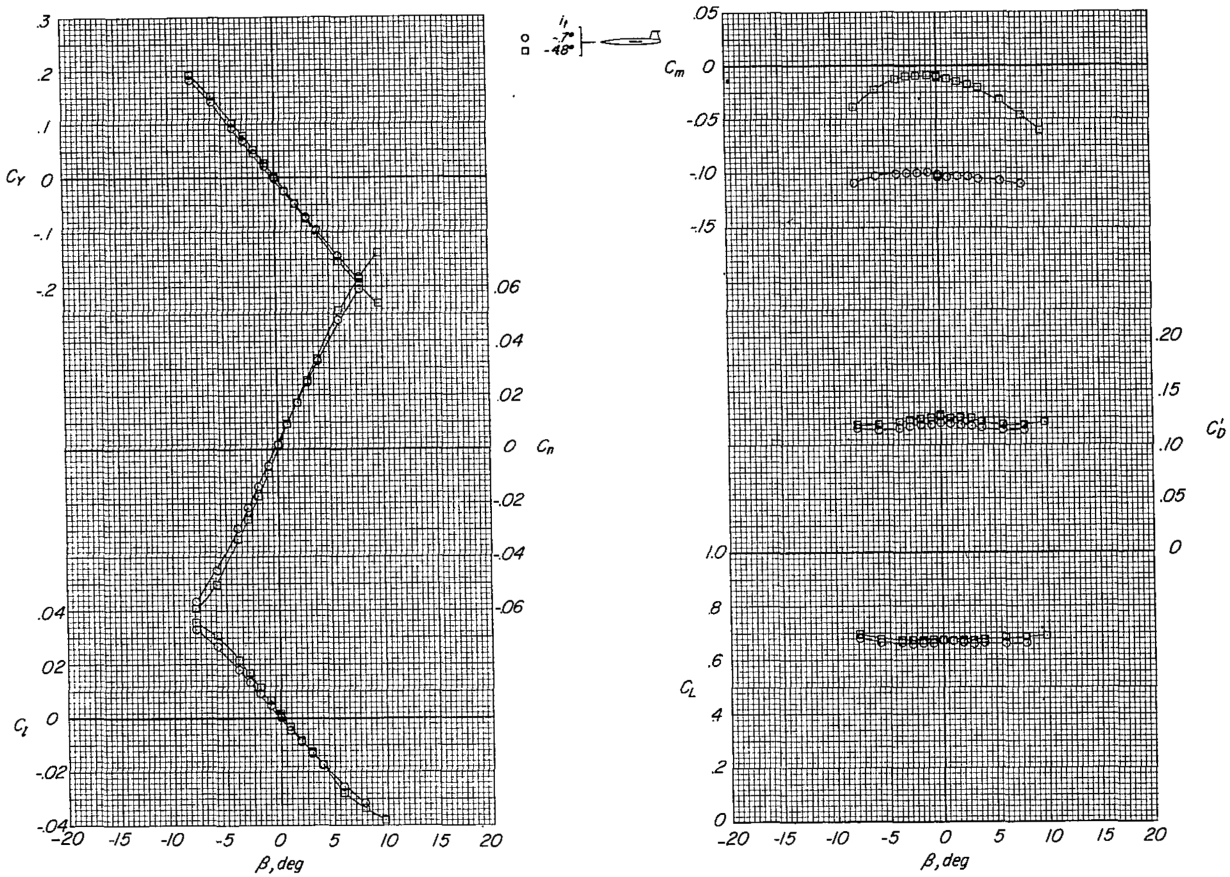

(b) M = 0.80.

Figure 23.- Continued.

[redacted]

[redacted]

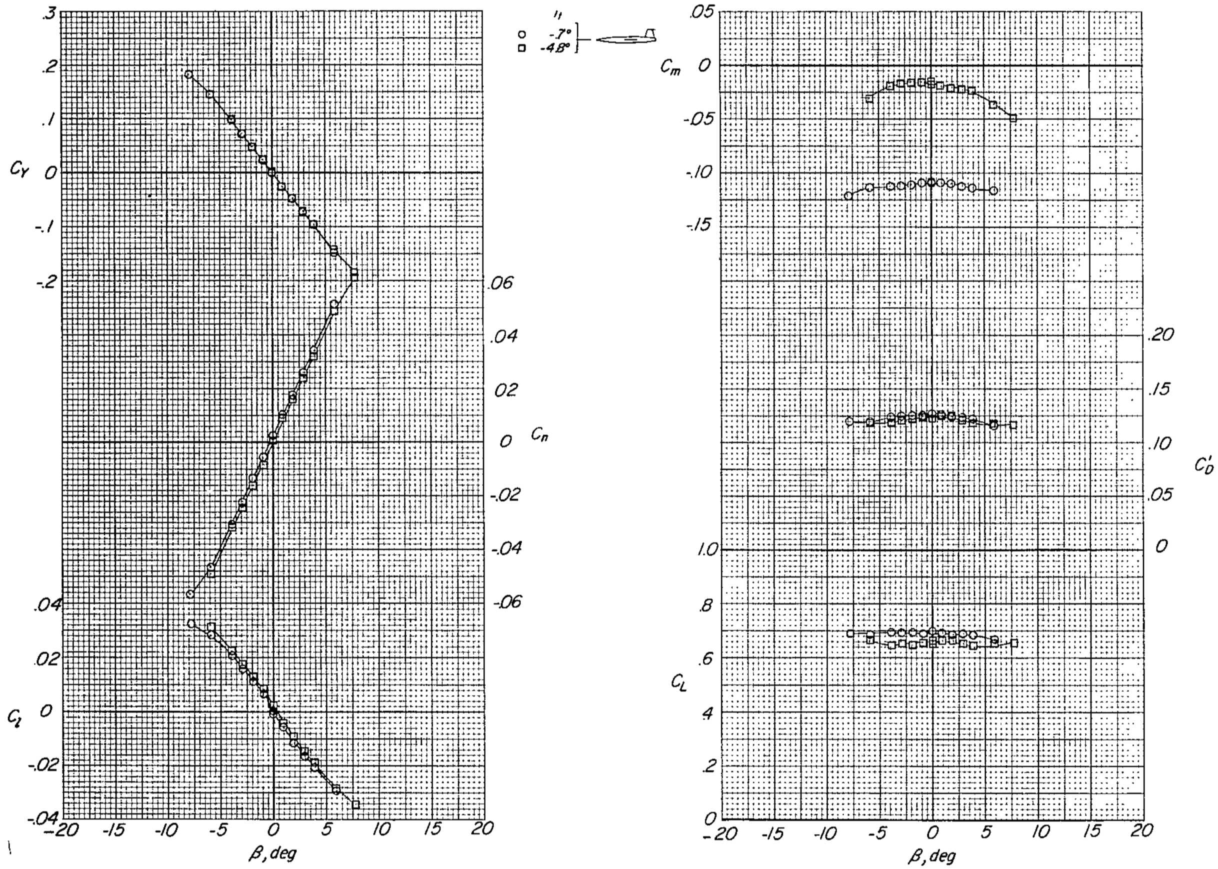

(c) M = 0.85.

Figure 23.- Continued.

CONFIDENTIAL

[redacted]

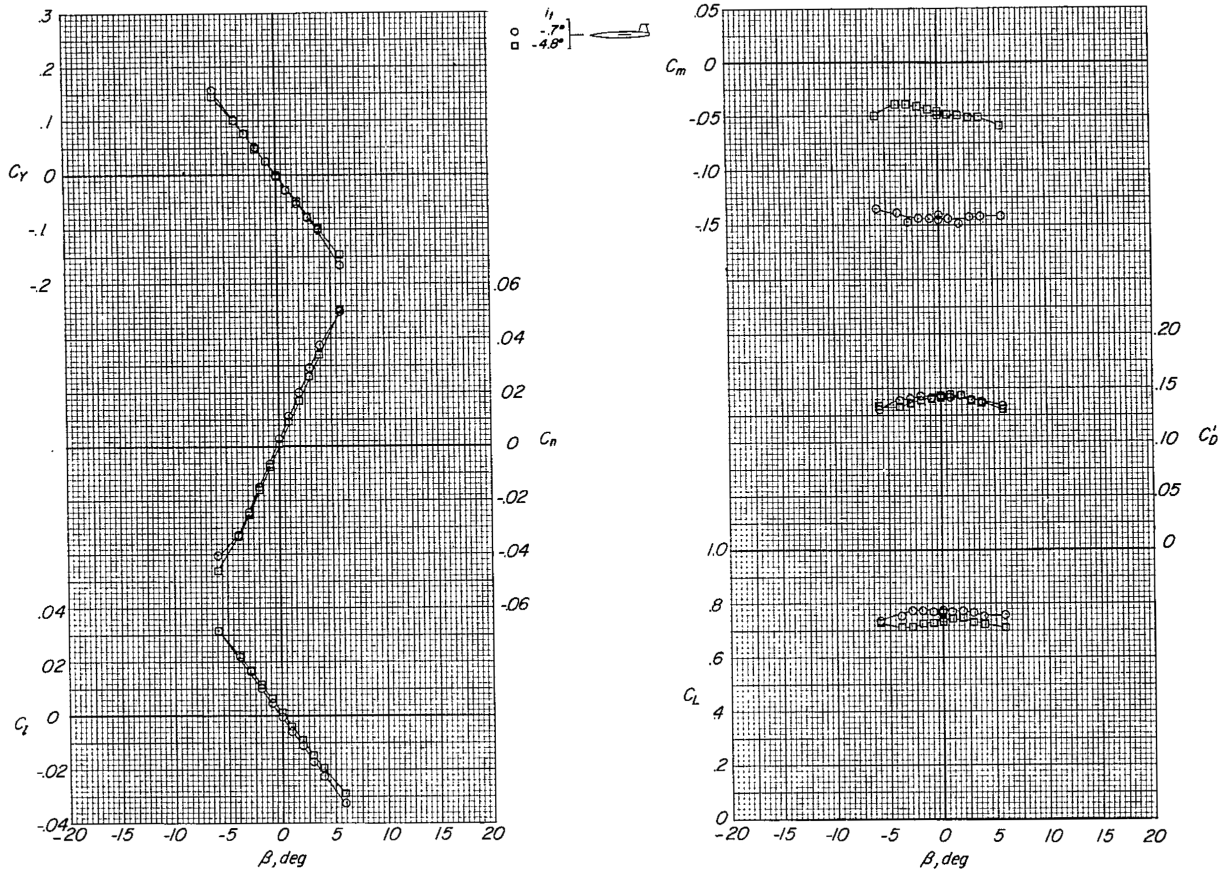

(d) M = 0.90.

Figure 23.- Continued.

[redacted]

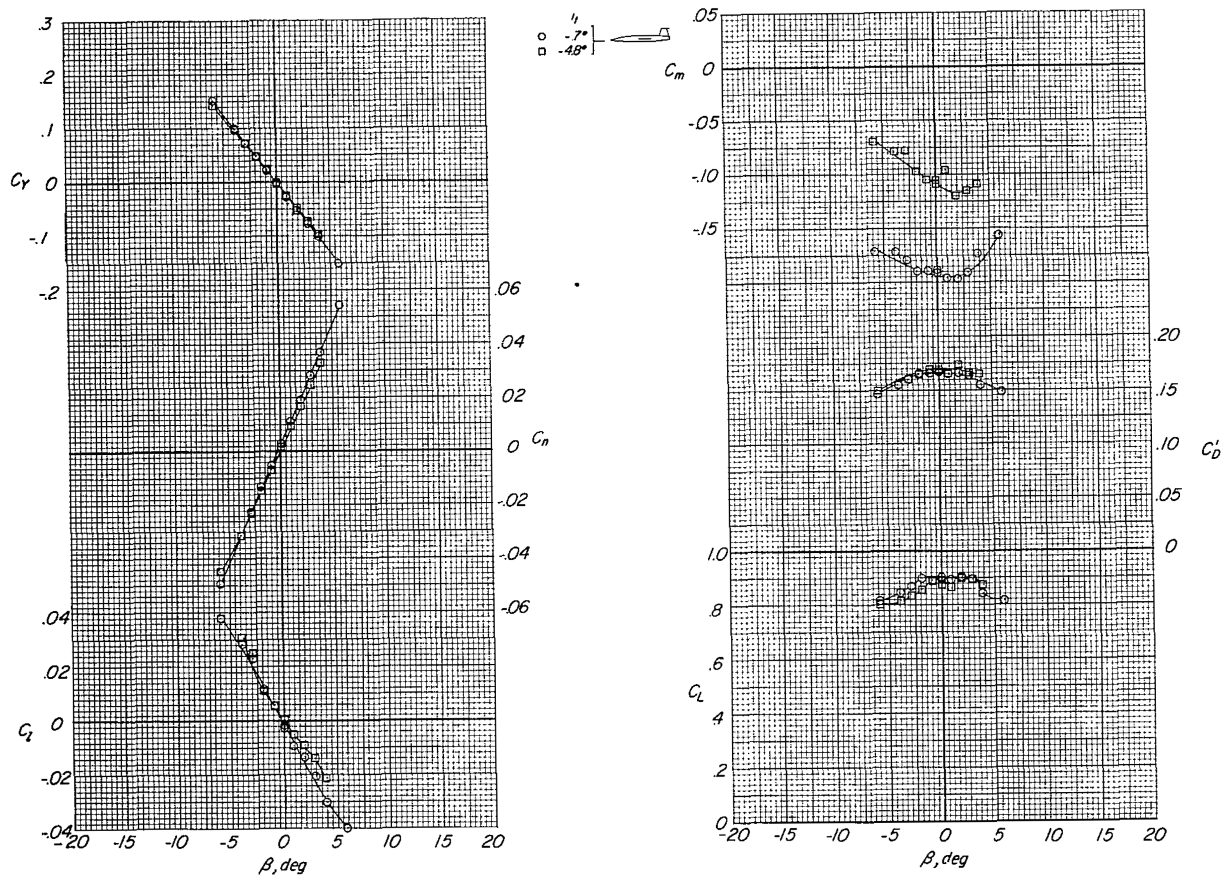

(e) M = 0.92.

Figure 23.- Concluded.

[redacted]

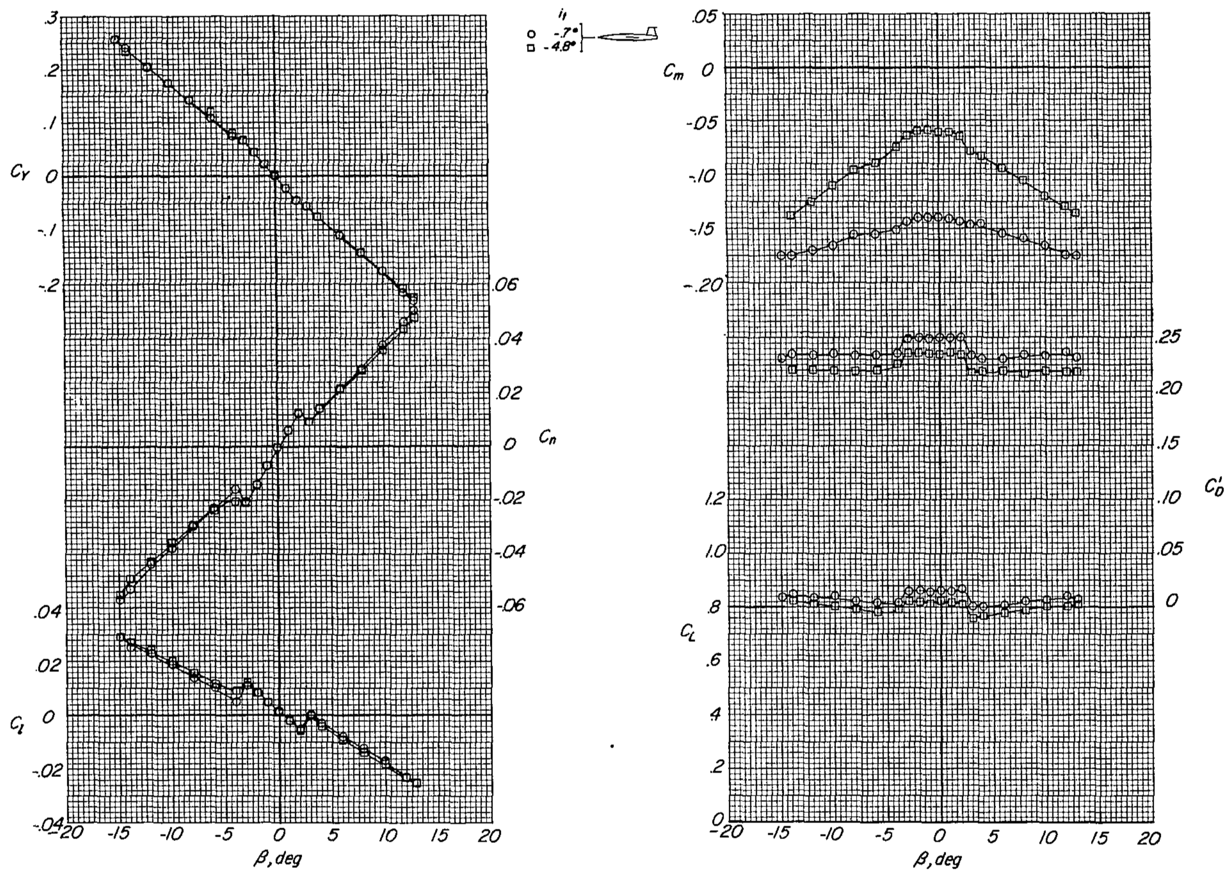

(a) M = 0.60.

Figure 24.- Effects of stabilizer deflection on aerodynamic characteristics of sideslipped model with the T-tail configuration with zero leading-edge overhang and mounted on a reduced-sweep vertical tail. Tail configuration 7; wing aspect ratio, 3.50; $\alpha = 15.6^{\circ}$.

[redacted]

[redacted]

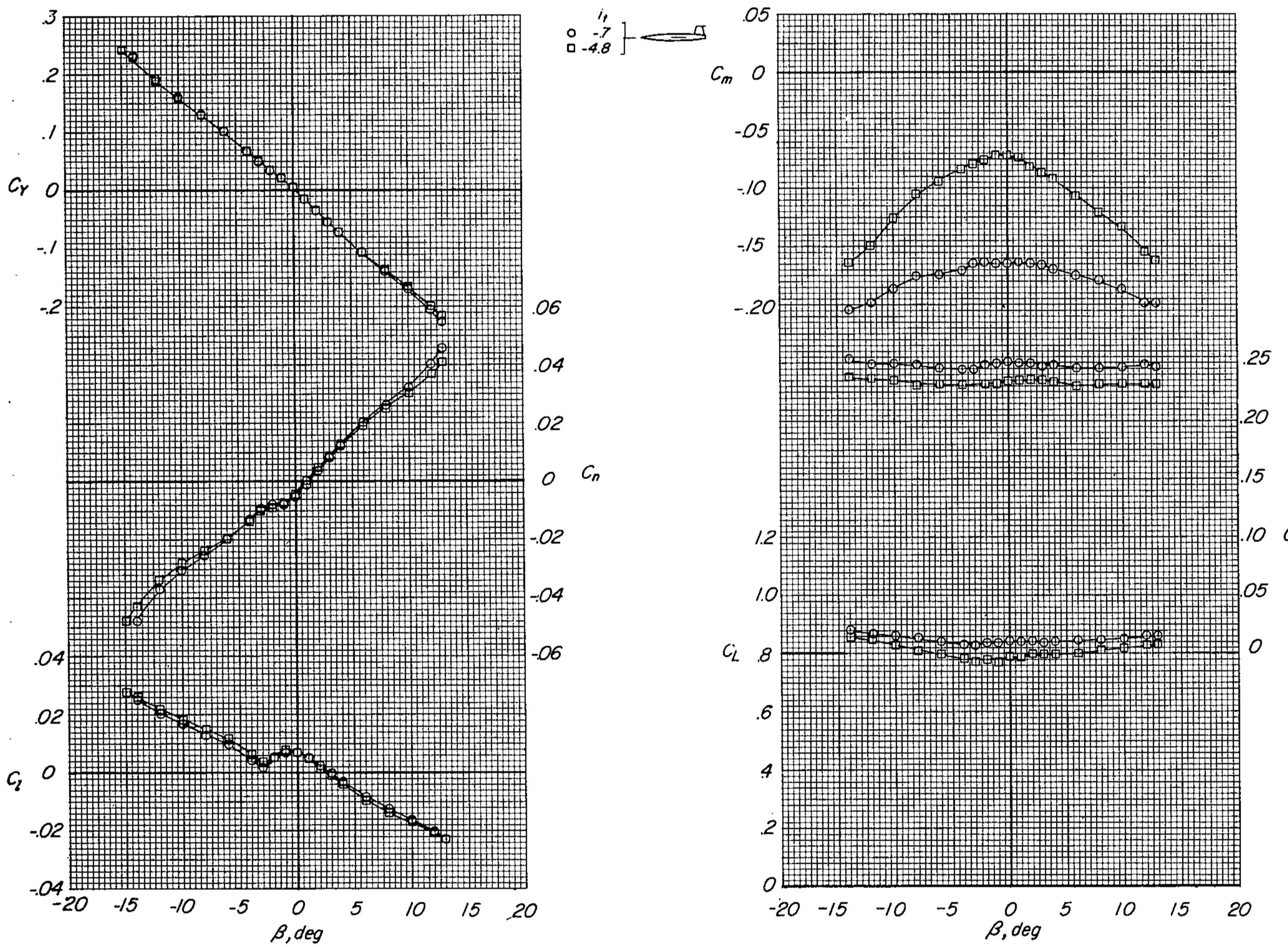

(b) M = 0.80.

Figure 24.- Continued.

[redacted]

[redacted]

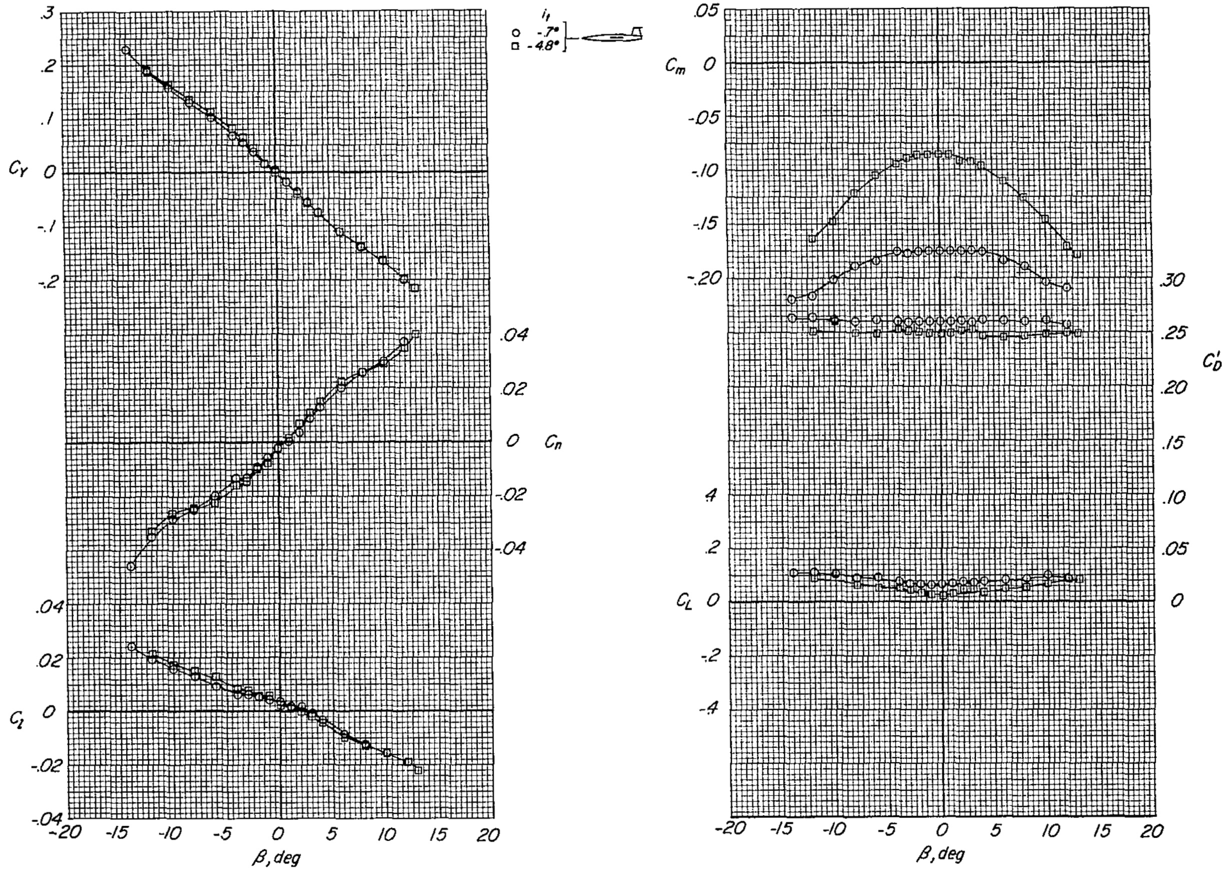

(c) M = 0.85.

Figure 24.- Concluded.

[redacted]

[redacted]